INSTITUT FÜR VERFAHRENSTECHNIK DES INDUSTRIELLEN UMWELTSCHUTZES
Montanuniversität Leoben
Franz-Josef-Straße 18
www.vtiu.com
A-8700 Leoben

Master Thesis

Improvement and Presentation of Two Novel, Innovative Filter Testing Methods

in corporation with

ICE Strömungsforschung GmbH

Submitted by:
Georg Reiss, BSc
0535107

Advisor:
Ao.Univ.-Prof. Dipl.-Ing. Dr.tech. Christian Weiß
Dipl.-Ing. Dr.mont. Gernot Boiger (ICE)

AFFIDAVIT

I declare in lieu of oath, that I wrote this thesis and performed the associated research myself, using only literature cited in this volume

Acknowledgement

I would like to thank Prof. Weiß for his commenting on my master thesis.

I am grateful to Gernot Boiger for his constant guidance, support and valuable feedback throughout my work. The collaboration with him was challenging, but also rewarding, and a gain in knowledge.

My thanks also go to Prof. Brandstätter, head of ICE Strömungsforschung GmbH, for the funding of my master thesis.

I am much obliged to my parents who supported me all my life, and enabled me to study in Leoben. It would not have been possible without them.

Above all, I wish to thank Katrein Kisza-Reiss who, with her cheerful and lovable nature, brought so much happiness into my life, and whose assistance I do not want to miss.

Kurzfassung

Verbesserung und Vorstellung zweier neuartiger, innovativer Filtertestverfahren

Die Prüfung von Filtermedien wird von zahlreichen Industrienormen beschrieben. Eine Vielzahl von unterschiedlichen Parametern, die bestimmt werden können, ist dort aufgelistet. Viele Prüfmethoden sind aber technisch und zeitlich sehr aufwendig. Zwei neuartige Prüfverfahren sind in Zusammenarbeit mit der Firma ICE Strömungsforschung GmbH entwickelt worden. Das *Durchlichtverfahren* beruht auf einem direkten Zusammenhang zwischen dem Druckverlust einer Filterprobe und den lokalen Grauwerten, die mittels Fotographie ermittelt werden. Diese Korrelation konnte in dieser Arbeit bestätigt werden. Des weiteren kann die Standardabweichung der experimentellen Ergebnisse verringert werden, weil mit dieser Methode repräsentative Proben ausgewählt werden können. Dadurch reduziert sich die Zeit beträchtlich, die für die Prüfung nötig ist, weil weniger Proben untersucht werden müssen, um Ergebnisse mit einer gleichen statistischen Genauigkeit zu erhalten. Die Anschaffungskosten für das *Durchlichtverfahren* sind relativ gering, die Benutzung ist einfach und die Implementierung in standardisierte Laborabläufe stellt kein Problem dar. Das zweite innovative Prüfverfahren ist in der Lage, die Partikeleindringtiefe in Filter mittels Fluoreszenz - Makrofotographie zu bestimmen.

Abstract

Improvement and Presentation of Two Novel, Innovative Filter Testing Methods

Filter testing methods are described by various industrial standards. A broad range of different parameters, which can be evaluated, are stated there. Nevertheless, many filter testing methods are complicated and time consuming. Two novel filter testing methods are developed in corporation with the company ICE Strömungsforschung GmbH. The first method, called *translucency examination,* makes it possible to find out a direct correlation between the pressure drop of filter samples and their local grey values, determined by photography. Furthermore, the deviation of the experimental results diminishes because representative samples can be selected. This yields in a reduced working time as fewer samples are needed to get results with an equally sufficient statistical accuracy. The acquisition costs for the *translucency examination* are relatively low, the handling is simple and it can be integrated into every standardized laboratory procedure without any problems. The second innovative filter testing method is capable of determining the particle penetration depth in filter media with the help of fluorescence macrophotography.

Table of Content

1 Introduction

Filtration processes play a vital role in our modern world. There is scarcely an application without filters involved. Above all, cleaning procedures in connection with environmental protection, like off-gas treatment or waste water treatment, do not manage without this technology. Further examples, apart from industrial processes, in everyday live are particulate filters for diesel engines, filters for ventilation and air conditioning or the uncomplicated filter for the daily coffee or tea in the morning.

Because filtration is so important for numerous applications, there are many industrial standards for the testing of filters. One drawback of many filter testing methods is the enormous time involved. Moreover, new possibilities to assess filter materials, like computational methods are neglected so far.

Boiger and Mataln (2009) developed a computer algorithm which is capable of determining the flow field, the pressure drop and the filtration efficiency on a real fibre geometry. The input data for the algorithm is an actual photograph of the fibre geometry, obtained by computer tomography. In cooperation with this research two novel, innovative filter testing methods were developed. The first new method, called *translucency examination,* is a procedure that is able to enhance the selection of representative filter samples. Furthermore, a connection between grey values and the pressure drop is assumed because of areas of varying thickness on the filter medium. These areas with higher or lower density are determined and assessed with a computer algorithm. An important guideline is that the developed process can be affordable for every laboratory. The second innovative method provides a process that is capable of evaluating the position of fluorescence particles within a filter, and reconstructs a 3-D distribution of these particles.

The starting point for this master thesis will be a brief survey of the state of the art in filter testing. Then, it will be tried to develop, verify and describe the two novel filter testing methods. The core of this thesis is to form a thorough working instruction for the developed processes. Subsequently, a filter medium will be chosen and assessed by using the newly proposed filter testing methods.

2 State of the Art in Filter Testing

A brief overview of different filter testing methods will be presented in this chapter. In order to obtain information of the suitability of different filter media for separation processes, it is important to know the design of textile filter media, material specific parameters and the operational behaviour.

2.1 Design of Textile Filter Media

> "Textile filter media in the form of textile fabrics consist of yarns and/or fibres. In the case of woven fabrics and/or knitted fabrics, yarns (filaments) form the structural elements, whereby the textile fabric is given its form and is stabilized by the crossing of several yarns or of a yarn with itself. With felts or nonwovens, fibres serve as the structural elements. The textile fabric is created here by needle-punching, fusing and/or bonding using a binding agent." (VDI 3926, 1994, p. 4)

2.1.1 Woven Fabrics

> "The typical characteristics of a woven fabric are predetermined by weaving type (filamentation), the textures in warp and weft directions, the properties of the warp and weft threads and by the finishing treatments following the weaving process. Woven materials with different properties can be obtained by varying these characteristics." (VDI 3926, 1994, p. 6)

2.1.2 Felts and Nonwovens

> "A differentiation is made between felts, fleeces and filament (spun-bonded) fleeces. The bonding of these materials can be effected mechanically by needling or by using water jet, adhesively with binding agents or cohesively with thermal or chemical methods. A distinction is made between felts and nonwovens in the case of materials mechanically bonded by needle-punching. These differ according to DIN 61210 in the intensity of the bonding. Needle-punched products free from binding agents with a gross density of ≥0.15g/cm³ are referred to as felts, all other products as nonwovens. With felts and nonwovens, the technological properties can be preset to great degrees by varying the influencing variables (fibre properties, design of the textile fabrics, manufacturing conditions)." (VDI 3926, 1994, p. 6)

2.2 Material-specific Properties of Textile Filter Media

The Verein Deutscher Ingenieure (VDI 3926, 1994, p. 10) proposes a list of different material specific data, which can be determined by common measurement methods. This data is of importance for the evaluation of the filter media for practical application and is listed in table 2.1.

Table 2.1: Recording of material-specific data of filter media (VDI 3926, 1994, p. 10)

	Data is		Symbol	Unit
	necessary	desirable		
1 Type of filter material	x		-	-
2 Chemical composition of the fibre	x		-	-
3 Trade name	x		-	-
4 Surface mass of the filter material	x		m_A	g/m²
5 Thickness of the filter material	x		d_5 [1]	mm
6 Air permeability	x		L_d	l/(dm²·min)
7 Permanent operating temperature	x		T	°C
8 Maximum tensile force				
8.1 longitudinal	x		F_H	N
8.2 transverse	x		F_H	N
9 Maximum tensile force elongation				
9.1 longitudinal	x		ε_H	%
9.2 transverse	x		ε_H	%
10 Load-elongation diagram	x		-	-
11 Shrinkage	x		S	-
12 Finishes	x			
13 Permanence				
13.1 Acid, alkali, solvent	x			-
13.2 Hydrolysis (water)	x			-
14 Fibre density		x	ρ_N	g/m³
15 Pore volume of the filter material		x	V_{px}	%
16 Bursting pressure		x	p_B	N/cm²
17 Melting point		x	T	°C
18 Combustibility		x		-
19 Water intake		x	W_A	%
20 Water retention capacity		x	W_n,W_t	%
21 Electrostatic behaviour: Surface resistance		x	R_{OT}	Ω
22 Data on supporting fabric		x		-
23 Biological resistance		x		-
24 Ageing resistance		x		-
25 Clinic instructions (washing)		x		-

[1] is equivalent to a_x

The next subchapters describe the most important measurement methods which are related to VDI 3926 (1994).

2.2.1 Mass per Unit Area (Weight per Unit Area)

"The term mass weight per unit area (weight) is used for the quantitative designation of a textile fabric. It is defined as the quotient of mass (in g) and surface (in m²).

The weight of a textile fabric with a determined test surface serves as test quantity.

The weight per unit area depends on the fibre type, the fibre fineness, as well as the type and design of the supporting fabric." (VDI 3926, 1994, p. 11f)

2.2.2 Thickness

"The thickness of a filter medium is defined as the distance between bottom and top side of a textile fabric, measured as the distance between two parallel measuring surfaces, between which the textile fabric is located at a measuring pressure of 200 Pa.

Test quantity is the distance measured between the bottom and the top sides of the filter medium (in mm) under the stated conditions." (VDI 3926, 1994, p. 12)

2.2.3 Gross Density

"The gross density of a filter medium ρ_{RX} is defined as the quotient from mass (weight) and the volume of the filter medium in relation to the standard thickness a_x according to DIN 53855. The unit of gross density is g/cm³.

The weight per unit area m_A (in g/m²) and the standard thickness a_x (in mm) are used as test quantities for determine the gross density.

The gross density is calculated using following formula:" (VDI 3926, 1994, p. 12)

$$\rho_{RX} = \frac{m_A}{1000 \cdot a_x} \qquad (2.1)$$

2.2.4 Air Permeability

"The air permeability describes the permeability of textile filter media against flowing air with a vertical flow against the plane of the layer. In general, filter media are tested at a differential pressure of 200 Pa (2 mbar).

The test quantity is the volume per surface area and unit of time: l/(dm²·min) or l/(m²·s). The size of the testing surface is 20 cm².

The air permeability is influenced, for example, by the weight per unit area, the thickness, the fibre fineness and the surface treatment. The air permeability of the material is stated by manufacturers in as-manufactured condition. The initial value is reduced in filtration operation due to dust deposits. Depending on the dust properties and the filter design, the reduction of air permeability in operation is 40 to 60%, in extreme cases 80 to 90%." (VDI 3926, 1994, p. 12f)

2.2.5 Pore Size Distribution and Mean Flow Pore Size

Akshaya and Krishna (2009, p. 2) show that the basic principle of determining the pore size distribution and the mean flow pore size, is based upon the measurement of differential pressure and flow rates through dry and wet filter samples. As long as the pores are filled with liquid the pressure drop is higher compared to the dry sample. The differential pressure which is required to remove liquid from a pore is related to the pore diameter D_p

$$D_p = \frac{4\gamma \cos\theta}{p} \qquad (2.2)$$

where γ is the surface tension of the wetting liquid, θ is the contact angle of the wetting liquid with the sample, and p is the differential pressure.

According to TOPAS (2008) at a certain point, the so called bubble point, the liquid filled pores will become gas permeable, which is shown in figure 2.1. At a certain differential pressure a sudden increase in flow can be measured. The real filter materials usually contain a wide range of pore sizes. Therefore, the bubble point corresponds to the opening pressure of the largest pore.

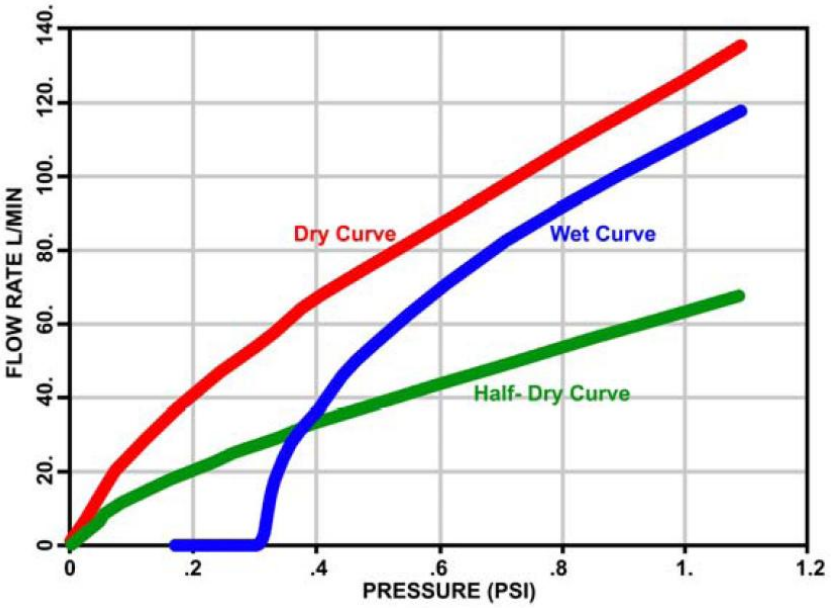

Figure 2.1: Variation of air flow rate with differential pressure (Akshaya and Krishna, 2009, p. 8)

As Akshaya and Krishna (2009, p. 8) have demonstrated, the bubble point diameter can be calculated with equation 2.2. To determine the mean flow pore size diameter a half dry curve has to be computed, which gives half of the flow rate through the dry sample at a given differential pressure, as shown in figure 2.1. The value where the half dry curve intersects the wet curve corresponds to the mean flow pressure. With this value and equation 2.2 the mean flow pore size can be calculated. The mean flow pore size is defined such that 50 % of the flow goes through pores larger than the mean flow pore size and 50 % through pores smaller than the mean flow pore size.

Akshaya and Krishna (2009, p. 9) say that a pore distribution can be computed when the flow rates through the wet F_w and the dry F_d filter medium are known. The formula for the distribution function f is given in equation 2.3

$$f = -\frac{d\left[\left(\frac{F_w}{F_d}\right)\cdot 100\right]}{dD_p}. \qquad (2.3)$$

An example of such a distribution is shown in figure 2.2.

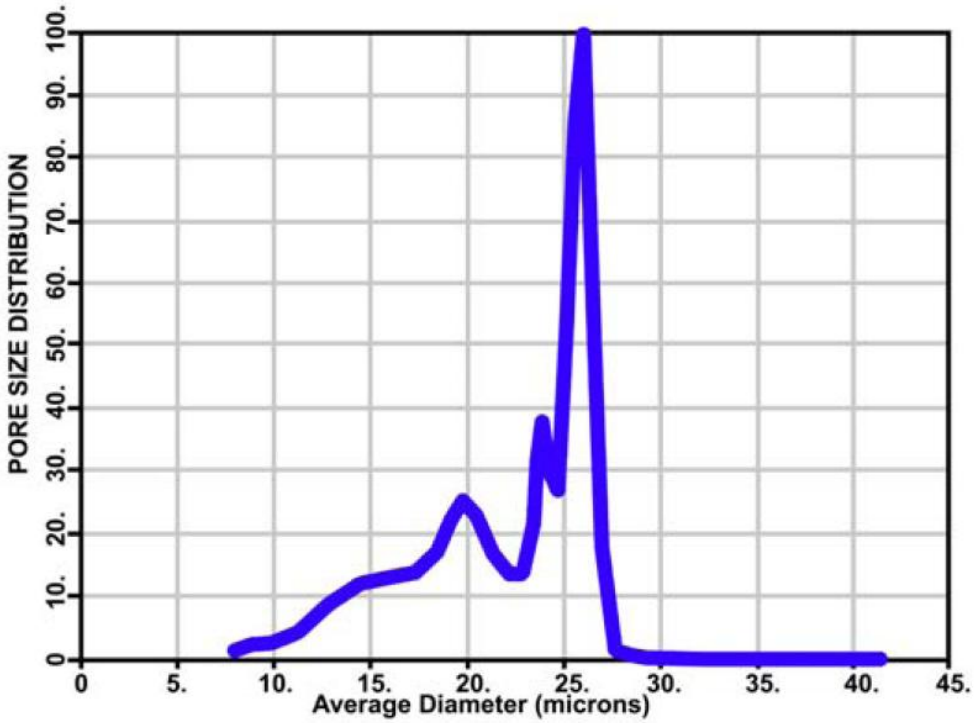

Figure 2.2: Pore distribution (Akshaya and Krishna, 2009, p. 9)

2.2.6 Pore Portion

"The pore portion of a filter medium is defined as the proportion of air spaces in the total volume contained in the fibres and between the fibres and yarns which the textile fabric accepts at standard thickness.

Test quantities for determining the pore portion V_{px} are the density of the fibre material ρ_N and the gross density ρ_{RX}. The pore portion (in %) is calculated according to

$$V_{px} = \frac{\rho_N - \rho_{RX}}{\rho_N} \cdot 100\% \qquad (2.4)$$

Conclusions about the manufacturing type of the filter medium can be drawn from the pore portion. Different fibre types, finishes and even the use of bonding agents with chemically stabilized nonwovens have a considerable influence on the pore portion of a filter material. Usual values of the pore portion for needle felt materials are between 75% and 90% and, with thermally stabilized nonwovens, between 50% und 80%." (VDI 3926, 1994, p. 13)

2.2.7 Strength and Deformability

"The strength and deformability of filter media can be described using measured results according to thermal and mechanical influence. The results of thermal influence include calorimetric and thermo mechanical characteristic values such as shrinkage. The characteristic quantities of mechanical influence include load-elongation behaviour with the static tensile test with the resulting values for the maximum tensile force and the maximum tensile force elongation, as well as the vaulting force, the tear growth strength and the resistance to abrasion." (VDI 3926, 1994, p. 13f)

2.2.7.1 Shrinkage

"Shrinkage is understood to be the dimensional behaviour of a filter medium after a predetermined time of being subjected to a thermal effect in hot air.

Test quantities for the determination of the shrinkage S are the starting length l_a and the shrinkage length l_s. The shrinkage S is defined as the ratio of the difference between the starting length and the shrinkage length ($l_a - l_s$) and the starting length l_a:

$$S = \frac{l_a - l_s}{l_a} \qquad (2.5)$$

The temperatures to which the filter material is exposed in this test depend on the material and require agreement. Usual temperatures are at least 10 °C above the maximum continuous operating temperature of the filter material stated by the manufacturer. The duration of the thermal influence is 1 hour for most filter media." (VDI 3926, 1994, p. 14)

2.2.7.2 Load-Elongation Behaviour

"The load-elongation behaviour refers to the relationships between tensile forces and the changes in length of strip-shaped measuring samples of filter materials.

The test quantities are the maximum tensile force and the maximum tensile force elongation, determined with the above mentioned strip-shaped samples.

The test piece (50 mm width with stabilized material; 200 mm free clamping length) is clamped in a tensile testing device. The relevant length of the strip-shaped sample is determined as a function of the tensile strength. It is usual to refer to the determined values as load-elongation diagram.

The load-elongation behaviour should be determined from at least 5 single samples in both longitudinal and transverse directions to the web. The measured values are determined arithmetically and recorded separately for longitudinal and transverse direction.

In addition to the maximum tensile force, the deformation speed is also of importance. This is set at 100 mm per minute for nonwovens according to [DIN EN 29073]. With other filter media, e.g. fabrics, this speed is set according to [DIN 53857] as a function of the maximum tensile force elongation." (VDI 3926, 1994, p. 14f)

2.2.7.3 Vaulting and Bursting Test

"The vaulting and bursting test is carried out according to DIN 53861 on a circular sample of the filter material to be investigated by subjecting it to compressed air. The sample, lying on a rubber membrane, is vaulted using compressed air, whereby the pressure-dependent vaulting expansion and/or the pressure required for bursting are determined." (VDI 3926, 1994, p. 15)

2.2.8 Permanence

"Assessments with textile filter media of the permanence (ageing behaviour) concern the influences of heat, air, steam, acids, alkalis, solvents, process gases and flue gases, water, light, as well as detergents during cleaning.

The permanence of filter materials against acids, alkalis, solvents and water can be of decisive influence for the possible applications. A distinction must be made when evaluating the permanence between the permanence of the fibre materials and the permanence of a finishing.

> Tests of the permanence require an initial treatment of the samples and a subsequent testing of the effect of the treatment. Such tests require special testing methods which must be applied in accordance with the material to be tested and which presuppose prior knowledge of the composition of the filter material. […] Such tests should be the responsibility of the manufacturer of the filter materials and the results of the tests should be requested from this source." (VDI 3926, 1994, p. 15f)

2.2.9 General Physical Characteristics

Moisture intake, the water retention value (water swelling value), the melting and decomposition temperature, the combustibility and flammability, and the electrostatic behaviour belong to the general physical characteristics.

Due to common synthetic fibres, which are only slightly influenced by moisture, the moisture intake value and the water retention value are not so important, and should be ascertained by the manufacturer.

Also the data on melting temperature and the more important recommended permanent application temperature should be requested from the manufacturer.

The burning behaviour of filter materials describes the burning and smouldering time, as well as the degree of destruction under the influence of a flame on textile samples hung perpendicularly.

When determining the electrostatic behaviour of filter materials, it has to be made a differentiation insofar as this involves aspects relevant to safety for conductive fibres. The following parameters are determined: the surface resistance R_{OT} (in Ω); the volume resistance R_A (in Ω·cm²) related to the surface area and the volume resistivity ρ_D (in Ω·cm). (VDI 3926, 1994, p. 16)

2.3 Testing Methods

The testing of operational behaviour of filter materials is very important for their characterization. The Verein Deutscher Ingenieure (1994, p. 29) recommends the testing of the following parameters for cleanable filters.

2.3.1 Pressure Loss across the Filter

With a constant volume flow and a constant raw gas concentration the pressure loss across the filter will increase during the measurement. At a certain maximum differential pressure the filter should be cleaned. This maximum pressure has to be specified according to the field of application. (VDI 3926, 1994, p. 29)

A flow law derived from numerous experimental studies, which is valid in case of fibrous filters not contaminated with particles, is given by VDI 3677 (1997, p. 7) in equation 2.6:

$$\frac{\Delta p}{\Delta L} = 64 \cdot (1-\varepsilon)^{1.5} \cdot [1 + 56 \cdot (1-\varepsilon)^3] \cdot \frac{\eta_f \cdot v_F}{D_F{}^2} \qquad (2.6)$$

where Δp is the pressure drop of the fibre layer, ΔL is the thickness of the fibre layer, ε is the layer porosity (pore volume fraction), η_f is the dynamic gas viscosity, v_F is the specific area load, which is the volume flow rate divided by the filter area and D_F is the fibre diameter.

2.3.2 Filtration Efficiency

To determine the filtration efficiency the dust content in the clean gas has to be measured. This can be done with a total filter installed in the clean gas channel. The amount of dust in the test filter is compared to the amount of dust collected in the absolute filter. (VDI 3926, 1994, p. 29)

To measure the amount of dust in a filter according to EN 779 (1994, p. 5-8) the gravimetrical measurement is used for synthetic dust. Another measurement technique used for atmospheric dust, which is smaller than synthetic dust, is a turbidity measurement of the filter before and after the filtration process. With the reduced translucency, the efficiency can be calculated.

If the filtration efficiency of lubrication oil filters should be determined the ISO 4548-12 (2000, p. 2-23) suggests a multi-pass test. This test requires the recirculation of unfiltered fluid through the filter element. The arrangement of the test rig consists of a contaminant injection circuit, a filter test circuit and a dilution and counting system. In the contaminant injection circuit the particles are dispersed, and injected in the filter test circuit. The filter test circuit comprises a pump, a test filter, a flow meter and a differential pressure gauge. In front of and after the test filter two sampling valves connect the filter test circuit with the dilution and counting system, where the particles in the upstream and downstream are counted with the help of two optical particle sensors.

3 Translucency Examination

This chapter describes the development process of a new filter testing method. The aim is to find a method to determine representative samples of a filter medium. For that, photographs of filter sheets are taken, and the differences in local grey values are evaluated.

Many filter media are inhomogeneous due to the production process. This means that one filter sheet consists of regions with higher density, and regions with lower density. It is assumed that the pressure drop is varying slightly over the filter sheet. In order to get a representative result many arbitrary samples have to be analysed, which usually takes a long time. In addition to that, if simulations of filter media are carried out, the investigated filter area is rather small and not representative, due to the limited computational capacity. In other words, to get a representative result from the simulation, many different portions have to be investigated.

With the *translucency examination* of the filter sheet it should be possible to determine and select representative samples. In that case the time for the filter testing and also the time for the simulations will diminish.

Moreover, it is assumed that the pressure drop corresponds to the local grey value of the proposed filter sample position.

3.1 Basic Principle

In chapter 2.3.2 a turbidity measurement of filter samples was presented. Due to the reduced translucency of the dust loaded filter the filtration efficiency can be calculated. The basic idea of this principle is used in this method. A photograph of the test filter on an overhead projector is taken. Figure 3.1 shows the photograph of a test filter.

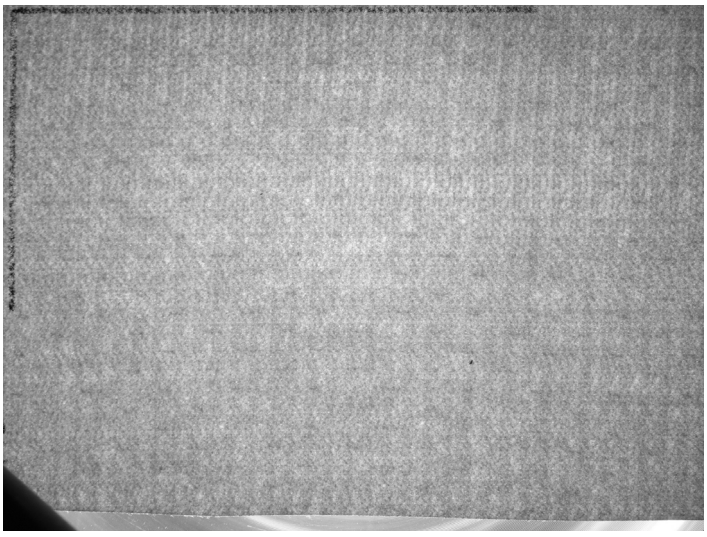

Figure 3.1: Photograph of the filter medium *A43 Fulda*

Regions with higher density appear darker than regions with lower density. This picture is the input data for a computer algorithm developed at the ICE Strömungsforschung GmbH. This algorithm is able to determine the positions of representative test samples, by evaluating the grey values of the filter sheet.

3.2 Experimental Assembly

Two main different devices form the basic setup for the procedure of the *translucency examination* and the determination of the pressure drop:

- *Translucency examination*
- Filter test circuit

3.2.1 Translucency Examination

The *translucency examination* shall comprise an overhead projector, a tripod and a camera. The assembly is shown in figure 3.2.

Figure 3.2: Assembly of the overhead projector and the tripod

To ensure a constant picture quality every test filter should be placed on the same position on the overhead projector. This is done by markings on the corners of the overhead projector. The camera settings, which should also be constant, are described in more detail in chapter 5. Once a photograph is taken, it can be transferred to a computer, and evaluated with the algorithm. The result will be a stencil which shows ideal positions for representative samples.

3.2.2 Filter Test Circuit

The filter test circuit is used to verify the initial assumption that the pressure drop and the evaluated grey values of filter samples correlate. The filter test rig described in the ISO 4548-12 (2000, p. 2-23) is the model for the filter test circuit used for the experiments, and shall include the following components. The arrangement of the filter test circuit is shown in figure 3.3:

a) A reservoir (a) which can contain at least 6 litre of oil, with the possibility to apply a pressure of about 6 bar. This pressure is used to force the oil through the filter test circuit; therefore, no oil pump is needed.

b) A compressor (b) to apply the pressure on the reservoir.

c) A pneumatic (c) and an electromagnetic agitating device in the reservoir to ensure a good mixing when particles are used.

d) A valve (d) to start and stop the testing manually.

e) A flow meter (f) and a flow control device (e) to measure and control the volume flow, and ensure definite operating conditions.

f) A fixture for the test filters (h).

g) A differential pressure gauge (g) which measures the pressure drop over the test filter.

h) A second reservoir (i) which contains the used oil after the test.

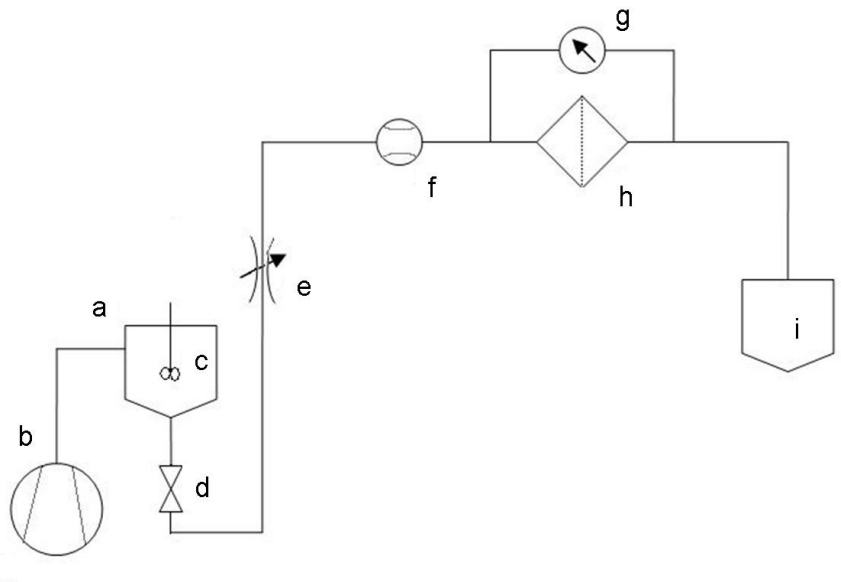

Figure 3.3: Diagrammatic arrangement of filter test circuit

The samples tested in this filter test have a circular shape with a diameter of 25 mm. The working procedure is explained in more detail in chapter 5.

3.3 Description of the Computer Algorithm

The evaluation of representative filter sample positions comprises two important steps. The first one is to take a picture of the filter sheet, and the second one is to adjust the parameters of the computer algorithm.

The picture of a filter sheet on an overhead projector is the input data for this algorithm. The first important step is to compensate for the circular light source, which influences the grey value distribution of the filter sheet. This fact is shown in figure 3.4.

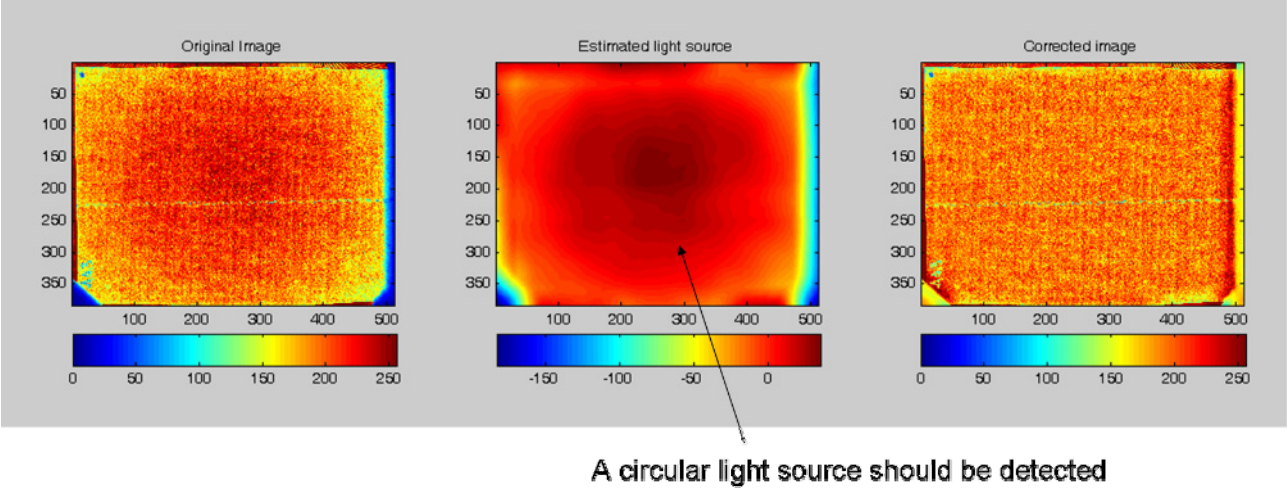

Figure 3.4: The result of the light source elimination

The left image illustrates the original photograph of the filter sheet. The emitted light of the bulb of the overhead projector has a circular shape. To determine this light source the program uses a rectangular “filter” with an adjustable size. In practice a size of 15% of the picture dimensions proved to be a sufficient value. The program scans every grey value and calculates the mean value of the “filter” area. The result of this calculation is the picture in the middle. It represents an estimated light source. These grey values are now subtracted from the original image. On the right hand side the corrected image is shown.

Subsequent to the light source elimination, the user is asked to define the diameter of the samples. With this data the program calculates the mean grey value at every pixel position within this sample region. This is very important because the information of the individual grey value at each pixel point is not sufficient for experimental purposes. Real filter samples have a diameter of 25 mm, and therefore, consist of hundreds of pixels, depending on the resolution.

The huge innovation of this algorithm is that it calculates the mean grey value of a circular shaped sample with an adjustable diameter. In figure 3.5 the differences between the grey values of the original picture (left) are compared with the mean grey values (right), calculated with a circular shaped sample. It is obvious, that the difference between the lowest and highest grey values of the original picture is much higher than the corresponding value in the processed and averaged image. In the latter picture the difference between the highest and lowest grey value is about 3%, whereas in the original image the difference is about 30% to 50%.

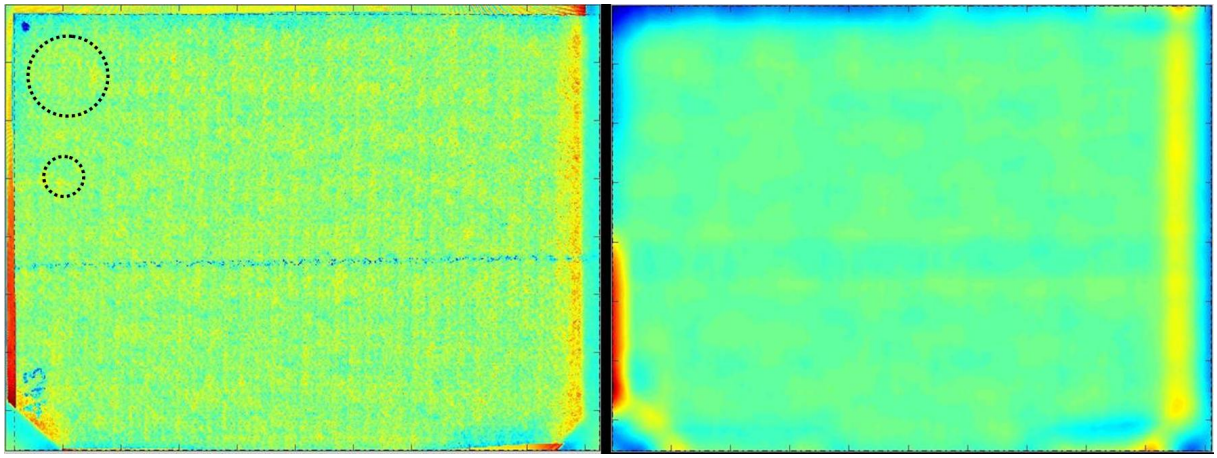

Figure 3.5: Comparison between the original (left) and the mean grey values (right). The calculation of the mean grey value of a circular shaped sample leads to more homogeneity (right); possibility of different sample diameters

Figure 3.6 shows three histograms which represent the above mentioned effects. The relative frequency is plotted over the grey values, which range from 0, which is black, to 256, which is white. The curve marked *selected paper* refers to the area of the picture where the filter sheet is located. This area has to be chosen by the user with the help of scroll bars. The distribution of grey values in the curve marked *selected paper* is the broadest one. After the program has calculated the mean grey values of the filter samples, the distribution is much narrower. The values are represented by the curve marked *Paper Mean*. The curve marked *Selected Area Mean* refers to the inner area of the filter sheet, which also can be chosen by the user. Due to light effects at the edges of the filter sheet, it is recommended to leave a margin of about 5 cm to the edges of the filter sheet.

It is obvious that the distribution of the medium sample grey values is a function of the diameter of the filter sample, with which the mean grey value is calculated. The smaller this diameter is, the larger the mean standard deviation of the distribution becomes. This is very important when areas for the simulation are to be determined, where the diameter of the samples is about 200 µm.

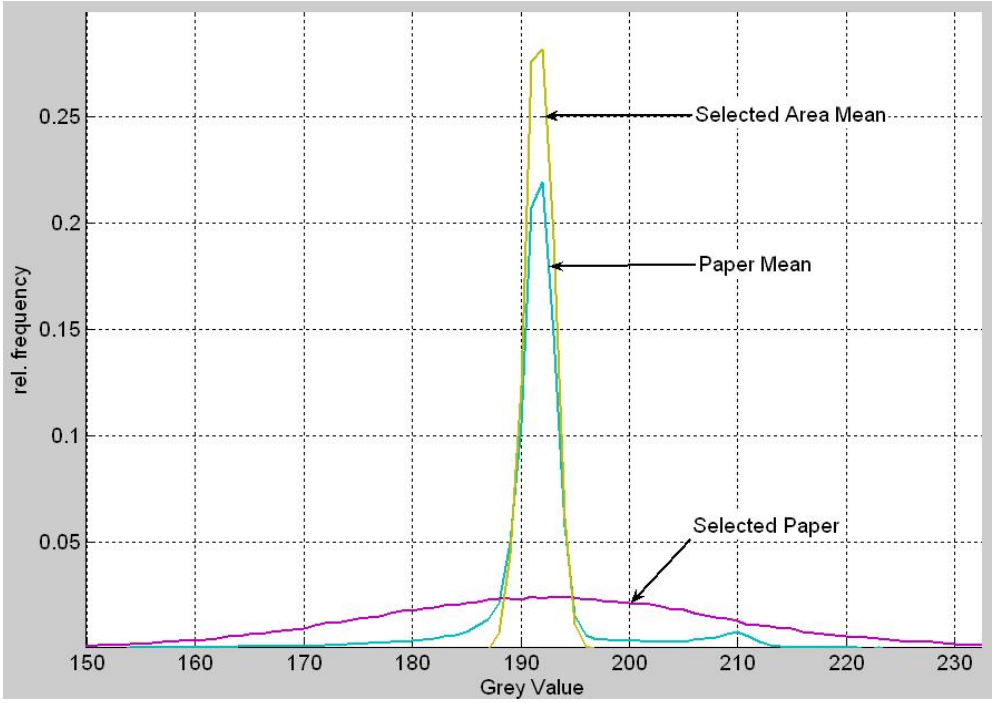

Figure 3.6: Histogram plotting grey values. The curve marked *selected paper* refers to the area of the picture, where the filter sheet is located. The curve marked *paper mean* refers to the grey values of the calculated samples. The curve marked *Selected Area Mean* refers to the inner area of the filter sheet, with a proposed margin of 5 cm.

The following input parameters can be adjusted by the user:

- *Range paper*: The user can define the range (minimum and maximum value) of the grey values.
- *Range mean:* The user can define the range (minimum and maximum value) of the mean grey value of a filter sample with the diameter which was defined by the user.
- *Range standdev:* The user can define the range (minimum and maximum value) of the standard deviation of the grey value of a filter sample with the diameter which was defined by the user.
- *Number of positions:* The user can define the number of grey values to sample. If *1* is inserted the program determines the position of the samples at the mean grey value. If *2* is inserted the program determines the position of the samples at the minimum and maximum grey value. If *3* is inserted the program determines the position of the samples at the minimum, the maximum and the mean grey value and so on.
- *Number of samples/position:* The user can define how many samples should be determined at each grey value *position*.

The result of the computer program will be a stencil which defines the positions of the different filter samples. The statistical data of the result is also saved. It comprises the minimum, maximum and mean grey value of the whole filter sheet and the selected area, as well as the respective deviations. In addition, the mean grey value and the deviation of each sample are saved. This deviation refers to the homogeneity of every sample. The stencil can be fixed with some paper clips to the filter sheet. With the help of a hammer and a punch the filter samples can be stamped. These filter samples are used for the determination of the pressure drop according to the working instructions described in chapter 5.

3.4 Process Development

3.4.1 Improvement of the Filter Test Circuit

The fixture in the filter test circuit was circular shaped and had a diameter of 25 mm. During the first experiments the filter samples for the first experiments were cut out with a scissor. The consequence of this procedure was that the filter sample did not fit the fixture exactly, especially at the edges. Therefore, the deviation of the pressure drop from one sample to another was higher than expected. In order to decrease this influence a pair of sealing rings were used as shown in figure 3.7.

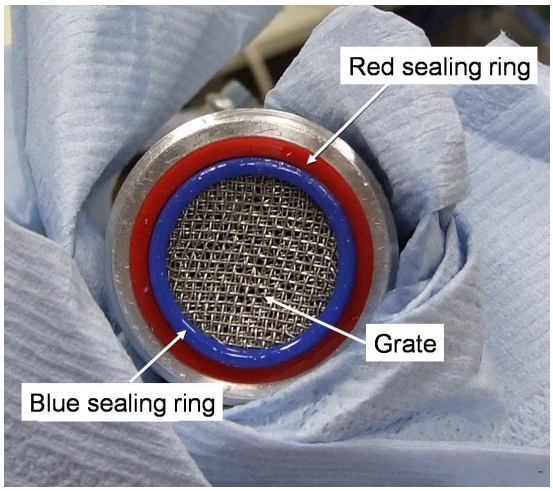

Figure 3.7: Assembly of the fixture

First the red sealing ring was put in the fixture. Than the grate was added for stability reasons. The filter sample was placed on the grate. Finally, the blue sealing ring was inserted to avoid leakiness at the edges.

Another improvement was the use of a punch instead of a scissor. Since a stencil was used, which located the filter samples, it was much easier to cut out these samples with the help of a punch than with a scissor. Because of this, every filter sample had the same size and shape.

3.4.2 Improvement of the Picture Quality

Another problem which occurred during the development process was that the reproduction of the pictures of the same filter sheet was not manageable. Even if two pictures were taken, one after the other, the mean grey value of the whole filter sheet differed. It was only 2%, but it made a comparison between different filter sheets virtually impossible. The reason why such a high precision was needed, was explained by the fact that the difference between the highest and lowest grey value of the filter sample positions was also only about 2%. This means that the filter sheets were rather homogenous.

The first thing which was checked, was the camera setting. The *manual modus* with the following setting was used:

Exposure time: 800

White balance: Neonlicht 2

Aperture value: 5.6

Flash: Stand by

ISO: 100

The second thing was the assumption that the emitted light of the bulb was not constant due to heat up effects. This fact was also stated in the EN 779 (1994, p. 6) and it was recommended that a certain time should pass, between the turn on of the bulb and the measurement. Therefore, at least 10 minutes should pass after the overhead projector was switched on.

The third thing was the influence of background light. The lighting conditions in the laboratory changed due to the position of the sun, and also the neon light had an influence. In order to decrease these effects, all curtains were drawn, and the light was switched off during the taking of the photographs.

Although these improvements have been carried out, the mean grey value of the whole filter sheet differs from one picture to another. Nevertheless, the deviation diminishes as plotted in figure 3.8.

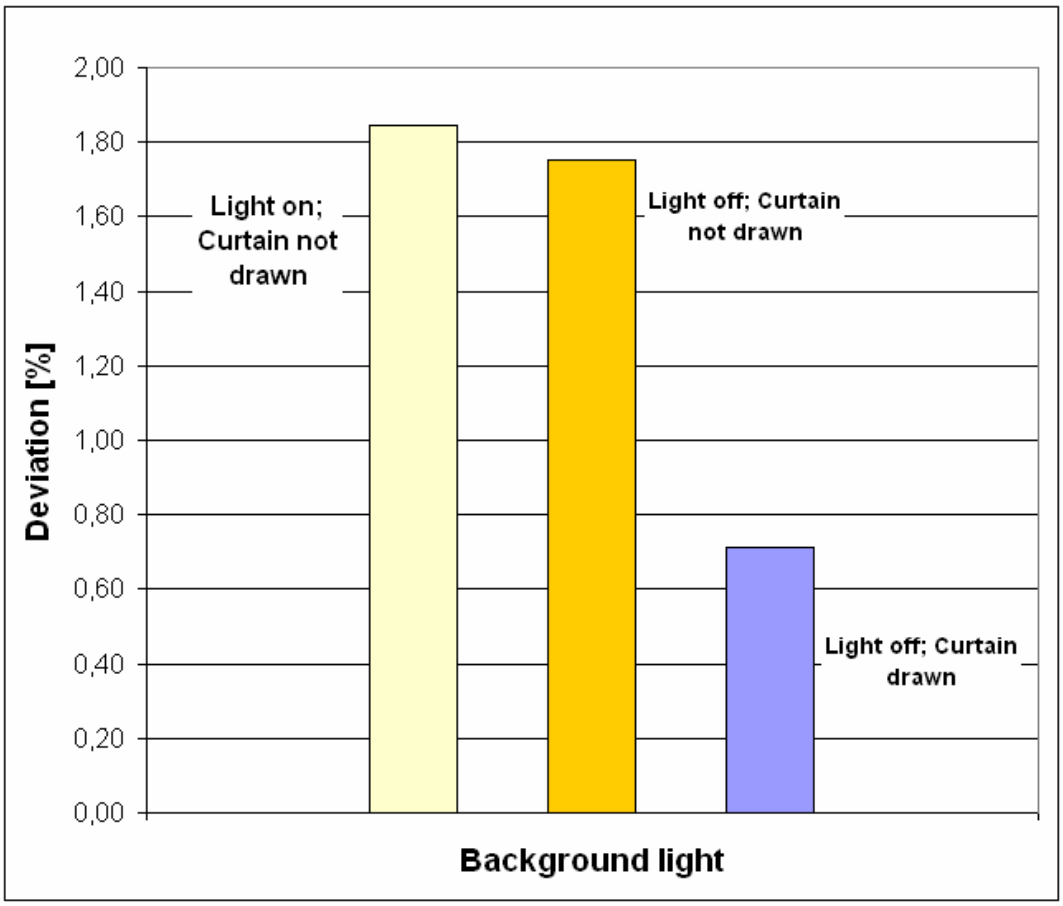

Figure 3.8: Deviation of the mean grey value under different background light conditions

To enhance the obtained improvement, it was necessary to set up a reference correction. The basic idea was to compare the mean grey value of a reference location with a defined value, and subtract or add the difference to all pixel values. Therefore, it should be possible to compare the mean grey value of all pictures. This procedure could be done because it was found out that the higher statistical moments of the grey value distribution stayed the same although the mean grey value differed. This meant that the whole distribution shifted towards another grey value.

In the upper left part of the overhead projector a red foil was placed. This foil acted as a reference location for the grey value correction. Several photographs were taken, and a mean value was calculated which then became the defined reference value. Now the first step in the algorithm was to determine the mean grey value of the reference location, and compare it to the reference value. Thus, the deviation of the mean grey value of two pictures of the same filter sheet decreased under 0.5%.

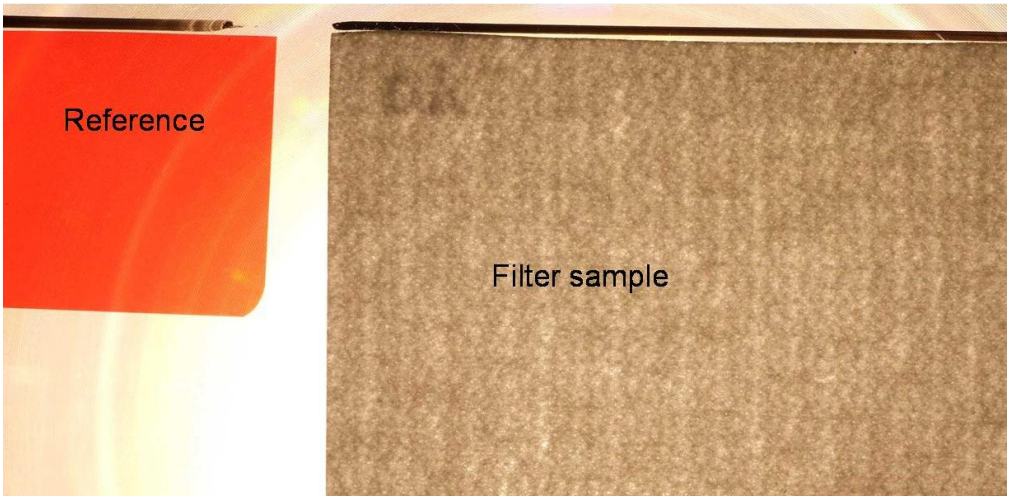

Figure 3.9: Filter sample with reference location

It seemed possible to compare filter samples of different filter sheets with each other. But the results showed that it was only reasonable to compare different filter samples of one filter sheet, which will be explained in the following section.

Two filter sheets of the type *A43 Fulda* were examined with the computer algorithm in order to get five samples with high density (low grey value), and five samples with low density (high grey value). The aim of this experiment was to find out, whether there is a correlation between the grey values and the pressure drop, or not. In addition, five randomly selected samples were taken, to compare the deviation of the measurement of the selected samples with the deviation of the randomly chosen samples. The results were evidence of a correlation between the pressure drop and the grey values. Another assumption was that the deviation within the selected samples is likely to be lower, compared to a random selection of samples. This second hypothesis could not be proven to be true.

These circumstances needed further assessment, which led to figure 3.10. The rectangular measurement values refer to one filter sheet of the type *A43 Fulda*, whereas the circular measurement values refer to another filter sheet of the same type. Two things can be observed in this figure. Firstly, the higher the grey values, the lower the pressure drop. Secondly, the deviation within one and the same filter sheet is much lower, compared to the deviation between two filter sheets although they have the same grey value, and should, therefore, have a similar pressure drop.

This led to the assumption that the grey value correction did not necessarily improve the experiments although possible light effects could be minimized. For further experiments only the samples of one filter sheet were compared with each other. Consequently, the reference foil was removed in order to increase the area for the filter sheet on the overhead projector.

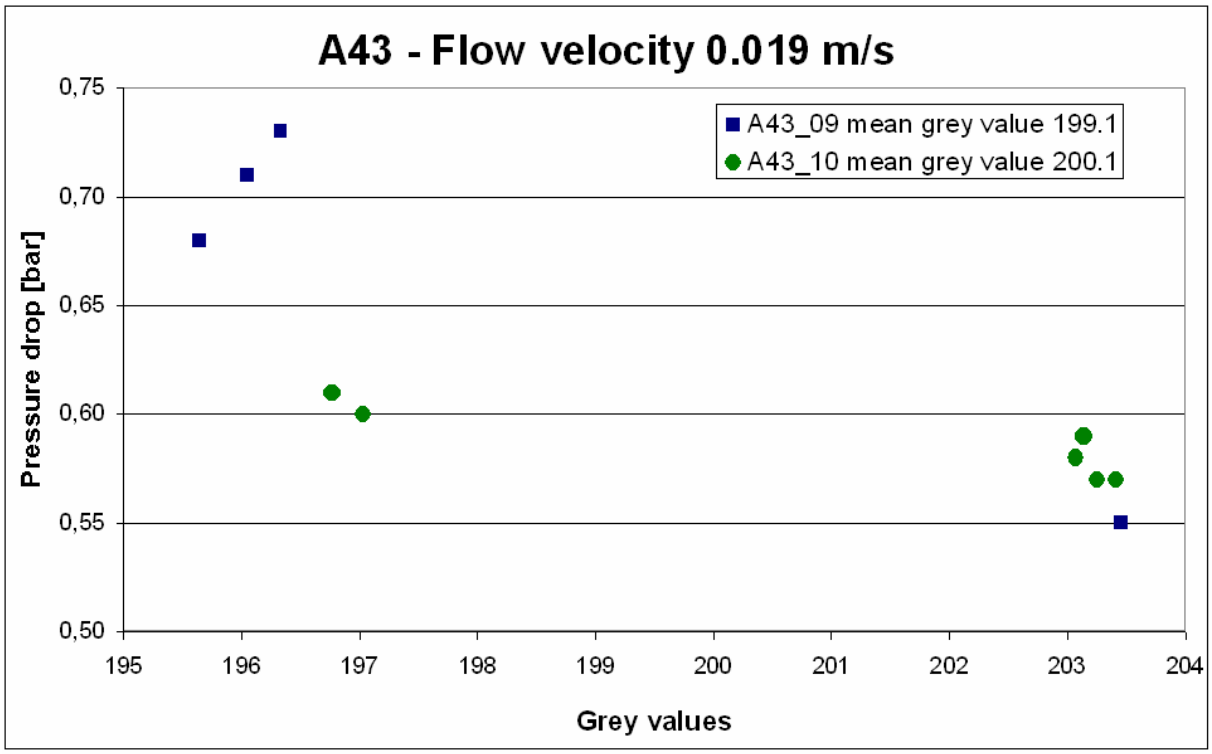

Figure 3.10: Comparison of the pressure drop in connection with grey values between different filter sheets of the same type

3.5 Experiment and Results

During the assessment of the *translucency examination* three different types of filter materials were tested. These filter media were *A55 Ahlstrom*, *A43 Fulda* and *Ti99*. Of each individual type five samples with a high grey value, five samples with a low grey value and five randomly selected samples were taken. That made 15 samples per filter material altogether. In addition to that, five filter samples with selected differing grey values were chosen of the filter material *A43 Fulda*. Therefore, each of these samples was supposed to feature a different pressure drop, according to the initial assumption. The latter setup was referred to as *worst case scenario*. An accurate description of the working procedure can be found in chapter 5. In this chapter the measurement data of the filter materials *A43 Fulda* and *A55 Ahlstrom* are discussed.

3.5.1 Translucency Examination

This subchapter describes the results and conclusions drawn from measurement data gathered by the *translucency examination*.

3.5.1.1 Proof of Dependence between Pressure Drop and Local Grey Values

The experimental results obtained by measurement in the laboratory are processed by means of visual evaluation, as well as statistical assessment.

3.5.1.1.1 Experimental Results

Figure 3.11 to figure 3.13 show the pressure drop of the individual samples of *A55 Ahlstrom* against the flow velocity. The information in the legend refers to the number of the sample (e.g. *P1*) and the current grey value of the sample.

The range of the grey values start from 0, which is black, to 256, which is white. This means that regions which appear darker on the image have a higher density, which should lead to a higher pressure drop. On the contrary, regions with lower density have a higher translucency, and appear brighter on the picture. Consequently, these regions should have a lower pressure drop.

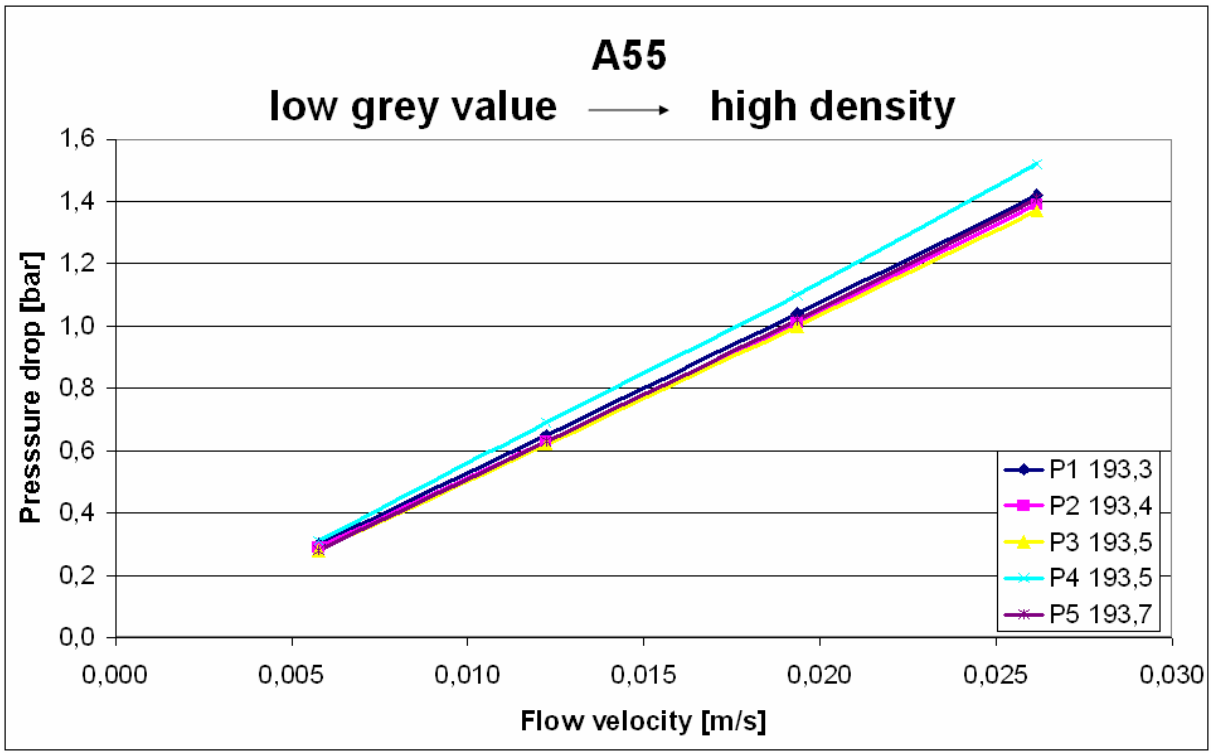

Figure 3.11: Pressure drop of *A55 Ahlstrom* filter samples with low grey values against flow velocity

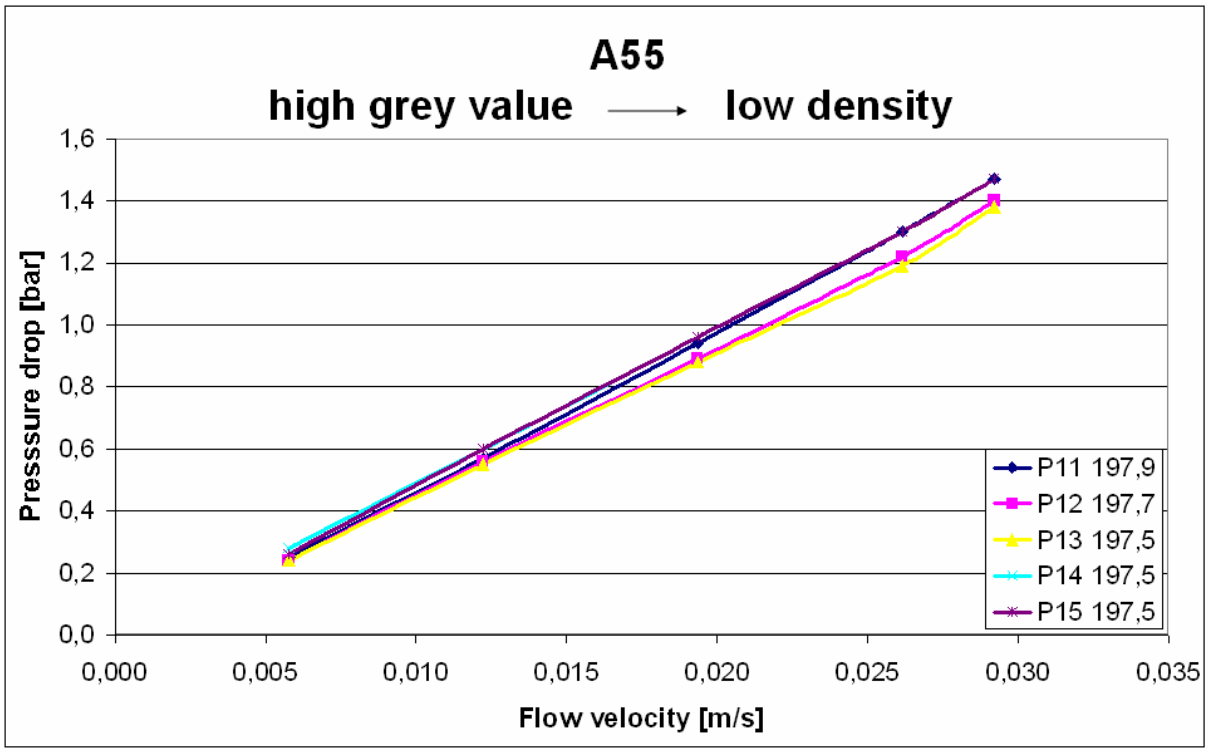

Figure 3.12: Pressure drop of *A55 Ahlstrom* filter samples with high grey values against flow velocity

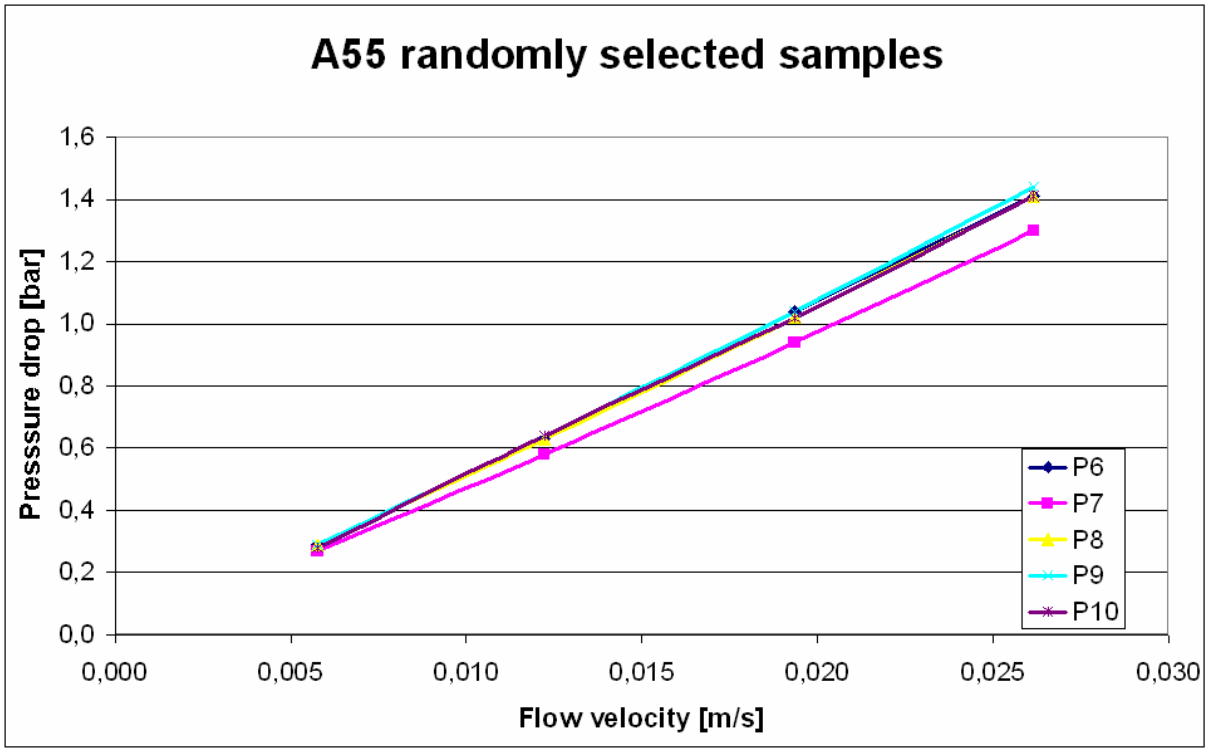

Figure 3.13: Pressure drop of randomly selected *A55 Ahlstrom* filter samples against flow velocity

Figure 3.14 is an evidence for the dependence between the grey values of the sample position and the pressure drop.

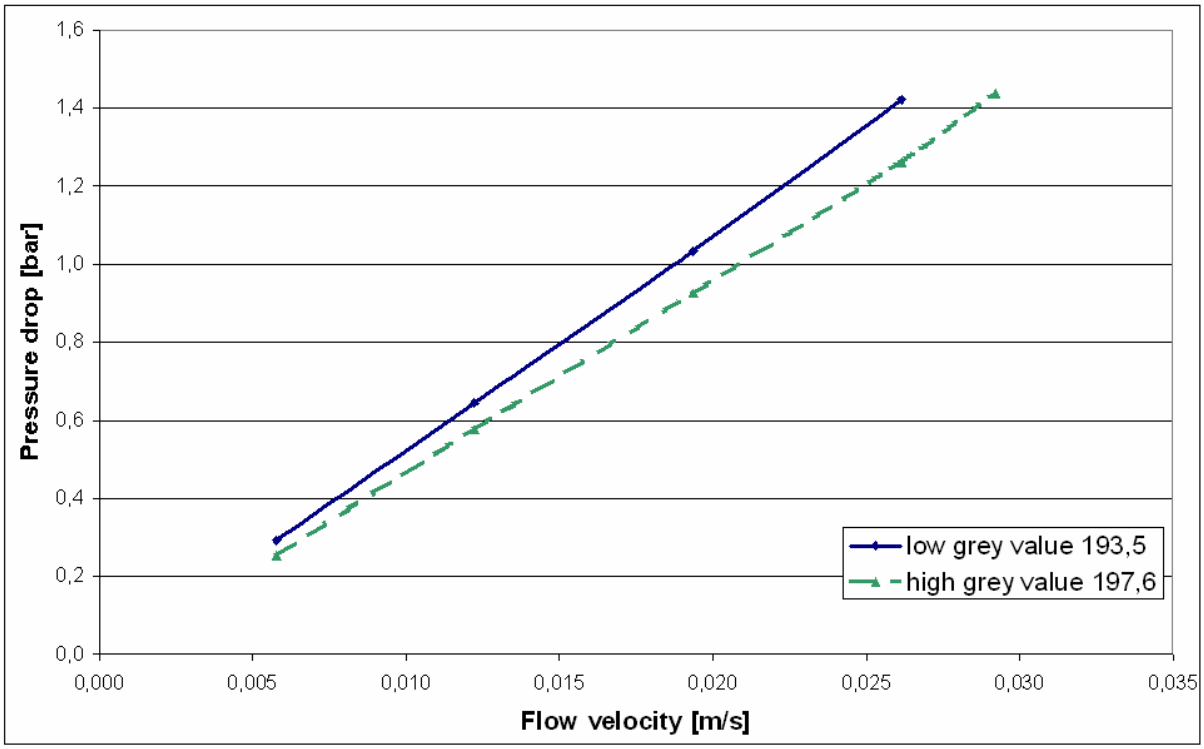

Figure 3.14: Comparison between the mean pressure drop values of *A55 Ahlstrom* against flow velocity

Figure 3.14 shows the pressure drop over the flow velocity as a mean value of the five samples with lower grey values, compared to the mean value of the five samples with higher grey values. The results confirm the assumption, that regions on the filter sheet, which appear darker, have a higher pressure drop than regions, which seem to be brighter.

In order to make the connection between the grey values and the pressure drop more clearly, a *worst case* experiment was carried out. The filter medium *A43 Fulda* was assessed with the *translucency examination* method. The goal was to find five samples with different mean grey values. Subsequently, the pressure drop of every sample was determined at five different flow velocities. Every pressure value was put in relation to the values of sample *P9* which had the lowest pressure drop. Therefore, relative pressure drop values for each flow velocity were obtained. In a last step, the mean pressure drop value of all flow velocities of one grey value was calculated. The results are shown in figure 3.15.

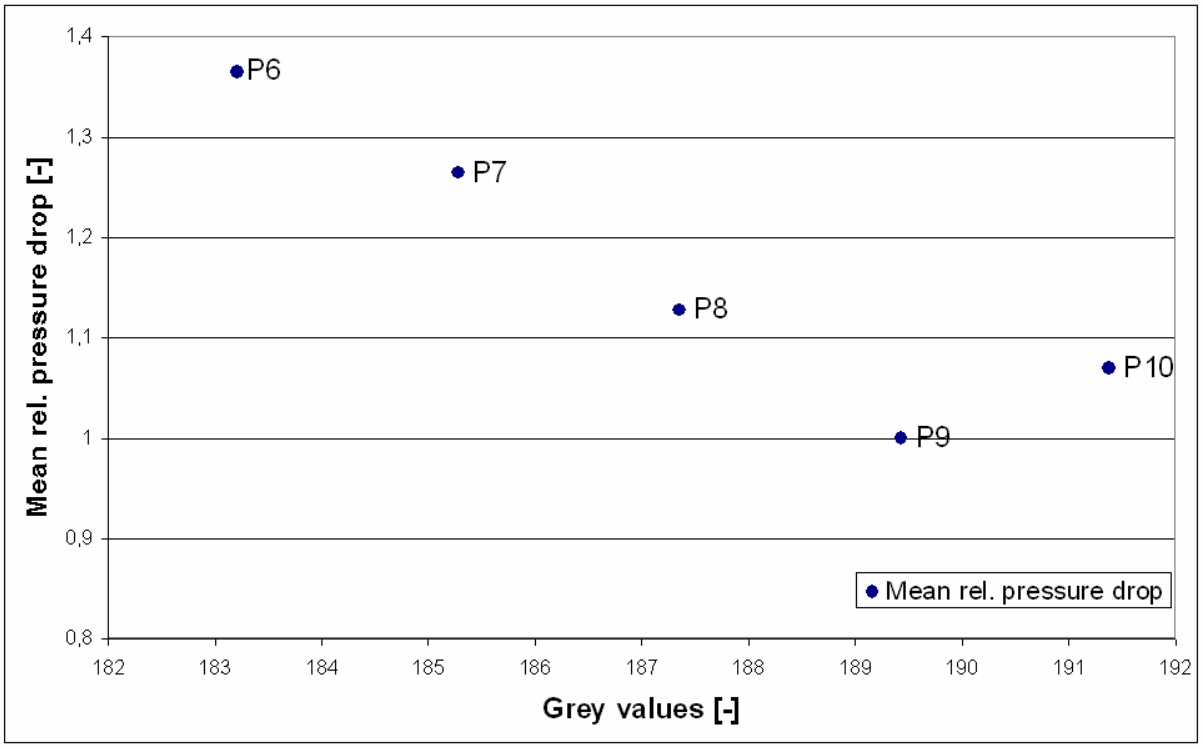

Figure 3.15: Relative pressure drop vs. grey values of filter *A43 Fulda*.

A certain trend can be seen, that with increasing grey values the pressure drop decreases. The only exception to the rule is the result of sample *P10*, where the pressure drop is slightly higher compared to sample *P9* although the grey value is higher as well. A thorough evaluation of the collected evidence leads to the conclusion, that this “trend-breaker” can be attributed to experimental error. A straight relation between pressure drop and local grey value is hereby considered to be proven. This is underlined by a methodical statistical *two way factorial* analysis, described in the next subchapter.

3.5.1.1.2 Statistical Evaluation

The experimental data of the high and low grey value pressure drop of the *A43 Fulda* filter was assessed with a statistical *two way factorial design* according to Box et. al. (1978, p. 228-231). In a *two way factorial design* two kinds of effects are considered: those of the *treatments*, and those of the *blocks*. In this case the blocks are essentially treatments as well. Both factors are of equal interest, and it will be assessed if theses factors have an influence on the results, or if the observed outcome can be contributed to statistical deviation. Furthermore, the *two way factorial design* provides the option to evaluate the possibility that these factors interact. Table 3.1 shows the basic setup of a *two way factorial design*.

Table 3.1: Results from randomized block design, general case (Box et. al., 1978, p.210)

		treatment						block
		1	2	···	t	···	k	average
block	1	y_{11}	y_{21}	···	y_{t1}	···	y_{k1}	
	2	y_{12}	y_{22}	···	y_{t2}	···	y_{k2}	
	⋮	⋮	⋮		⋮		⋮	⋮
	i	y_{1i}	y_{2i}	···	y_{ti}	···	y_{ki}	$\bar{y}_i$
	⋮	⋮	⋮		⋮		⋮	⋮
	n	y_{1n}	y_{2n}	···	y_{tn}	···	y_{kn}	
treatment average				···	$\bar{y}_t$	···		$\bar{y}$ = grand average

In this *two way factorial design n* levels of the block factor *FV* (*n* = 4 different flow velocities), *k* levels of the treatment factor *GV* (*k* = 2 different grey values), and *r* replications (*r* = 5 pressured drop values per group) are evaluated. The corresponding sums of squares, S_{FV} for factor *FV*, S_{GV} for factor *GV*, S_I for the interaction between *FV* and *GV*, S_e for error, and *SoS* for total, are given by the formulas according to Box et. al. (1978, p. 231)

$$S_{FV} = rk\sum_i (\bar{y}_i - \bar{y})^2 \qquad (3.1)$$

$$S_{GV} = rn\sum_t (\bar{y}_t - \bar{y})^2 \qquad (3.2)$$

$$S_I = r\sum_t \sum_i (\bar{y}_{ti} - \bar{y}_t - \bar{y_i} + \bar{y})^2 \qquad (3.3)$$

$$S_e = \sum_t \sum_i \sum_j (y_{tij} - \bar{y}_{ti})^2 \qquad (3.4)$$

$$SoS = \sum_t \sum_i \sum_j (y_{tij} - \bar{y})^2 \qquad (3.5)$$

wherein $\bar{y_i}$ is the block average, $\bar{y_t}$ is the treatment average, $\bar{y_{tij}}$ refers to the j^{th} element in the i^{th} block and t^{th} treatment and $\bar{y}$ is the grand average. Table 3.1 shows the nomenclature for a *two way factorial design*. In this case every block and treatment consists of five different measurement values. The results of this evaluation are summed up in the table 3.2 and 3.3.

Table 3.2: Two way factorial design. Test of parameter influence on pressure drop. Part 1

Flow velocity [m/s] and grey values - A43

Samples	low grey values		high grey values		**Mv:**
V [m/s]	SoSInteraction:		SoSInteraction:		
	0,000910		0,001792		
0,006	Residual:		Residual:		**0,171**
	0,00000	**0,18**	0,00002	**0,15**	
	0,00000	**0,18**	0,00004	**0,16**	
	0,00006	**0,19**	0,00002	**0,15**	
	0,00000	**0,18**	0,00004	**0,16**	
	0,00000	**0,18**	0,00002	**0,15**	
	SoSResidual:		SoSResidual:		
	0,00008		**0,00012**		
	Mgroup:	**0,18**	**Mgroup:**	**0,15**	
0,012	SoSInteraction:		SoSInteraction:		**0,376**
	0,000078		0,000136		
	Residual:		Residual:		
	0,00000	**0,41**	0,00032	**0,31**	
	0,00014	**0,42**	0,00014	**0,34**	
	0,00014	**0,42**	0,00006	**0,32**	
	0,00006	**0,40**	0,00014	**0,34**	
	0,00032	**0,39**	0,00000	**0,33**	
	SoSResidual:		SoSResidual:		
	0,00068		**0,00068**		
	Mgroup:	**0,41**	**Mgroup:**	**0,33**	
0,019	SoSInteraction:		SoSInteraction:		**0,594**
	0,000125		0,000205		
	Residual:		Residual:		
	0,00020	**0,66**	0,00090	**0,49**	
	0,00020	**0,66**	0,00040	**0,54**	
	0,00020	**0,66**	0,00010	**0,51**	
	0,00026	**0,63**	0,00040	**0,54**	
	0,00068	**0,62**	0,00000	**0,52**	
	SoSResidual:		SoSResidual:		
	0,00152		**0,00180**		
	Mgroup:	**0,65**	**Mgroup:**	**0,52**	
0,026	SoSInteraction:		SoSInteraction:		**0,799**
	0,000775		0,001573		
	Residual:		Residual:		
	0,00048	**0,89**	0,00090	**0,67**	
	0,00048	**0,89**	0,00090	**0,73**	
	0,00048	**0,89**	0,00040	**0,68**	
	0,00078	**0,84**	0,00040	**0,72**	
	0,00144	**0,83**	0,00000	**0,70**	
	SoSResidual:		SoSResidual:		
	0,00368		**0,00260**		
	Mgroup:	**0,87**	**Mgroup:**	**0,70**	
	Mgv:	**0,53**	**Mgv:**	**0,43**	
Mov=0,48					

Table 3.3: Two way factorial design. Test of parameter influence on pressure drop. Part 2

	Decomposition of Variance Table:						
	Sum of Squares	**Degrees of freedom**	**Mean Square**	**Ratio of Mean Squares**	Distr.:	**Significance**	
Grey value effect:	S_{GV} = 4,6278	k – 1 = 1	4,6278	**13269,57**	**F1,32**	**100,00**	%
***FV* effect:**	S_{FV} = 2,1284	n – 1 = 3	0,7095	**2034,32**	**F3,32**	**100,00**	%
Interaction effect:	S_I = 0,0272	(n-1)(k-1) = 3	0,0091	**26,00**	**F3,32**	**100,00**	%
Model error:	S_e = 0,0112	nk(r-1)=32	0,000349				
Total:	*SoS* = 6,7945	*nkr-1* = 39					

The following list explains the abbreviations used in table 3.2:

- Mgroup: Mean pressure drop of a group. One flow velocity and one grey value.
- Mgv: Mean pressure drop of a certain grey value at all flow velocities
- Mov: Mean pressure drop of all individual pressure values
- Mv: Mean pressure drop at a certain flow velocity of all grey values
- SoSInteraction: Sum of Squares Interaction
- Residual: Quadratic difference between Mgroup and individual values
  $Residual = (x_i - Mgroup)^2$
- SoSResidual: Sum of Squares Residual $SoS\,Residual = \sum_{i=1}^{n} Residual$

The following list explains the abbreviations used in table 3.3:

- The *sum of squares* can be calculated with equations 3.1 to 3.5.
- The *mean square value* is calculated as the fraction between the *sum of squares* and the *degrees of freedom*.
- The *ratio of mean squares* is the fraction between the *mean square value* of the effects and the *mean square value* of the model error.
- This value is then compared to the F-distribution at a certain significance.

The tested parameters for this two way factorial design are:

- Grey value effect
- Flow velocity (*FV* effect)
- Interaction effect between grey values and flow velocity effect

In this case the outcome is quite remarkable. The influence of the flow velocity on the pressure drop is calculated to be significant with a probability level of 100,00%. This is obvious, does not need further attention and can serve as a plausibility check for the outcome. The interesting thing is that the grey values also have a highly significant effect on the pressure drop. The probability level is calculated to be 100,00%. The two columns in table 3.2 refer to the following data:

- low grey values → selected samples with the *translucency examination* and low grey values; *A43 Fulda*
- high grey values → selected samples with *translucency examination* and high grey values; *A43 Fulda*

The samples with low and high grey values are originated from one and the same filter sheet of the type *A43 Fulda*. The statistical evaluation confirms with an evident certainty that the mean pressure drop values, from samples with low grey values, differ significantly from the mean pressure drop values, from samples with high grey values. The notable probability of 100,00% can be attributed to the high number of samples used for the statistical evaluation. This fact can also be taken as evidence that the “trend-breaker” in figure 3.15 is caused by a measurement error.

Another remarkable outcome is that the interaction effect between the flow velocity and the grey values has a probability of 100,00%. When figure 6.3 is considered this interaction can be seen. The higher the flow velocity, the higher the differences between the pressure drop of low and high grey value samples.

3.5.1.2 Deviation of the Pressure Drop

The computer algorithm does not only calculate the mean grey value of the samples, but also the deviation of the grey values within these samples. This deviation will be called *inner deviation*.

An assumption was that the inner deviation may have an effect on the deviation of the measurement results of the pressure drop. The higher the inner deviation, the more inhomogeneous the sample is. The samples of the filter medium *A43 Fulda* have a higher inner deviation compared to the filter medium *A55 Ahlstrom* and *Ti99*. Therefore, it seemed

reasonable that the deviation of the pressure drop of the *A43 Fulda* would be higher too. In figure 3.16 the mean value of the deviation of the pressure drop of the higher and lower grey values is plotted over the mean value of the inner deviation. Both values are related to their mean value and multiplied by a factor of 100, in order to get a percentage. The numbers in the diagram refer to the current grey value. The results in this figure show no definite connection between the pressure drop deviation and the inner grey value deviation.

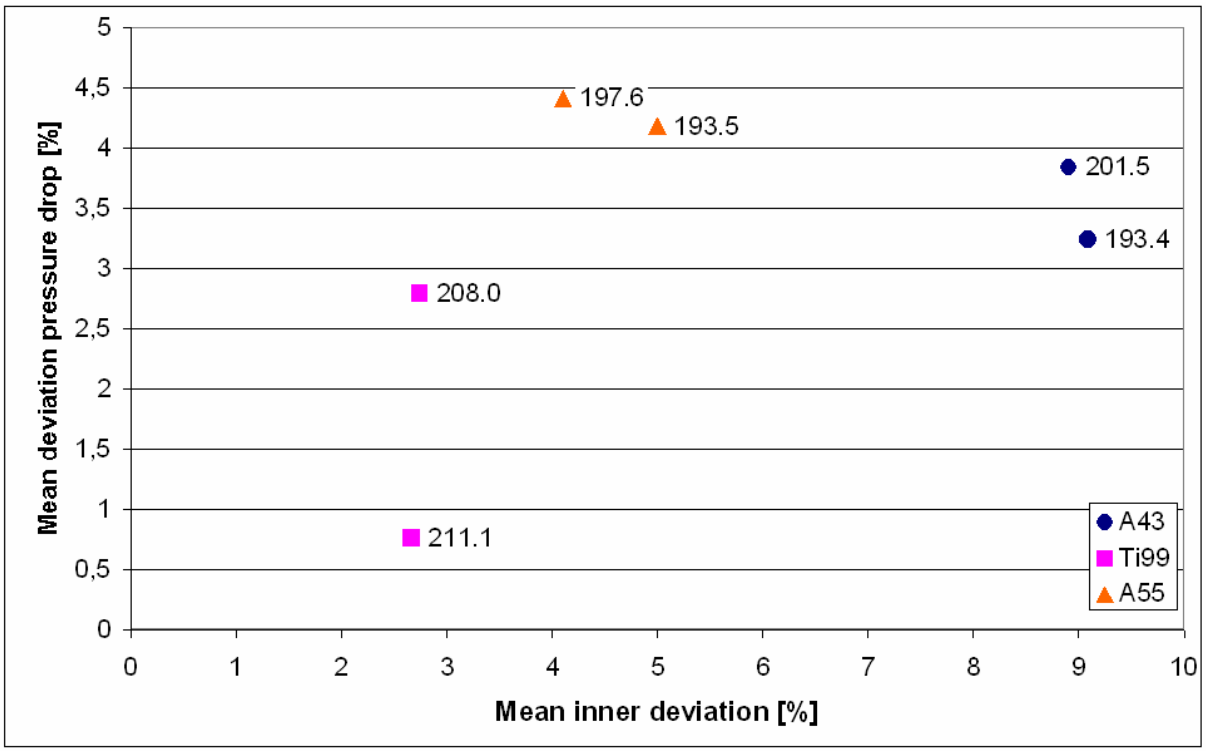

Figure 3.16: Comparison between the deviation of the pressure drop and the inner deviation

In figure 3.17 the deviation of the experimental data is plotted against the flow velocity. The value on the y-axis is the deviation divided by the mean value times 100. It is equal to a relative deviation in percent. In the *worst case* scenario each filter sample has a different grey value, ranging from the lowest to the highest possible value. In figure 3.17 four curves are plotted. The relative deviation of the experimental data of the *worst case* scenario is the highest, and ranges between 12% and 14%. The samples which are taken randomly have a deviation of about 6%. The samples, chosen with the help of the translucency examination, have the smallest relative deviation in the range of 3 to 4%.

Before this work it was state of the art in the laboratory at the ICE Strömungsforschung GmbH to choose the samples arbitrarily. With the help of the *translucency examination* it is now possible to decrease the deviation under 4%, which is an astonishing outcome. Thus, it will be sufficient to test smaller sample quantities, with the same result. This proceeding will reduce the time for experiments dramatically.

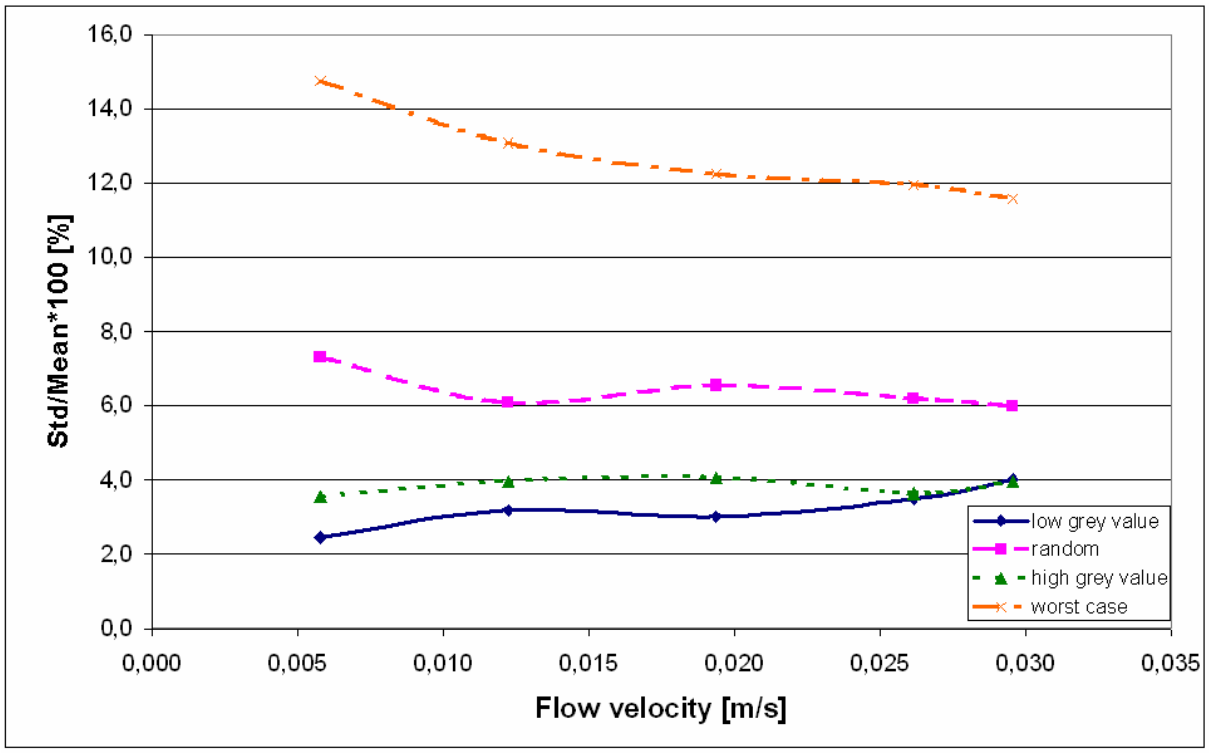

Figure 3.17: Comparison between the deviations of the experimental data of the filter type *A43 Fulda*

3.5.1.3 Conclusion

A direct correlation between the grey values of filter samples and the pressure drop is found, and confirmed with well established methods of statistical evaluation. As the grey values have an influence on the pressure drop, the results of the experiments depend on the position on the filter sheet where the samples are taken. The functioning of the *translucency examination* is proven by several experiments with different filter fibre materials. In addition to that, the deviation of the measurement results can be decreased by 30% with the help of the *translucency examination*, compared to the ordinary method which was used to choose samples.

What is not yet possible with the *translucency examination* is a direct prediction of the pressure drop, when the grey values of the samples are known. The simple reason for this is that the grey values depend very strongly on the background light and on the settings of the camera. What can be said is, that samples with higher grey values have a lower pressure drop and vice versa. In the same way, it is not possible to compare the grey values of different filter media with one another. An example is the comparison between the filter materials *Ti99* and *A43 Fulda*. The *Ti99* has higher grey values than the *A43 Fulda*, but the pressure drop of the filter *Ti99* is distinctly higher. This is due to the fact that its filter material has a brighter white than the *A43 Fulda*, and therefore has a higher basic grey value.

One problem which has to be pointed out, is the fact that it is only possible to compare samples of the same filter sheet. Even the standardization of the photographs of different filter sheets of the same material, with the help of a reference adjustment, failed to be sufficient. The results of different sheet samples are not yet comparable with each other because of background light effects and unstable camera settings. One thing which can be tried in the future, is to make five individual photographs of each filter sheet, and take the mean value of the results. This procedure is likely to be more effective than the standardization.

Another problem is that the manufacturer uses different types of coloured stripes, in order to help distinguish between diverse filter media. These coloured stripes have an influence on the grey value distribution of the whole filter sheet, and make the task of obtaining valid results more difficult.

3.5.2 Permeability

This subchapter describes another significant finding accomplished within this thesis. It refers to the permeability of filter materials. Mataln et. al. (2007) describe the fluid-structure interaction of deformable filter media in the context of filtration processes. The assumption is that the permeability of filter media changes at relevant flow velocities due to deformation of the filter structure.

3.5.2.1 Proof of Relevant Filter Fibre Deformability

Schnitzer and Ripperger (2007, p.228) describe the Darcy equation 3.6 as a potential model, especially for filter materials with small, branched out pores, that relates the pressure drop Δp to the flow velocity v_F.

$$\Delta p = \frac{\eta_f \cdot s}{K_D \cdot A_f} \cdot \dot{V} = \frac{\eta_f \cdot s}{K_D} v_F \qquad (3.6)$$

V is the flow rate, A_f corresponds to the cross section of the filter, s is the thickness of the filter, η_f is the viscosity of the fluid and K_D is the permeability of the filter. Substituting the fraction, s divided by K_D, by the thickness-related permeability K_D' and rearranging the equation 3.6 yields:

$$K_D' = \frac{\eta_f}{\Delta p} v_F \qquad (3.7)$$

The flow velocity v_f and the pressure drop Δp can be obtained by measurement. The viscosity η_f for paraffin oil is 160 mPas. Equation 3.7 gives the opportunity to calculate the

thickness-related permeability K_D' which is supposed to be constant for all relevant flow velocities.

In figure 3.18 the thickness-related permeability K_D', determined by equation 3.7, is plotted against the flow velocity v_f. The thickness-related permeability of the filter medium *A43 Fulda* is constant for all examined flow velocities. The *A55 Ahlstrom* shows a slight change in the thickness-related permeability. The comparison between the lowest and highest flow velocity shows a difference of roughly 7%. The highest change in the thickness-related permeability can be observed in the *Ti99,* with 20% difference between the lowest and highest flow velocity.

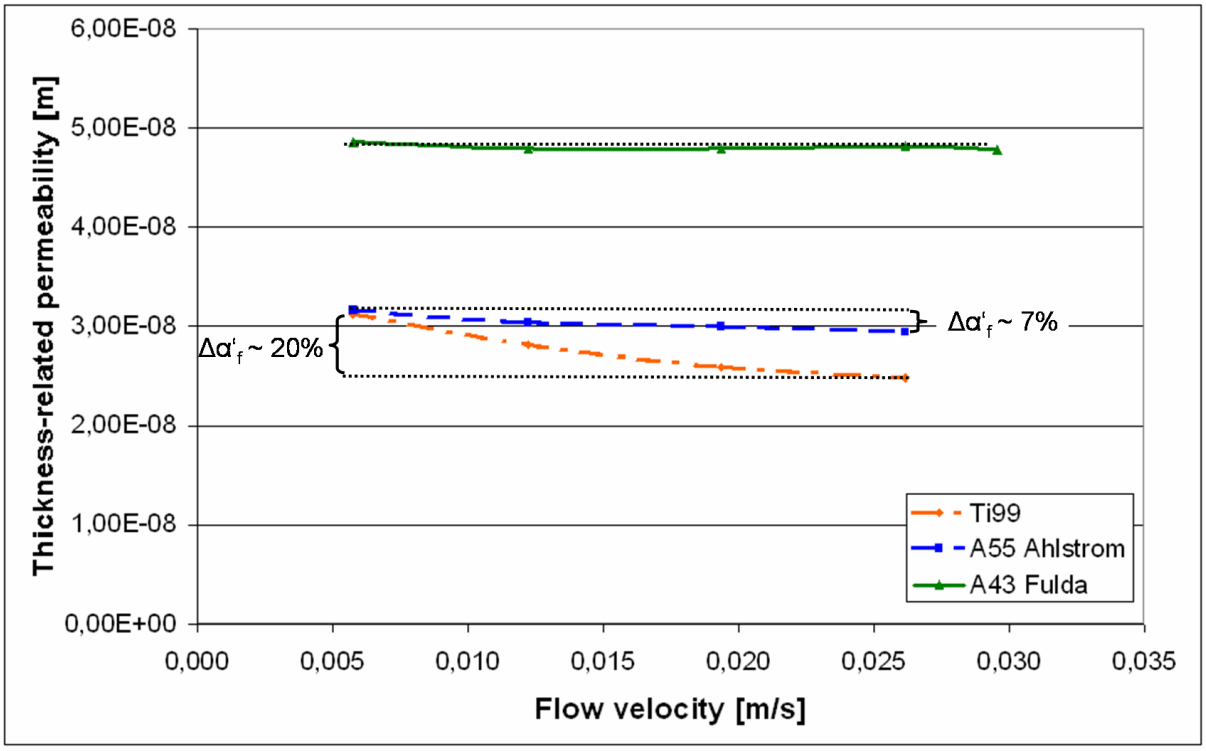

Figure 3.18: Dependence of the permeability on the flow velocity

Through a comparison between the Darcy equation and the equivalent model of the Hagen-Poiseuille equation Schnitzer and Ripperger (2007, p. 228) derive the following relation for the permeability K_D:

$$K_D = \frac{\varepsilon^3}{2 \cdot \mu \cdot (1-\varepsilon)^2 \cdot S_v^2} \qquad (3.8)$$

wherein ε is the mean porosity of the filter medium, S_v is the specific surface of the filter related to the volume of the fibres and μ is a correction factor for the model that takes the detour into account, which the fluid has to make in order to pass the fibres.

The change in the permeability plotted in figure 3.18 can be interpreted, considering equation 3.8, as follows: As the specific surface S_v of the filter is constant, the porosity ε has to change in order to explain the differences in permeability of the same filter medium at different flow velocities. Due to deformation of the filter material the porosity ε of the filter medium decreases, and therefore also the permeability declines. Glass fibre filters like *Ti99* are structurally weaker compared to polymer based filters like *A55 Ahlstrom* or *A43 Fulda*. These types of filters are more stable, which can be observed in figure 3.18 where their permeability is constant or changes only slightly.

In figure 3.19 the filter of the type *A43 Fulda* has a linear connection between the pressure drop and the flow velocity. The *A55 Ahlstrom* filter shows a slight non-linear behaviour at higher flow velocities. The *Ti99* has the highest non-linear manner. This fact can be explained considering the structure of the filter medium. While the *A43 Fulda* and the *A55 Ahlstrom* have a rather high stability, the *Ti99*, which is a glass fibre fleece, can be deformed relatively easy. For this reason, the deformation of the *Ti99* filter is higher, at higher flow velocities, and the pores will change their size due to the forces acting on the filter.

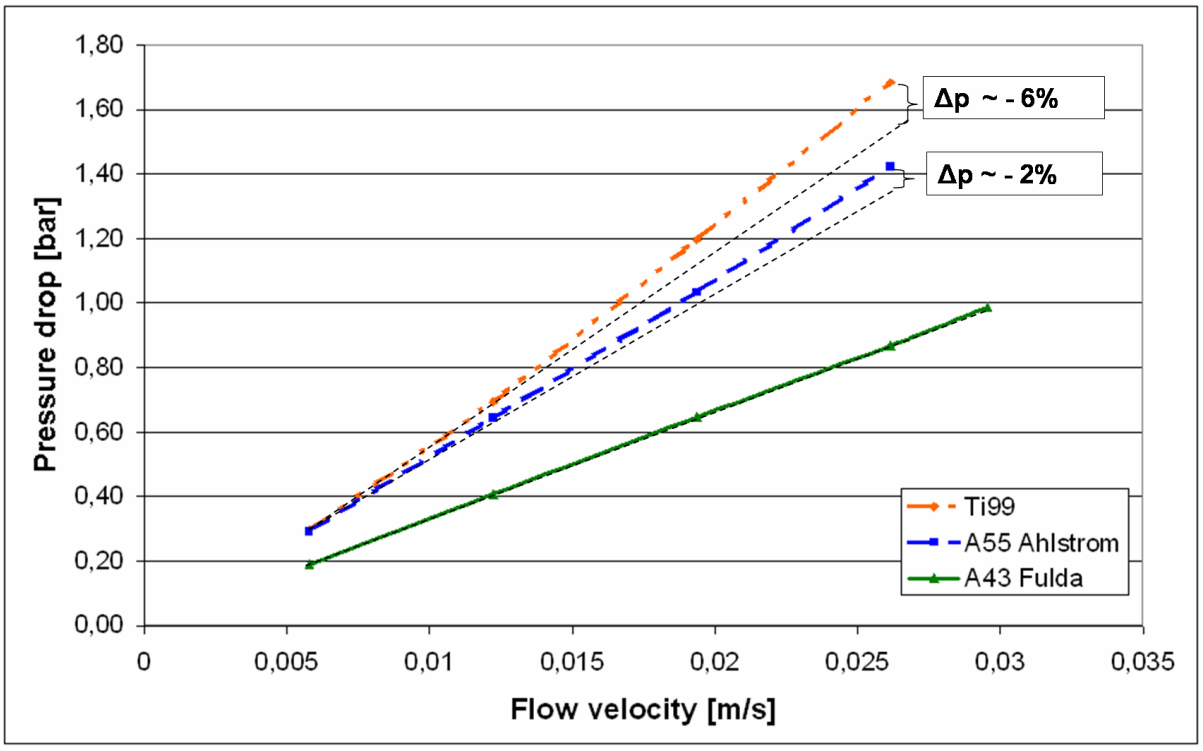

Figure 3.19: Influence on the permeability of different filter materials

3.5.2.2 Conclusion

The assessment of the experimental data, in connection with the Darcy equation, leads to the conclusion that the flow velocity has an influence on the permeability. The non-linear behaviour of the pressure drop of some filter materials can be explained by the fact of the changed permeability. This is a very important finding for filter fibre design. It points to the fact that the MFP value (mean flow pore size) changes relevantly with the flow velocity due to deformation of the filter fibre structure. Materials with lower stiffness are more prone to that effect than others, as the comparison between the *A43 Fulda* and the *Ti99* glass fibre fleece is an evidence for this conclusion.

3.6 Applicability and Outlook

The *translucency examination*, presented in this chapter, is an entirely new tool which will probably improve the quality of filter testing methods. A dependence between the grey values and the pressure drop was found, as well as the fact that the deviation of the experimental results is significantly lower. There are two main different areas of application for this innovative process.

- The application in the daily laboratory use. The deviation of the experimental results can be decreased. Therefore, the amount of work involved can be reduced because the samples, chosen with the *translucency examination*, are likely to be more representative. Thus, fewer samples are needed to achieve equivalent statistical significance. On the other hand, it is possible to determine the highest and lowest possible pressure drop of one filter material, which is also an interesting parameter. To sum up, the *translucency examination*, used as a preparation for the actual filter testing, is a powerful tool to increase the accuracy of the measurement method and, decrease the working time.

- It can be used as a starting point in simulation techniques. A simulation software, developed by Boiger and Mataln (2009), is capable of dealing with the assessment of filter materials. Pressure drop, flow field and the deposition of particles in a real fibre geometry can be calculated. The innovation and basis for this algorithm is the implementation of a real fibre geometry, which is a photograph obtained with the help of computer tomography of the original filter medium. The problem is that the investigated areas of the filter sample are in the range of 200x200µm, which is a reasonable compromise between benefits and computational effort. A justified objection to the results of this simulation is that the investigated area is too small to be representative. This problem can be solved with the help of the *translucency examination* because the filter area, where a photograph should be taken, can be determined beforehand, which ensures that representative sample positions are selected.

In order to simplify the handling of this method, it will be reasonable to alter the assembly of the camera and the tripod, by replacing the tripod with a fixture for the camera on the overhead projector. This ensures that the camera arrangement, and also the detail of the photograph, is constant for all measurements. If the filter sheet is placed on the same position on the overhead projector every time, which can be established by using marks on the overhead projector, the control of the computer algorithm can be made simpler. Usually the user has to select the area of the picture where the filter is located. This is described in more detail in chapter 5. If, due to the steady camera arrangement, the position of the filter is constant in each photograph, a default value can be defined, so that the same picture area is evaluated every time.

Furthermore, an arrangement with a cloth that covers the overhead projector and the camera will improve the measurement method. This assembly will ensure that no unwanted background light in the laboratory will influence the picture quality, so that the grey values will be representative for the filter sample. If this assumption can be proven to be true in further experiments, it should be possible to assess filter sheets only by means of their grey values. The only thing which has to be done is to examine a filter sheet of a certain type once, and evaluate the pressure drop in dependence on the grey values. All other filter samples of the same type can then be assessed only by the *translucency examination*. If the grey values are in a determined range the quality of the filter sheet will be sufficient for the particular purpose.

In summary, the *translucency examination* is a procedure which can be used to improve the measurement techniques in filter testing. The relatively low acquisition cost for the overhead projector and the camera are incentives and a definite advantage of this method. Moreover, the handling is uncomplicated and does not required special training. Fast results can be obtained, and a simple incorporation in standardized laboratory procedures is possible.

4 Particle Penetration Depth

This chapter sums up the development process of a method capable of estimating the particle penetration depth in non-woven filter materials.

One important characteristic of filter materials is the filtration efficiency. It represents the percentage of separated particles with different diameters in a filter material. The tests for filtration efficiency are rather complicated and time consuming. The filter is considered a black box. This means that the qualitative aspects of particle deposition are not considered to be as important as the quantitative mass balance between inlet and outlet. This approach is sufficient for several applications, but especially producers of filter media are concerned with deposition mechanisms within filter materials.

Wang (2001, p. 166) describes the deposition of particles in filters as follows. When a particle moves towards the filter fibres, many different forces act on it. It will leave the streamline of the fluid, which it originally followed, mainly due to Brownian motion, caused by thermal forces, and particle inertia. When the distance between the particle and the fibre becomes less than the particle radius, it deposits on the surface of the fibre. Whether the thermal forces or the particle inertia are the main reason for the deposition depends mainly on the particle diameter, the gas velocity and the fibre diameter. Particles with a diameter larger than 1 µm are deposited for the most part due to particle inertia, whereas Brownian motion plays a greater role for particles smaller than 0.1 µm. Another type of forces, contributing to the deposition, are electrostatic forces, especially for even smaller particles because both, particle inertia and thermal forces are relatively weak, due to small particle diameters.

A simulation software developed by Boiger and Mataln (2009) is able to determine the flow, the pressure drop and the particle deposition in a real fibre geometry. The distribution of particles with different diameters in the filter can be estimated. Before this work, there was no opportunity to compare the results of the simulation with experimental data.

Klauth et. al. (2007, p. 119) use a fluorescent macrophotography in combination with digital image analysis to visualise the concentration distribution of fluorescent microspheres in porous media slices. They achieve good results, and describe the fluorescent macro-photography as a fast and reliable method that delivers same results as established microscopic methods. One weakness of this method is that it is destructive. Klauth et. al. (2007, p. 119-122) reconstruct spatial distributions of the colloid particles by investigating different slices of a soil column. This is not appropriate for filter materials, but the application of macrophotography in connection with fluorescent particles can be used as a verification of the simulation results.

4.1 Basic Principle and Theoretical Background

To estimate the particle penetration depth in a filter material, fluorescent particles are used. The particles are obtained from microparticles GesmbH (Berlin). To acquire the pictures of the deposited particles in a loaded filter an assembly of a camera, a drive set and a laser is used. The settings of the camera are chosen in a way that the depth of field is as low as possible. Therefore, different layers of the filter and thus different particles are in the focus plane, while all the others are blurred. A program developed by Boiger (2009, p. 221-225) uses techniques, based upon multi-focus image fusion, to evaluate focused picture areas. These focused particles are then reconstructed in a 3-D distribution.

4.1.1 Fluorescent Particles, PIV Camera, Laser

During the progress of this method monodisperse fluorescent particles (Rhodamine B PMMA) with three different diameters were used. They have a size of 19.78 ± 0.18 µm, 41.12 ± 0.76 µm and 61.35 ± 1.42 µm. It is necessary that the particles fluoresce at a wave length of 532 nm, produced by the used New Wave Research laser. The camera, used to take the pictures, is ordinarily applied to particle image velocity (PIV). According to LaVision (2002, p. 129) it is recommended to use a 532 nm bandpass filter in order to suppress background light. The filter can be mounted on the regular camera lens. The camera contains a sensitive charge coupled device (CCD) chip which is capable of detecting very low intensity light signals and processing them very fast. Figure 4.1 shows a simplified model of one pixel of the CCD chip.

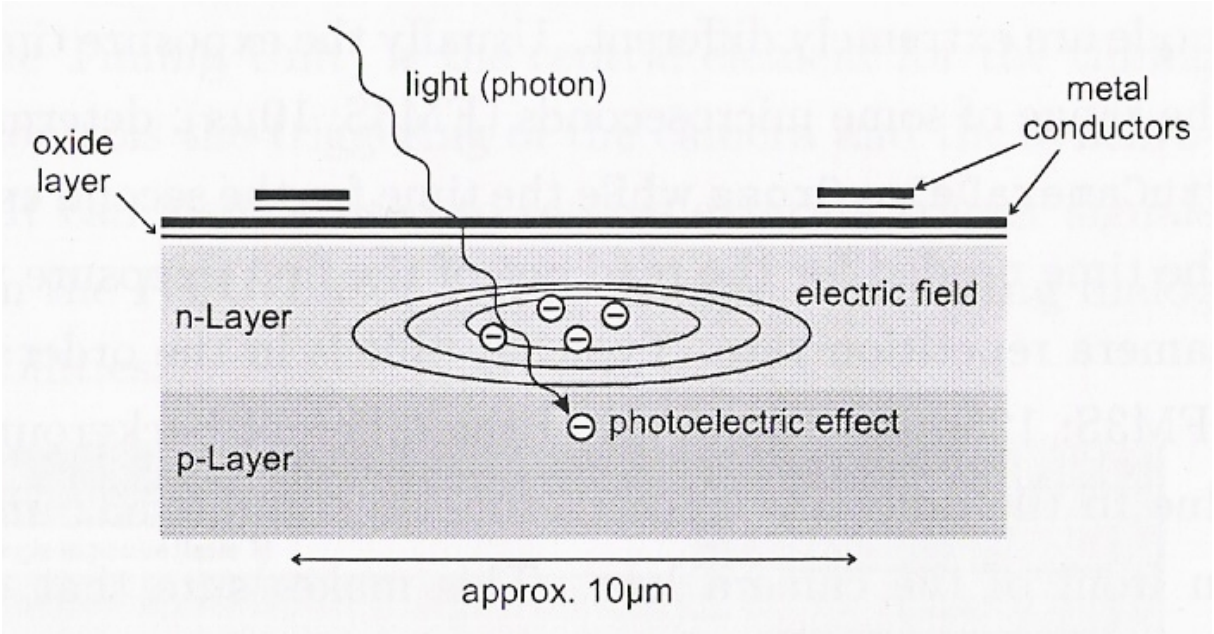

Figure 4.1: Simplified model of a pixel (LaVision, 2002, p.113)

LaVision (2002, p.113) describes the function of the CCD chip as follows. Photons, reaching the chip, are converted to electric charges, based on the photoelectric effect. The solid state sensor contains an array of pixels (picture elements). Each pixel consists of a semiconducting substrate with a p-layer (cathode) and an n-layer (anode) with an insulating oxide layer and metal conductors on the surface. A small applied voltage generates an electric field in the semiconductor. A photon produces an electron-hole pair in the p-n-junction, and the electrons migrate towards the minimum electric field. Here the electrons are accumulated during the exposure time.

The laser used for the measurement is an Nd:YAG laser. Every laser comprises three main components: a laser material, a pump source and an oscillator. In this case the laser material is a crystal where Nd^{3+} ions are incorporated in YAG (yttrium-aluminium-garnet), the pump usually is a krypton flashlamp or a smaller semiconductor laser and the resonator is a set of high reflective mirrors. (LaVision, 2002, p.15) Figure 4.2 shows the components of the laser.

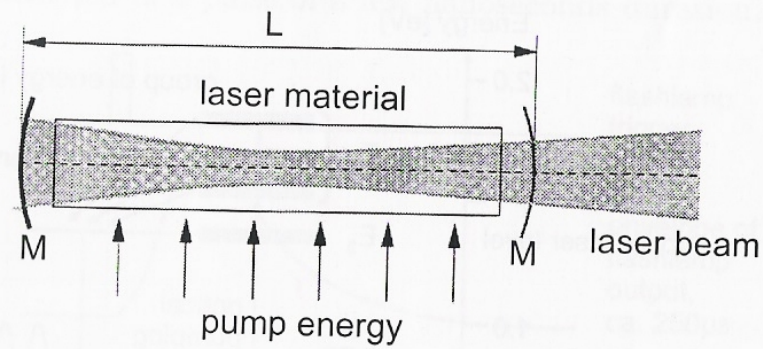

Figure 4.2: Components of a laser (LaVision, 2002, p.15)

The laser beam diameter is ordinarily very small. In order to get a sufficiently large beam, which can illuminate the whole filter sample, a set of lenses is used. The basic assembly is shown in figure 4.3.

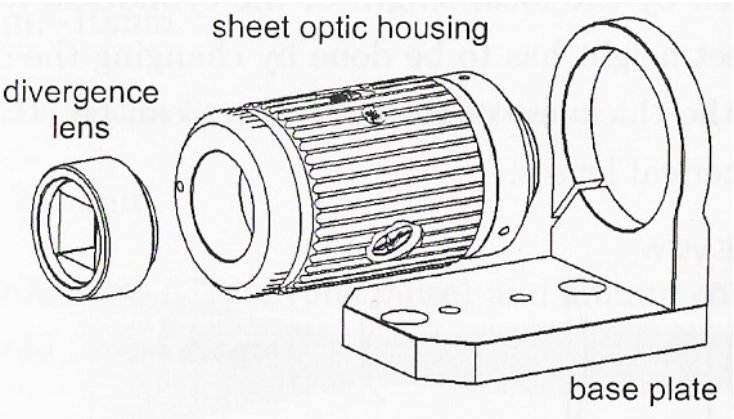

Figure 4.3: Sheet optics on base plate (LaVision, 2002, p.29)

The regular lens configuration is used to produce a light sheet (LaVision, 2002, p.30). For the particle penetration depth the position of the laser and the divergence lens are adapted to get a steady illumination of the filter sample.

Figure 4.4 shows a comparison between the pictures of a loaded filter with background light (left) and laser light (right).

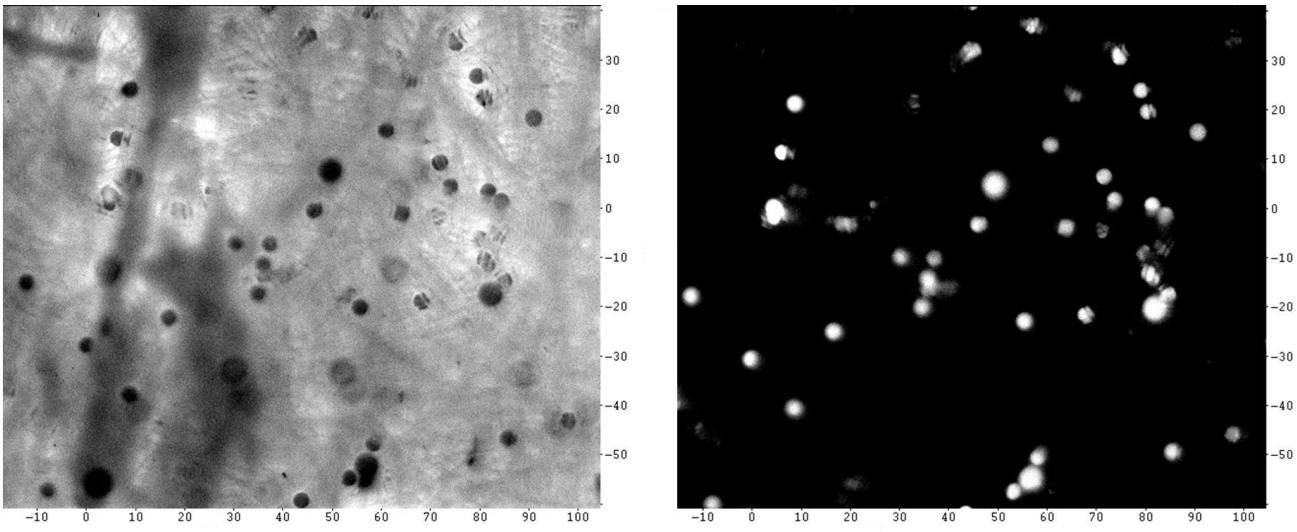

Figure 4.4: Comparison between loaded filter with background and laser light

It is possible to obtain pictures with the position of the particles, but without the filter fibre geometry.

4.1.2 Depth of Field

Many photographs contain objects at varying distances to the camera. The distribution of the sharpness in such a photograph depends on various factors. The object focused by the camera and the objects near to that appear to be the sharpest ones. Other objects, which are behind or in front of the focused distance, lose sharpness gradually in the picture. This sharpness-loss is not significant within a certain distance which is called depth of field (DoF) of the camera. It depends on various factors, but the important ones in this case are the aperture used (decreasing the aperture will increase the DoF), the distance of the focused object (the nearer the object, the shorter the DoF) and the focal length (the longer the focal length, the shorter the DoF).

According to Conrad (2006, p.1) a camera can focus only on one plane. If the objects are points they will be imaged as a disk, if they are not in the focus plane. This disc, known as blur spot, is bigger when it is farther away from the focus plane. However, when the disc is small enough it cannot be distinguished from a point, and appears sharply on the

photograph. The diameter of such a blur spot, which still appears sharply, is known as the circle of confusion (COC) and equals *2R*.

Figure 4.5 illustrates the geometric optics of a symmetrical lens.

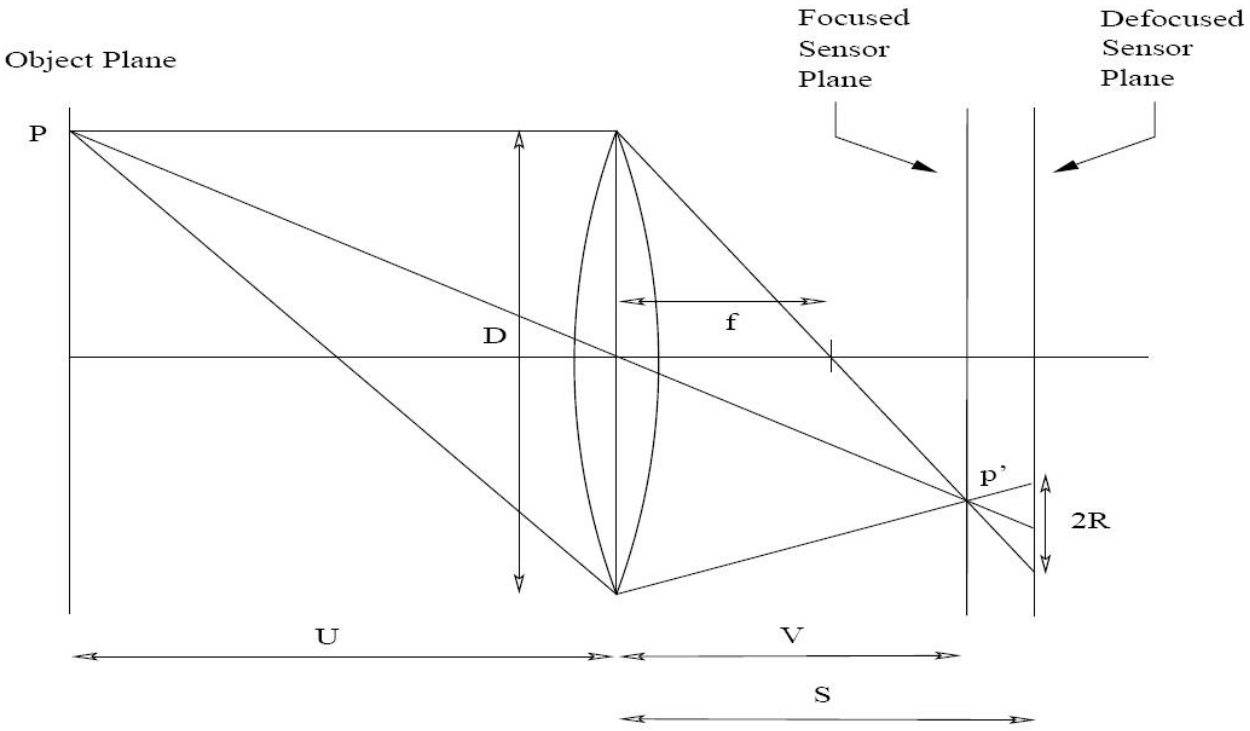

Figure 4.5: Geometrical model for symmetrical lenses (Eltoukhy and Kavusi, 2003, p. 334)

Eltoukhy and Kavusi (2003, p. 333) derive an equation which will allow to estimate the radius of the blur circle *R*. The problem is reduced to geometric optics which is basically only useful for analysis of first order effects. However, diffraction-related effects which can be determined by physical optics are not significant for this application because the spatial resolution of most sensor arrays is quite below the diffraction limit. In the case of the thin-lens geometrical model in figure 4.5, the point *P* at the distance *U* is focused as point *p'* on the image plane at *V*. The lens equation 4.1 relates the position of the two points, *U* and *V*, with the focal length *f* of the lens.

$$\frac{1}{f} = \frac{1}{U} + \frac{1}{V} \qquad (4.1)$$

Each lens possesses a finite aperture which is assumed to be circular, and the diameter is denoted *D*. The diameter of the aperture *D* is related to the f-number *N* by the reciprocal value of *D*:

$$N = \frac{f}{D}. \qquad (4.2)$$

With the f-number *N* the object lens can be adjusted. The actual distance of the sensor plane to the lens, *S*, will enable us to estimate the radius of the blur circle *R*. Similar triangles are used and the following equation is derived:

$$\frac{D}{V} = \frac{2R}{S-V} \tag{4.3}$$

R is expressed in terms of camera parameters using the lens equation:

$$R = \frac{1}{2}DS\left(\frac{1}{f} - \frac{1}{U} - \frac{1}{S}\right) \tag{4.4}$$

This relation demonstrates that the larger the aperture, the larger the blur circle engendered. Using the above relation for the blur circle, the depth of field is derived for a lens system, where *R* becomes the largest acceptable blur circle in the image. It depends on the sensor resolution and human visual acuity limits. Combining equation 4.3 with the lens equation 4.1 yields

$$U_{far} = \frac{Uf\left(1 - 2\frac{R}{D}\right)}{f - 2\frac{R}{D}U} \tag{4.5}$$

$$U_{near} = \frac{Uf\left(1 + 2\frac{R}{D}\right)}{f + 2\frac{R}{D}U} \tag{4.6}$$

$$DOF = U_{far} - U_{near} \tag{4.7}$$

Where U_{near}, U_{far} are the distances to the nearest and farthest object planes with blur circles less than or equal to the chosen *R* and *U* is the distance to the in-focus object plane. This means that U_{near} and U_{far} define the area where all objects are in focus.

Conrad (2006, p.5-6) substitutes the magnification *m*

$$m = \frac{V}{U} \tag{4.8}$$

into the given equations 4.5 and 4.6 rearranges them, and yields

$$U_{near} = \frac{U}{1 + \frac{N \cdot 2 \cdot R}{f \cdot m}} \qquad (4.9)$$

$$U_{far} = \frac{U}{1 - \frac{N \cdot 2 \cdot R}{f \cdot m}} \qquad (4.10)$$

In contrast to photography it is important to decrease the DoF to a minimum for this process. Equations 4.9 and 4.10 help to understand how the DoF can be influenced by the settings of the object lens. The f-number *N* stands in the denominator. When the f-number *N* is smaller the denominator in equation 4.9 is also smaller, and therefore the value for U_{near} is higher. Similarly, if the lens focal length *f* is higher, the denominator decreases, and U_{near} will become higher too. Because of the minus sign in the denominator in equation 4.10, the distance U_{far} decreases under the same conditions. Consequently, the DoF diminishes, which is illustrated in figure 4.6.

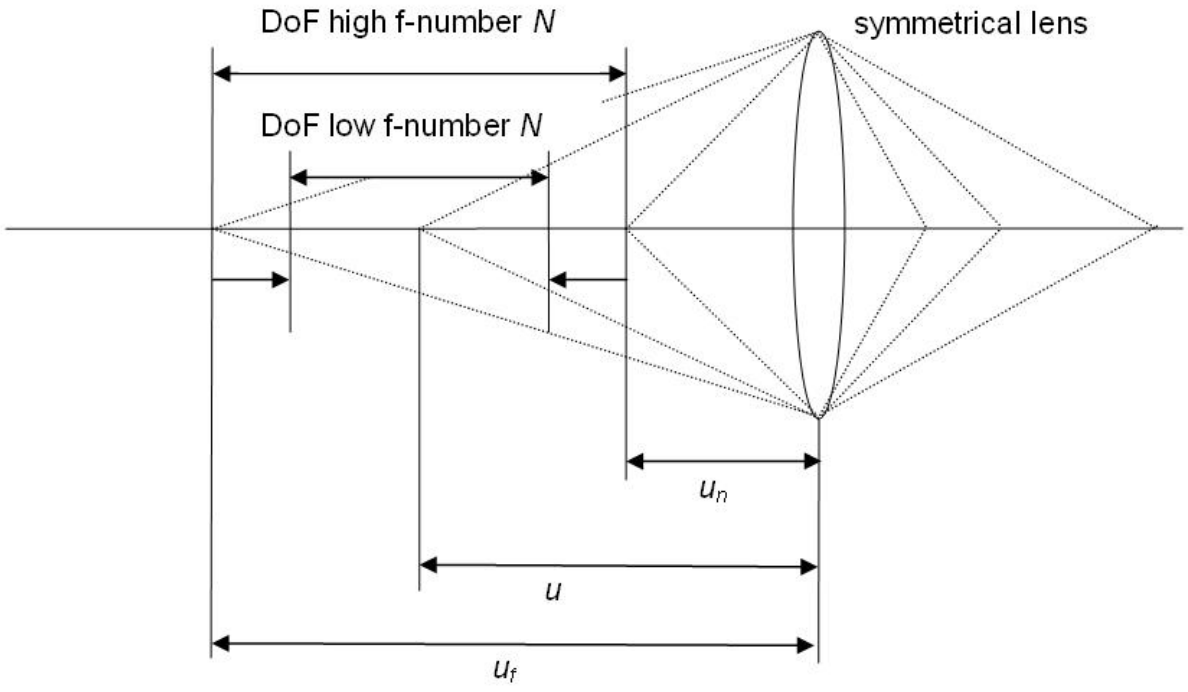

Figure 4.6: Connection between DoF and f-number *N*

These considerations lead to the certainty that in this case it is necessary to use a low f-number *N* and a high focal length *f*. It will also be useful to place the object as near as possible to the camera lens.

4.1.3 Image Fusion

According to Boiger (2009, p. 222-223) procedures also used for multi-focus image fusion are able to assign specific sharpness values to 2D objects, and combine differently sharp regions with each other. The focus measures used in this algorithm are Energy of Image Gradient (EOG) and Sum Modified Laplacian (SML). For further details see Maruthi and Sankarasubramanian (2007) and Huang and Jing (2007). Figure 4.7 demonstrates how the EOG highlights sharply depicted regions (high grey-scale gradient) and forfeits blurred ones (regions of smaller grey-scale gradient). In multi-focus image fusion the EOG is used to acquire one picture where all objects are sharply represented, out of several pictures where only some objects are focused. In this work, however, the EOG is merely used to distinguish sharp and blurred objects.

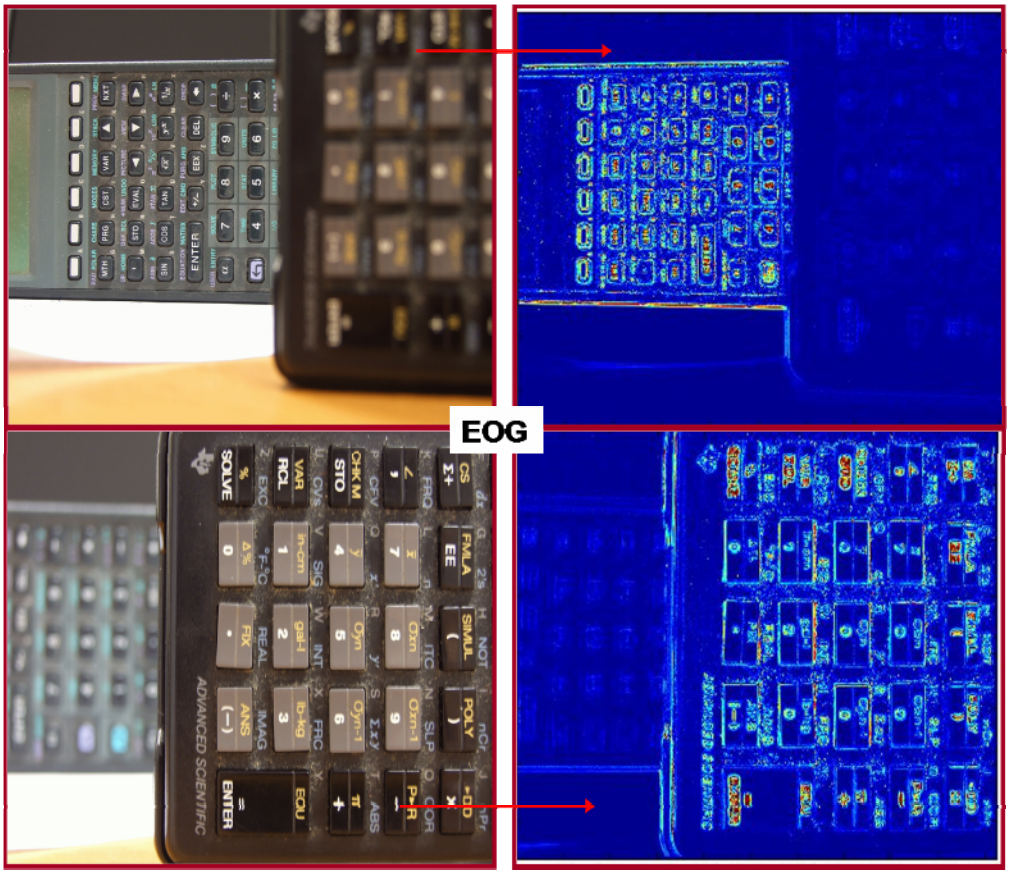

Figure 4.7: Example of the basic functionality of the EOG focus measure (Boiger, 2009, p.223)

4.2 Experimental Assembly

The evaluation of the particle penetration depth can be split up in four different working steps. Firstly, the determination of representative filter samples with the help of the *translucency examination*. Secondly, the loading of the filter sample with *PMMA Rhodamine*

B particles. Thirdly, the taking of the pictures with the *PIV camera* and the *laser*. And fourthly, the evaluation of the pictures with the multi-focus *image fusion* algorithm.

4.2.1 Determination of Representative Filter Samples

The filter samples are chosen with the *translucency examination*. Further details of the process itself can be obtained in chapter 3. A thorough working instruction is available in chapter 5.

4.2.2 Loading of the Filter Samples

In the experiment monodisperse fluorescent particles (Rhodamine B PMMA) with three different diameters are used (**19.78** ± 0.18 µm, **41.12** ± 0.76 µm and **61.35** ± 1.42 µm) .The assembly of the filter test circuit is the same as described in chapter 3. A detailed working instruction is offered in chapter 5.

4.2.3 Particle Detection Facility

The particle detection facility comprises three main components:

- Particle image velocity (PIV) camera with a CCD chip extended by an optical bellows (see figure 4.8).

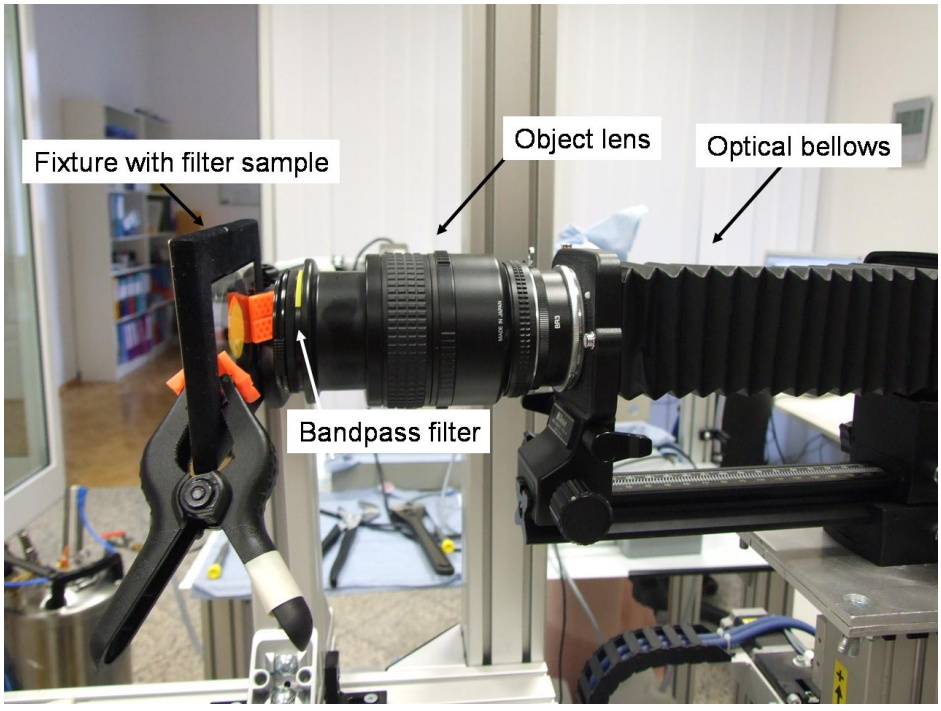

Figure 4.8: LaVision, Imager Intense. PIV camera with optical bellows.

- Laser: New Wave Research; Model: Solo III 15 Hz (see figure 4.9). Light frequency 532nm; Pulse length: 3 – 5 ns. Beam width: 3mm.

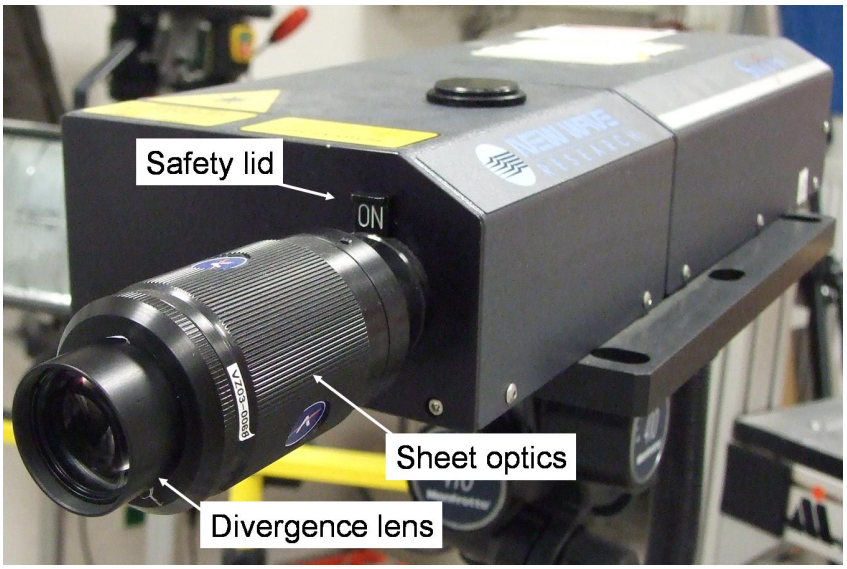

Figure 4.9: New Wave Research laser with divergence lens

- Drive set: Systec (see figure 4.10). Three degrees of motional freedom. Minimal step width: 10µm. Software: Motion Basic.

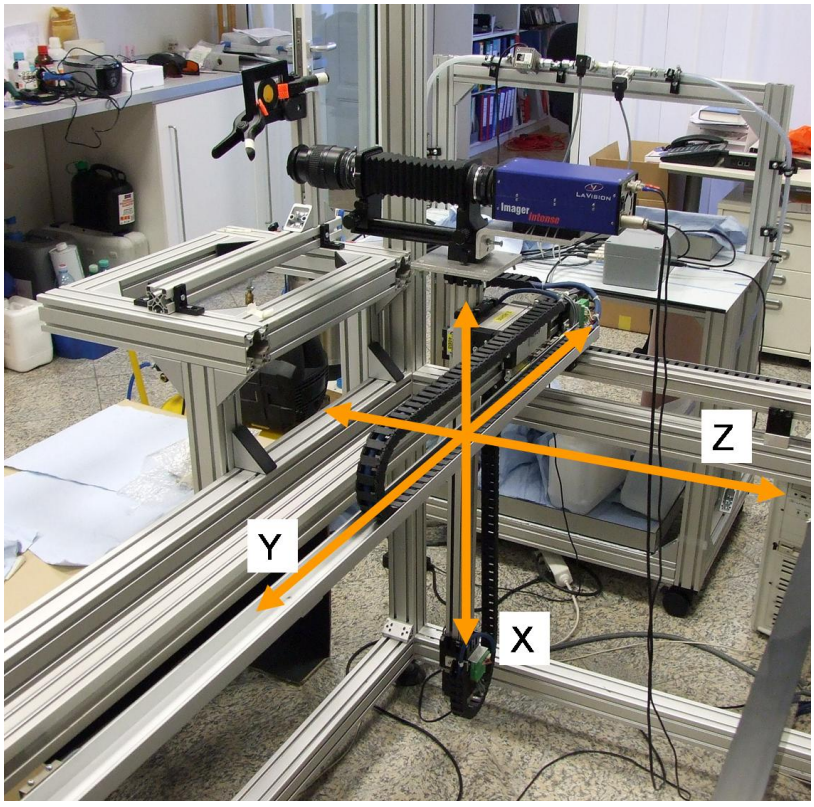

Figure 4.10: Motion Basic Drive Set and PIV camera placed on it

The loaded filter, coming from the filter test circuit, is placed in a fixture as shown in figure 4.11. It is screwed on the fitting of the *motion basic drive set,* and the camera is placed in front of the fixture with the smallest possible distance.

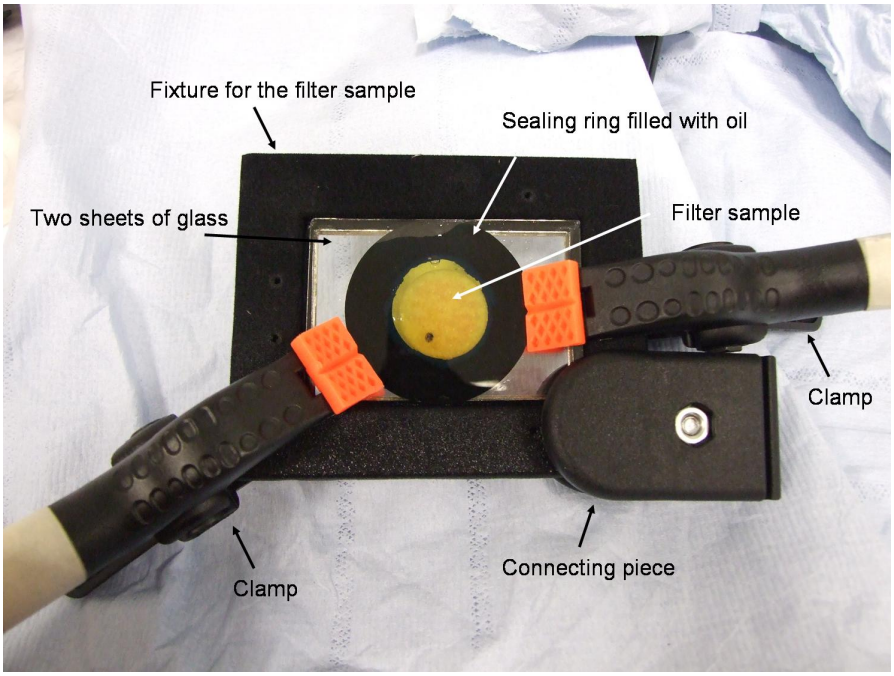

Figure 4.11: Preparation of the filter sample

The laser is located such that it aims at the filter sample. Figure 4.12 shows the basic set-up.

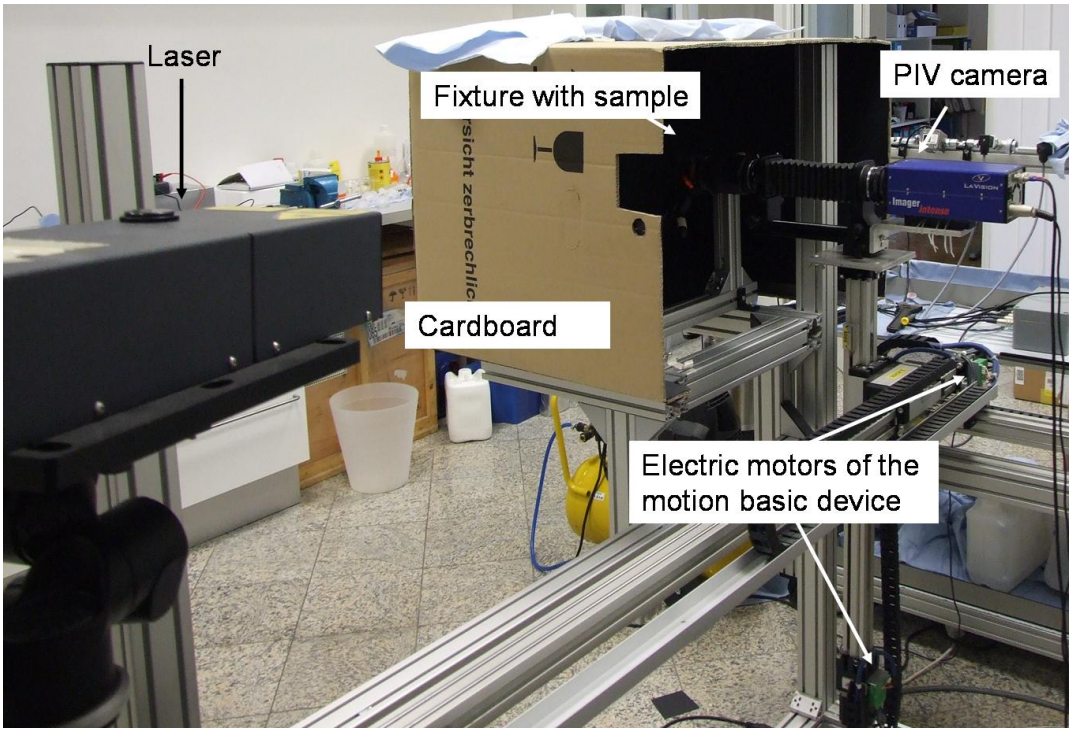

Figure 4.12: Test assembly for the particle detection facility

The *PIV camera,* the *laser* and the *motion basic drive set* can be controlled with a *LabView* program. The settings of the object lens of the *PIV camera* are adjusted to get a minimal depth of field. The program procedure is as follows: Firstly, the laser is switched on, and the settings (e.g. intensity, frequency) can be entered. Secondly, the camera takes a picture of the illuminated particles. Thirdly, the *motion basic drive set* changes the position of the camera in the z-direction, so that the distance between the camera and the filter sample increases. The smallest possible finite drive set shift is 10 µm, but for this application 20 µm have been found to be sufficient. After some seconds the camera takes another picture, and the procedure continues till 40 to 50 photographs at different depth positions are taken. Figure 4.13 shows a sketch of the procedure.

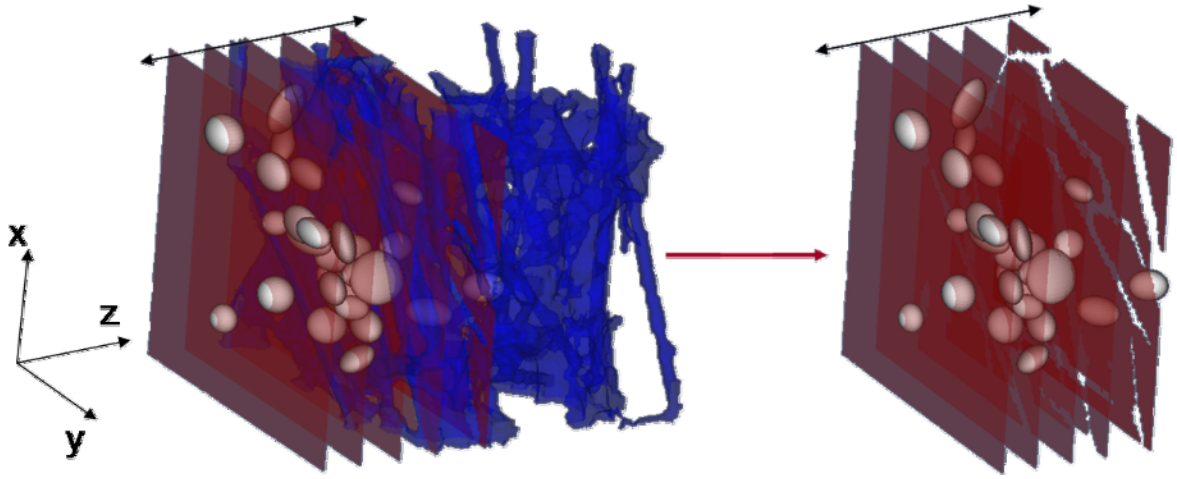

Figure 4.13: Measurement principle behind the laser fluorescence macroscopy method to determine 3-D particle distribution. Focal plane (red) is moved through the fibre structure (blue) and particles (grey) are highlighted (Boiger, 2009, p. 219)

4.3 Description of the Computer Algorithm

The photographs taken with the method mentioned above are the input data for an optical evaluation algorithm created by Boiger (2009, p. 221-226). The algorithm programmed in *MatLab* is capable of recognizing particles in 2D pictures and reconstructing them as 3-D objects. It mainly consists of three phases:

- 2D shape recognition: This procedure is comprised of built-in *MatLab* functions from the image processing toolbox. It was enhanced by the ability to automatically remove background light effects (by courtesy of Prof. Paul O'Leary, Institute of Automation, University of Leoben). Figure 4.14 shows an exemplary result of the 2D shape recognition function. Five nuts are recognized as individual objects, counted and their pixel area is evaluated.

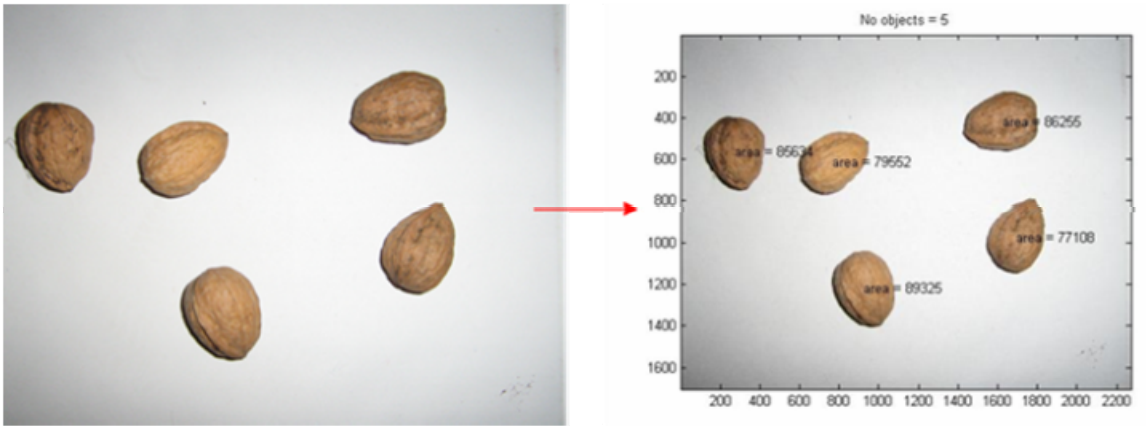

Figure 4.14: Exemplary result of 2D shape recognition function (Boiger, 2009, p. 222)

- Evaluation of object specific sharpness value: With the help of a multi-focus image fusion procedure, described in more detail in the *subchapter 4.1.3 Image Fusion,* specific sharpness values can be assigned to 2-D objects.

- Construction of digital 3-D objects in vector space: After 2-D objects are recognized, and their focus measure is determined in every photograph, the algorithm compares the focus measure in every picture. Figure 4.15 and 4.16 shows the connection between the original image and the evaluated focus measure for two different depth planes. The value of the focus measure is highest when the particles are in focus. Different particles are recognized as individual, nearly circular shapes. If the centre-to-centre distance between a shape in two pictures is notably smaller than the mean shape radius, these shapes are made out to belong to the same particle. Subsequently, the centre point with the highest focus measure is stated to be the 3-D objects centre position. Furthermore, the medium diameter of the centre-shape becomes the diameter of the object. A sketch of the principle reconstruction procedure is illustrated in figure 4.17.

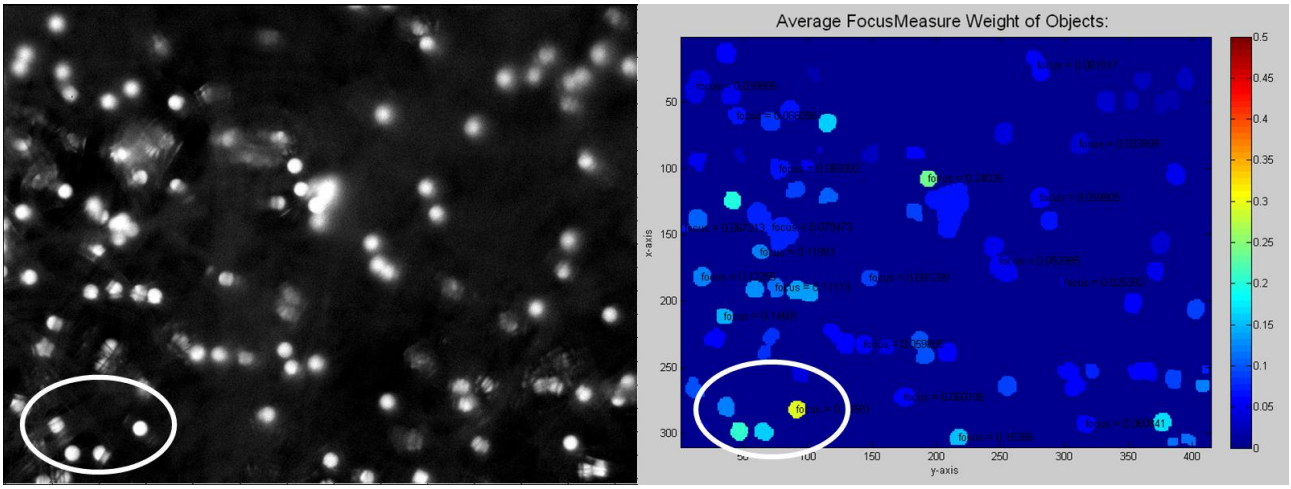

Figure 4.15: Comparison between the original image and the evaluated focus measure (7th depth plane)

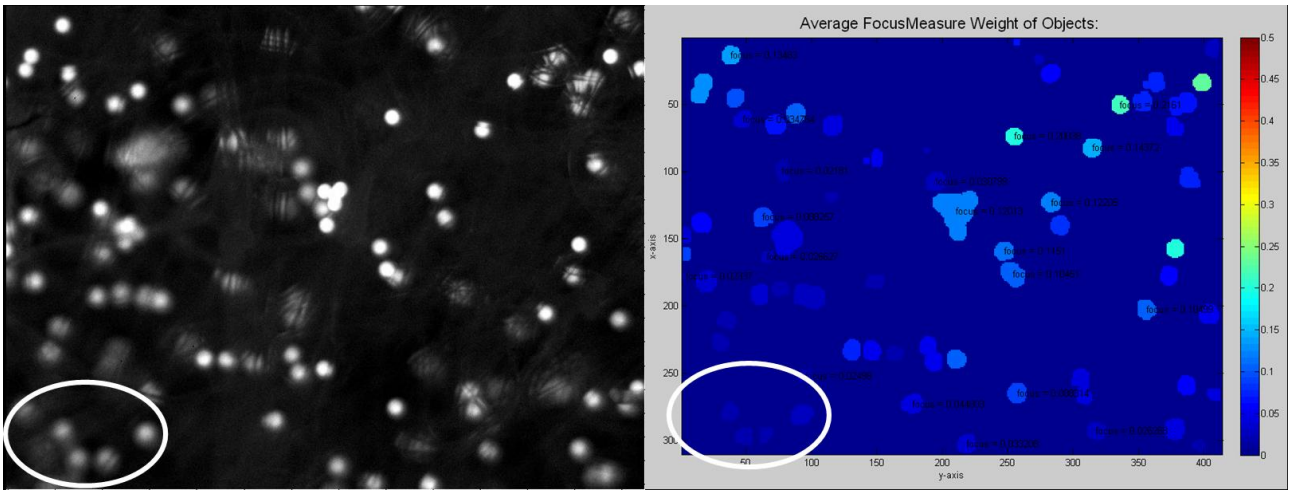

Figure 4.16: Comparison between the original image and the evaluated focus measure (18th depth plane)

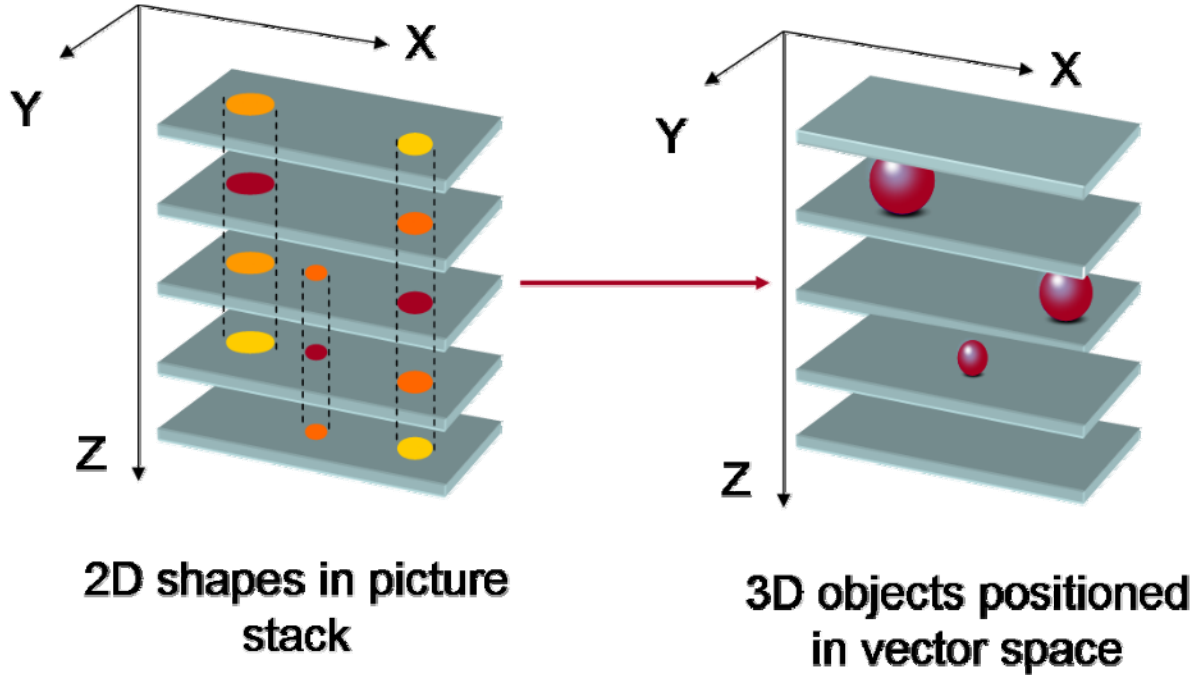

Figure 4.17: Principle operational sequence of the construction of 3-D objects (Boiger, 2009, p.224)

The algorithm is not only capable of providing a 3-D distribution of particles in a filter fibre material as shown in figure 4.18, but can also present other visualized results, as well as numerical results like: a count of objects per depth plane, relative covered picture area per depth plane or medium object diameter of objects per depth plane. Exemplary results are shown in figure 4.19.

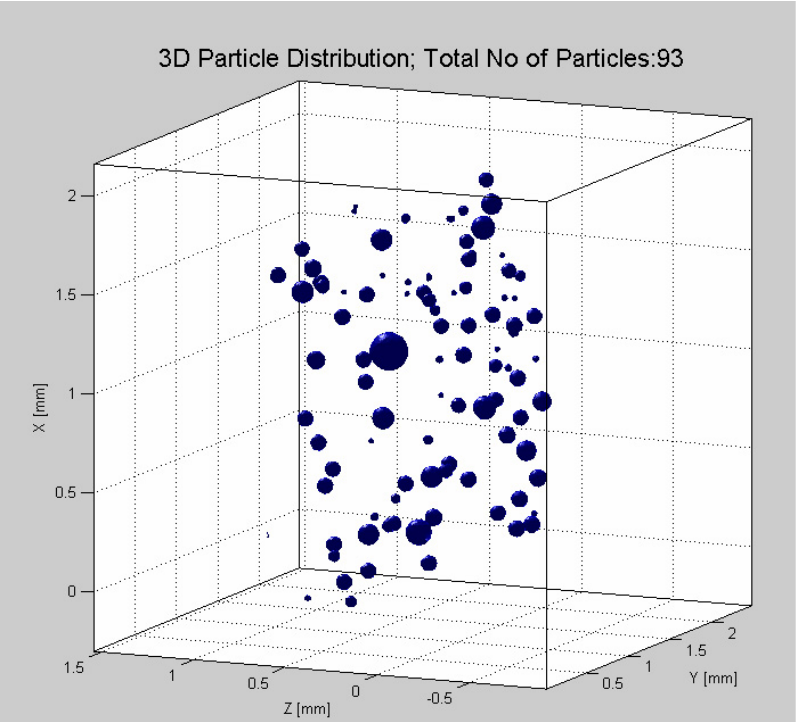

Figure 4.18: Final result of reconstructed 3-D particle distribution in a real fibre filter geometry

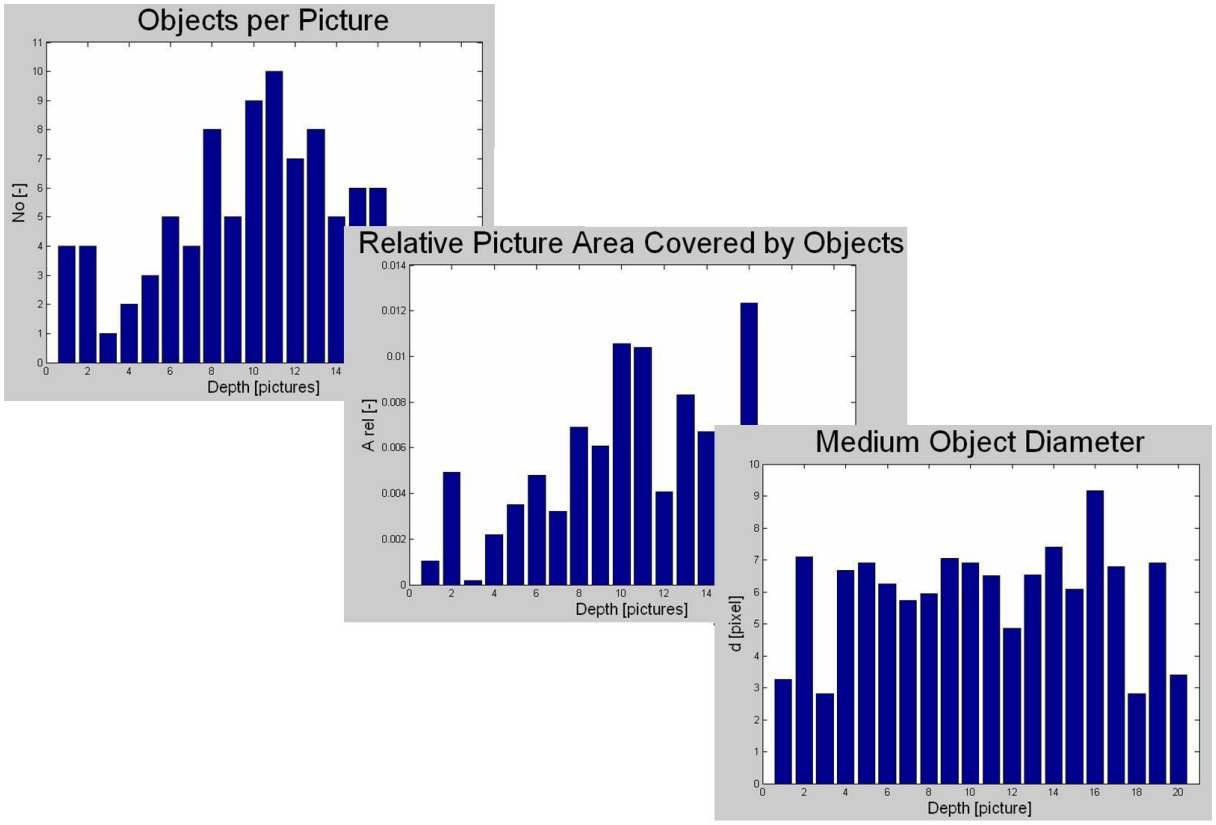

Figure 4.19: Exemplary results of the evaluation of 3-D test particle distribution.

Figure 4.20 to 4.22 show the evaluated mean diameter of different particle fractions. The particle radius in *pixel* is plotted against the number of the respective picture (depth plane). The first picture, showing a focused particle, is located in the filter medium. The last photograph with a calculated particle radius should be situated on the surface of the filter medium. The computer algorithm determines the relative radius r_r of the covered picture area in pixel. With the knowledge of the resolution *Res*, the particle diameter *d* can be converted into µm as shown in equation 4.11.

$$d = \frac{2r_r}{Res} = \frac{2 \cdot 5.4}{0.26} = 41.5\,\mu m \qquad (4.11)$$

The resolution according to the camera settings is 0.26 pixel/µm (see chapter 4.4.2).

Table 4.1 contains a comparison between the evaluated and the actual particle diameters. It is obvious that the particles on the pictures appear slightly larger than they really are. This attributes to the lustre of the particles, caused by the laser light.

Table 4.1: Comparison between the actual and the evaluated particle diameters

Actual particle diameter	Evaluated particle diameter
19.78 ± 0.18µm	24.49 ± 3.78µm
41.12 ± 0.76µm	41.57 ± 3.62µm
61.35 ± 1.42µm	63.73 ± 3.07µm

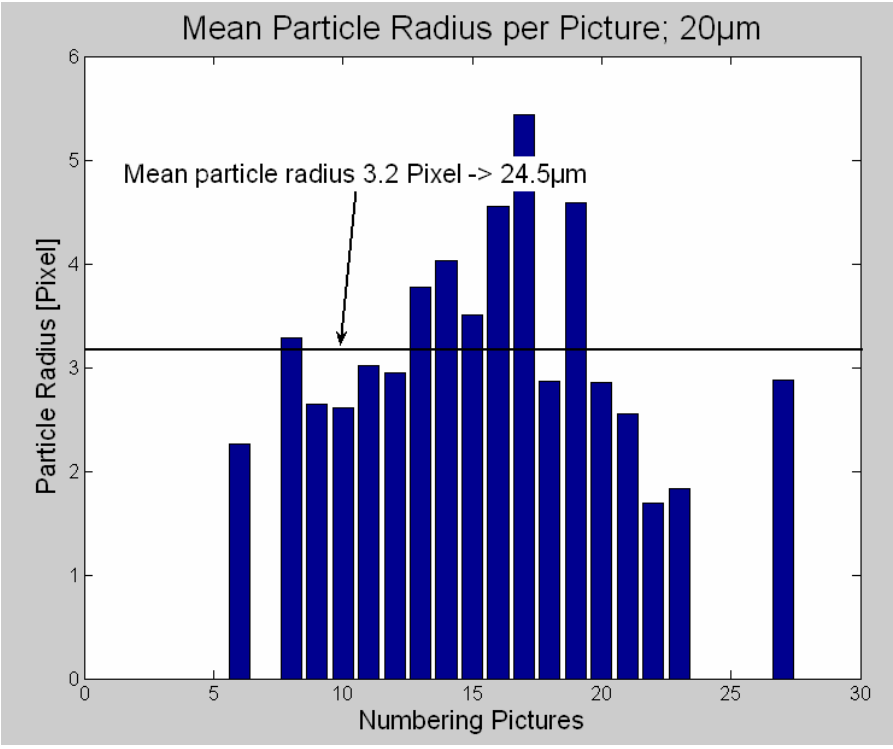

Figure 4.20: Distribution with evaluated particle diameter 20µm

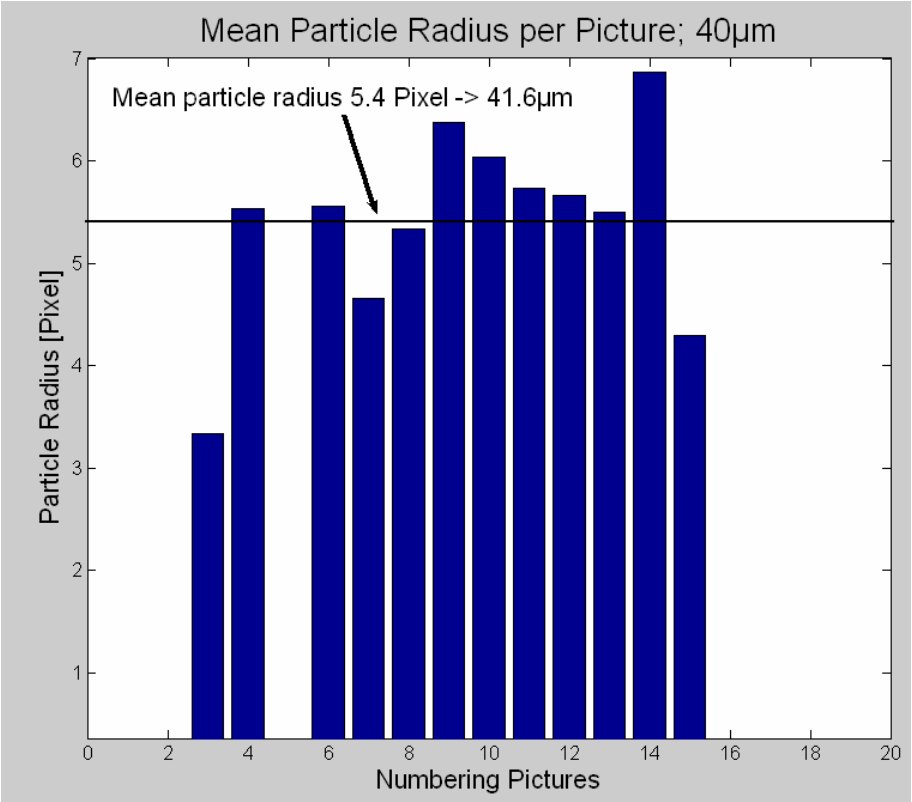

Figure 4.21: Distribution with evaluated particle diameter 40µm

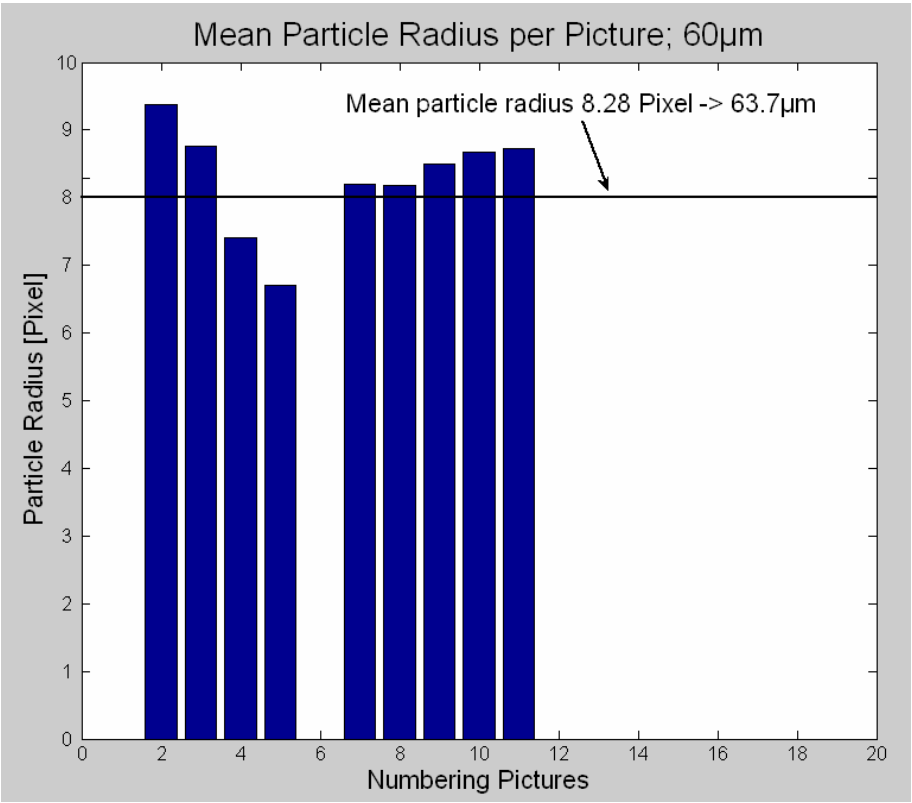

Figure 4.22: Distribution with evaluated particle diameter 60µm

The program features several input parameter. The quality of the results can be influenced mainly by three factors:

- threshold value for the focus measure (*thres*)
- *radius extension*
- number of erode operations (*noOps*)

The threshold value defines a percentile of the maximum focus measure value. It is in the range between 0 and 1. The recommended value for all particle sizes is 0.05. If the focus measure value of a particle is below the threshold value, the shape will be discarded. Therefore, the higher the threshold value, the more shapes, and thus the more “real particles” will be ignored.

The radius extension increases the radius of the shape of the particles in pixel. This means that particles, which are close to each other, are recognized as one particle when the radius extension is high (see figure 4.16). This operation is very useful when particles are partly hidden behind filter fibres. Therefore, they appear as several individual particles although these supposedly individual particles belong only to one particle. An example is shown in figure 4.23. The recommended radius extension value for all particle sizes is 2.

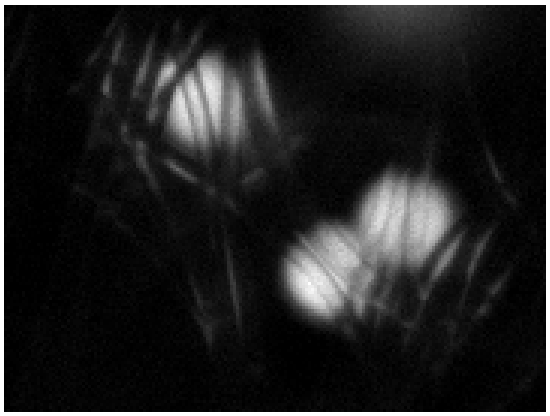

Figure 4.23: Hidden particles which may appear as several individual particles in the computer algorithm

The computer algorithm comprises a function which is capable of deleting unwanted scattered light effects. This function decreases the size of every detected object by a certain amount of erode operations. In this case the edges of white areas, which represent particles, are painted over with a line of black pixels. The user can define how often this erode operation shall be carried out. Subsequently, the size of the particles which are left over is increased by a similar operation, with the difference that now white pixels are used. For particles with a size bigger than 30 µm a *noOps* of 2 can be used. When the particle size is smaller the *noOps* has to be decreased to 1 because otherwise also small particles are deleted. This fact is illustrated in figure 4.24; the original picture is shown in figure 4.25.

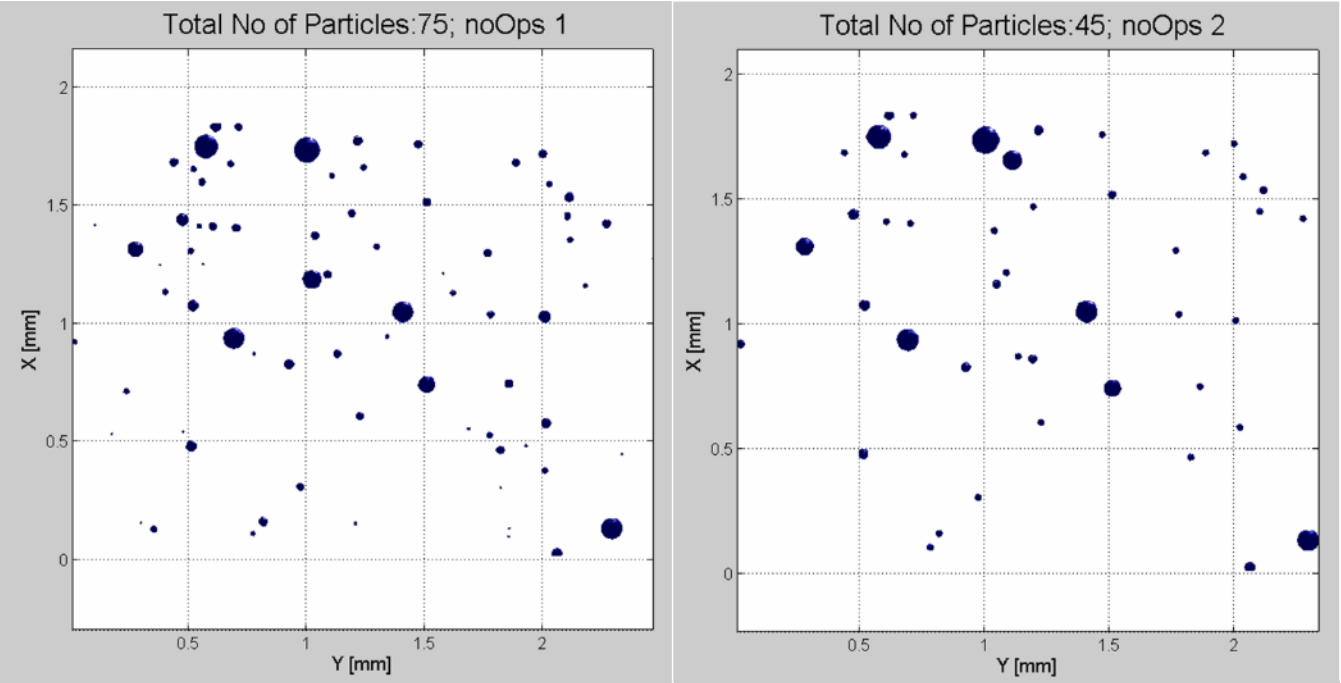

Figure 4.24: Comparison of the results between different *noOps* values for the filter sample *A43 Fulda* and a particle size of 20 µm

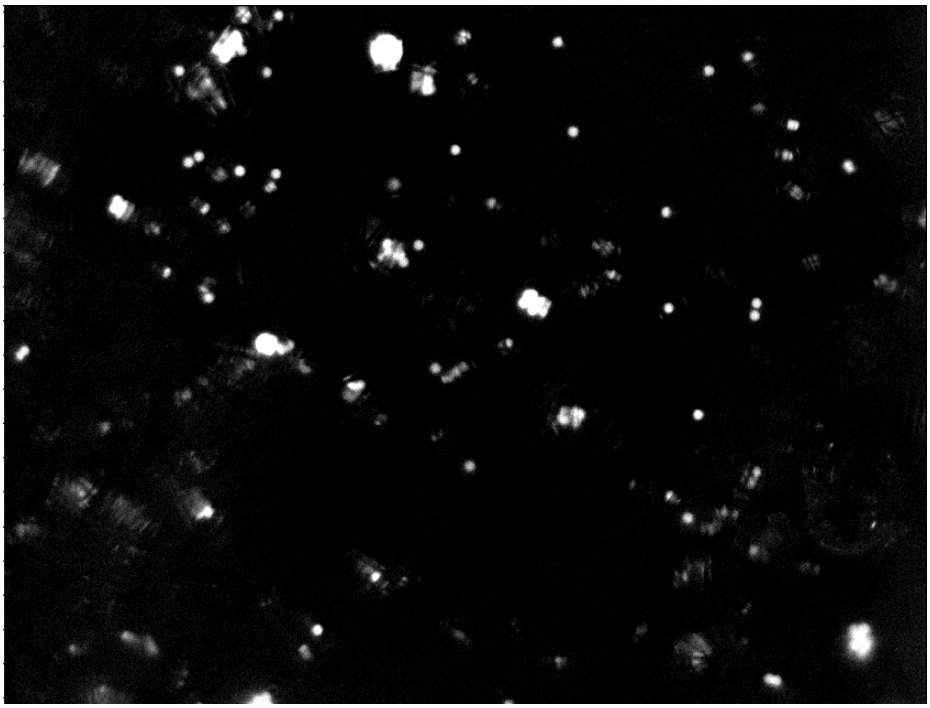

Figure 4.25: Original image of an A43 Fulda filter loaded with particles with a diameter of 20 µm

A *noOps* value of 2 erodes not only scattered light effects, but also particles. With this setting the algorithm detects 30 particles less than with a *noOps* value of 1.

4.4 Process Development

4.4.1 Verification of the 3-D Algorithm

Together with Boiger (2009, p. 226) a simple macroscopic experiment was carried out in order to verify the functionality of the 3-D reconstruction method. The particle distribution in filter media was approximated with five white, macroscopic spheres with diameters in the range of 3 cm to 8 cm. These spheres were hung on black threads, and located in an empty black cardboard. The basic set-up is shown in figure 4.26. An ordinary digital camera was placed in front of the spheres. The settings of the camera were chosen to obtain the lowest possible depth of field. A similar approach, compared to the microscopic imaging, was chosen, in a way that the camera was moved in steps of 1 cm after every picture. Therefore, also the focal plane shifted through the spheres. Subsequently, the obtained pictures were evaluated with the 3-D reconstruction algorithm. Figure 4.27 is an evidence for the functionality of the algorithm. The picture on the left hand side shows the position of the spheres located in the experimental set-up. On the right hand side the screenshot of the proposed 3-D distribution, evaluated with the 3-D algorithm, is shown. Due to good agreement between the results and reality, a verification of the functionality of the algorithm is considered to be achieved.

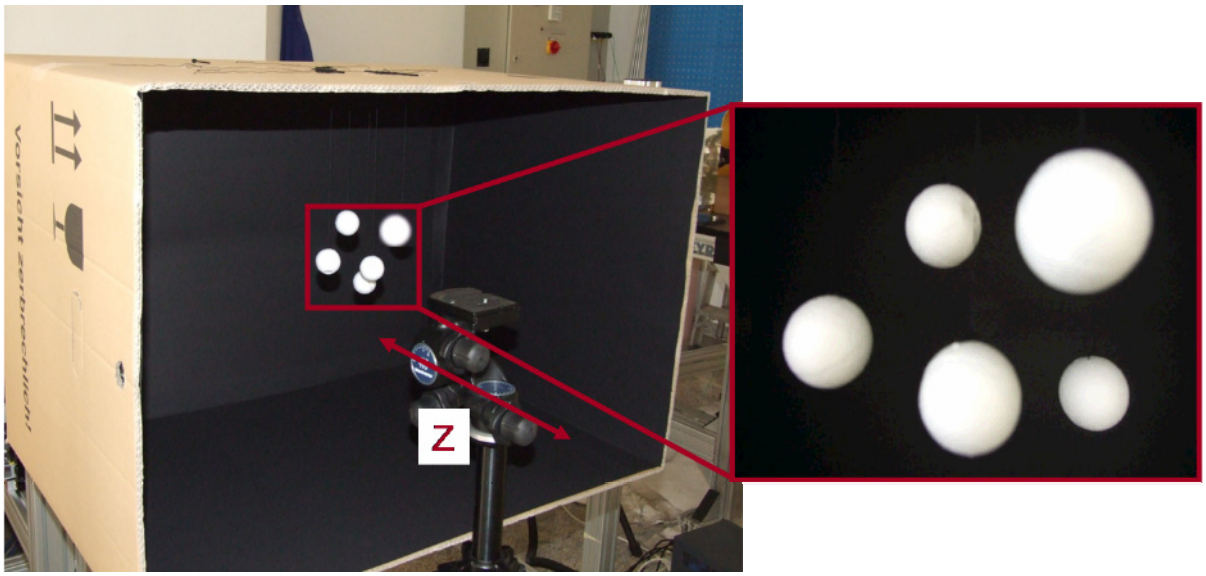

Figure 4.26: Set-up of a simple scene to verify the functionality of the 3-D particle reconstruction method (Boiger, 2009, p. 226)

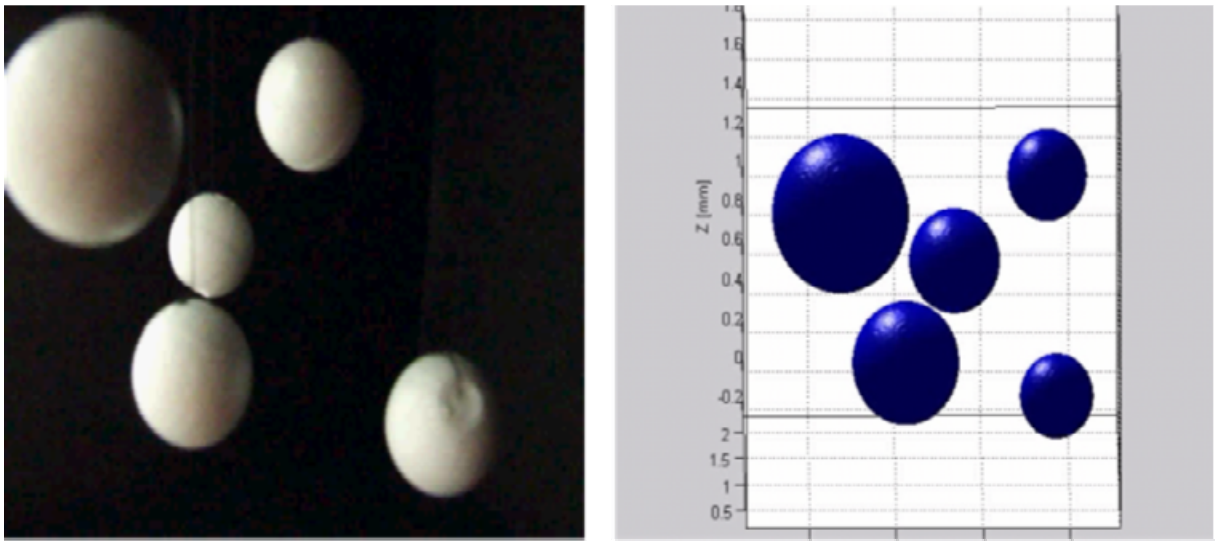

Figure 4.27: Comparison between a real picture of a sphere distribution and the 3-D result of the computer algorithm (Boiger, 2009, p. 227)

4.4.2 Resolution

As in most filtration applications the diameter of the particles is in the range of 1 µm to 100 µm, therefore, the resolution of the camera has to be very high. To enhance the quality of the pictures, two improvements were carried out:

- Macro object lens with a focal length of 60mm
- Optical bellows

The macro object lens is used in photography for objects which are rather close to the camera. With the help of the optical bellows it is possible to place the camera in front of the filter sample at a distance of 5 to 10 cm. Figure 4.28 shows a comparison of the resolution in pixel per µm between different optical bellows settings and different object lenses.

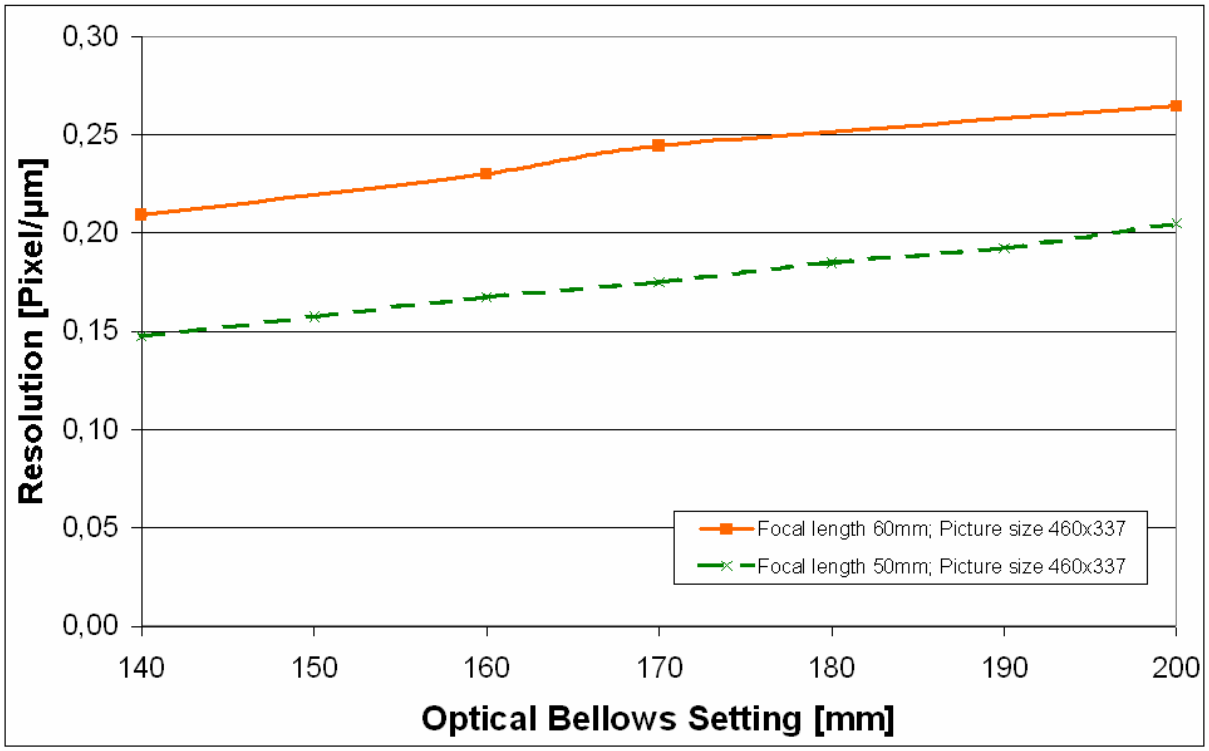

Figure 4.28: Comparison of the resolution in pixel per µm between different optical bellows settings and different object lenses.

The picture size is limited to a resolution of 460 x 337 due to the calculation time of the algorithm. It is not reasonable to use higher resolutions because the algorithm has to evaluate up to fifty pictures at the same time. The two curves in figure 4.28 represent the resolution of two different object lenses. The continuous line stands for the macro object lens with a focal length of 60 mm, whereas the dotted line corresponds to an ordinary object lens with a focal length of 50 mm. The higher the resolution in pixel per µm, the better is the quality of the picture. Due to the use of the macro object lens, the resolution of the picture is increased by 40 %. Another fact is that with a longer optical bellows setting the resolution will also increase. The only drawback is that with a higher resolution the area of the filter sample, which is photographed, will diminish. This circumstance is shown in figure 4.29.

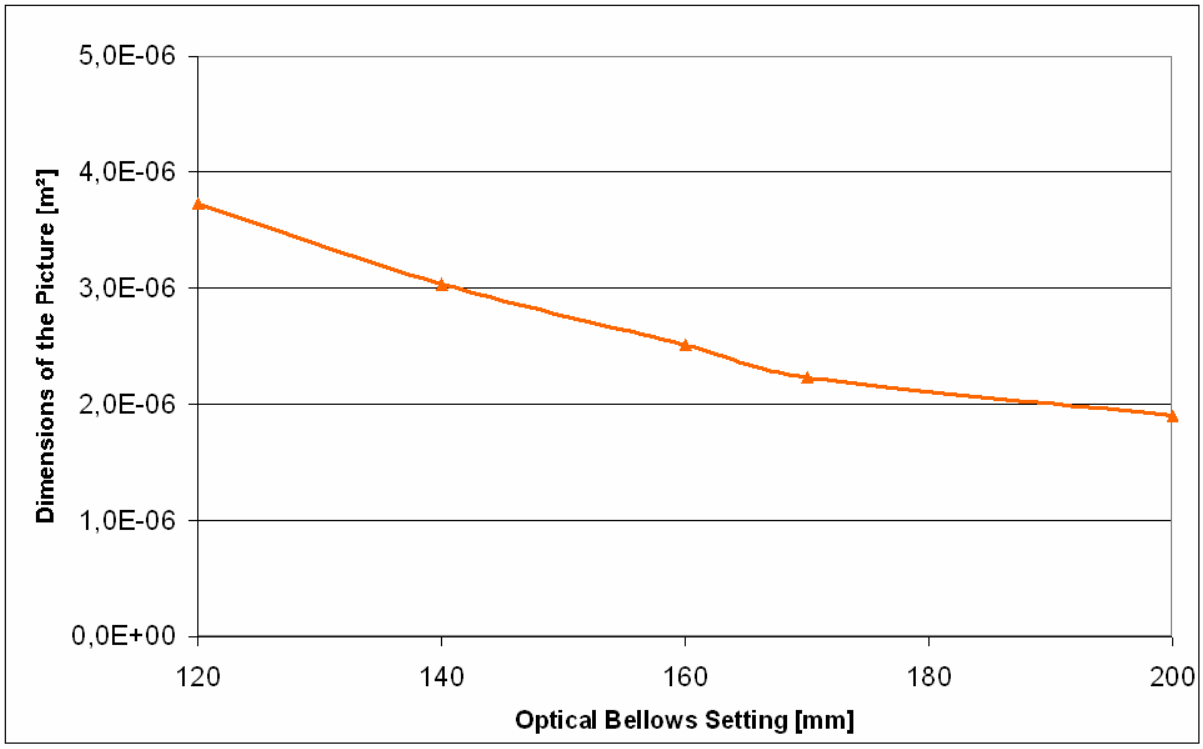

Figure 4.29: Photographed filter sample area (Resolution: 460 x 337) with different optical bellows settings.

However, an optical bellows setting of 200 mm is chosen in order to resolve particles of a diameter down to 10 µm because otherwise the particle size will be too small for an optical evaluation.

In order to compensate for the smaller filter sample area, which is photographed, five different positions within the filter sample are selected. These samples represent roughly 3% of the entire filter sample area. To ensure that the evaluated regions are equivalent, filter samples with a low interior grey value deviation are chosen. These samples are selected with the *translucency examination* method (see chapter 3).

4.4.3 Index Match of Optical Refractive Indices

The usage of fluorescence particles enables to obtain photographs of particles, within the filter, but without the filter fibres. Nevertheless, the filter fibre structure causes some problems regarding the quality of the photographs. As these fibres are solid bodies, particles can be hidden behind them, and the sight in the filter material is limited.

The idea to solve this problem was to use a type of oil with the same refractive index than the filter material. If the filter fibres, and the oil surrounding it, have the same refractive indices, the filter fibres tend to become invisible. Different types of oils with different refractive indices were applied to *A55 Ahlstrom*, *A43 Fulda* and *Ti99*. The optical results can be seen in figure 4.30.

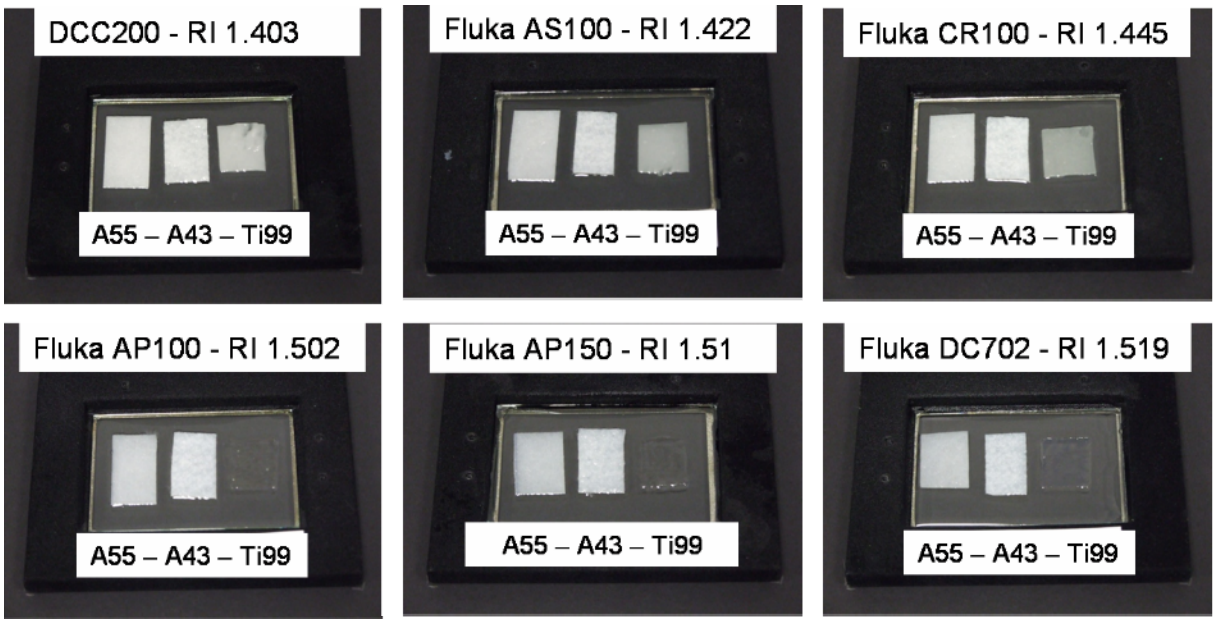

Figure 4.30: Comparison of the index match between filter samples and different oils

The heading lists the name of the used silicon oil and the corresponding refractive index (RI) provided by the supplier. The polymer based filters of the type *A55 Ahlstrom* and *A43 Fulda* are not affected by the treatment and remain opaque, whereas the glass fibre filter *Ti99* becomes transparent at a refractive index of 1.502. It is thus possible to increase the sight in this type of filter by using oil with a refractive index of about 1.5. In the experiments paraffin oil with a refractive index of 1.48 is used. It is a compromise between the index match and the acquisition costs for the oil.

4.4.4 Picture Quality

The CCD chip of the PIV camera is very sensitive. If the exposure time of the camera is too high, scattered light will be seen on the photograph. Therefore, also filter fibres will be seen on the photograph. The algorithm is only capable of dealing with pictures like these to a certain extend. Nevertheless, if the pictures are too bright, the distribution of the particles within the filter fibres cannot be determined.

The main problem was that the maximum possible exposure time was 1 ms. Otherwise the background light in the laboratory had too strong an influence. Within this short period of time it was not possible to gain pictures with a constant quality. Some pictures appeared to be brighter, whereas others were darker. This was caused by the varying number of laser shots during the exposure interval because the laser firing rate was in the range of 1 to 15 Hz.

The solution to this problem, with a slight and cheap adjustment, is shown in figure 4.12. A cardboard with black interior walls is put over the fixture with the filter sample. The side where the camera is located can be covered with towels. A small gap on the side of the

cardboard makes it possible for the laser to shoot at the filter sample. Thus, it is possible to increase the exposure time up to 5 seconds, without disturbing scattered light.

Another improvement is the adopting of the *Motion Basic* software for this particular procedure. The camera can be moved in three dimensions with the help of three different electric motors. With a computer program, the camera is positioned in front of the filter sample, and moved 20 µm away from the sample after each picture. This movement causes some vibrations of the frame. Consequently, the pictures are blurred. To solve this problem a delay of 2 seconds between the changing of the position and the taking of the picture is implemented in the computer software.

4.5 Conclusion and Outlook

The method presented in this chapter is capable of determining the particle penetration depth in filter media, and evaluate a 3-D model, as well as statistical distribution values. It is verified with a simple macroscopic 3-D model. The results of the method can be used in two different areas.

Firstly, as a comparison to the simulation results of the filter efficiency. The real particle distribution within the filter fibre geometry can be compared to the simulated one.

Secondly, as an important information for producers of filter material. It can be assessed where and to what extent particles with different diameters are deposited in a certain filter medium.

One drawback, apart from the expensive set-up and the high amount of time involved for the experiment, is that although the filter fibre material can be faded out to a certain extent, it is not possible to make out all particles in the filter material. Particles are still hidden by fibres, and especially small particles, which ordinarily have a higher penetration depth, are harder to detect. A possible way out of this condition is presented in chapter 4.4.3 where special oils are used, which have the same refractive index compared to the filter fibres. Thus, the filter material becomes transparent, and it will be possible to detect particles within the entire thickness of the filter sample. Up to now, only glass fibre fleeces are inclined to become transparent, whereas polymer based filters still stay opaque.

Another possibility for an improvement is that the computer algorithm evaluates, among other things, also the particle diameters of detected particles. Therefore, it should be possible to use polydisperse mixtures of particles, and reduce the time for the experiments. The problem is that diameters of detected particles tend to be higher than they really are, which is shown in table 4.1. This problem can probably be solved by determining a correction value, converting the evaluated diameter into the actual diameter. This correction value has to be obtained by several measurements, comparing the estimated to the real diameters. Thus, polydisperse mixtures of particles can be used because the size and position of each particle

can be determined. It will be reasonable to use two different polydisperse mixtures because the exposure time for small particles has to be higher, compared to bigger particles. Therefore, a mixture with a range from 10µm to 30µm, and a mixture with a range from 30µm to 60µm is recommended.

5 Working Instructions

The following subchapters describe the working procedures of the *translucency examination* and the particle penetration depth. All necessary working steps are explained in detail. Chapter 5.5 presents a list of the required equipment and materials used in these methods.

5.1 Working Instruction - *Translucency Examination*

Read the following working instruction carefully and thoroughly!

5.1.1 Preparation of the Filter Sheet

- Usually the edges of the filter sheets are right-angled. If this is not the case a rectangle has to be drawn on the filter sheet. It helps the user to select the filter area in the program.
- The upper left corner of the filter sheet should be marked as shown in figure 5.1. This is very important because the upper left corner of the stencil is put on this corner.

5.1.2 Taking the Pictures

- The tripod [1] is placed over the overhead projector [2] as shown in figure 3.2.
- The camera is fixed on the tripod. The filter sheet is placed on the overhead projector within the markings, to ensure constant conditions for each filter sheet.
- The position of the tripod and the zoom of the camera [3] have to be changed to get a picture of the filter, which takes up most of the area. In many cases a zoom of 150 is recommended.
- A ruler is placed on the filter and a picture is taken in the *automatic modus* (see figure 5.1). With the information of the width of the picture the program can calculate a scaling factor. After the picture is taken, the ruler can be removed.

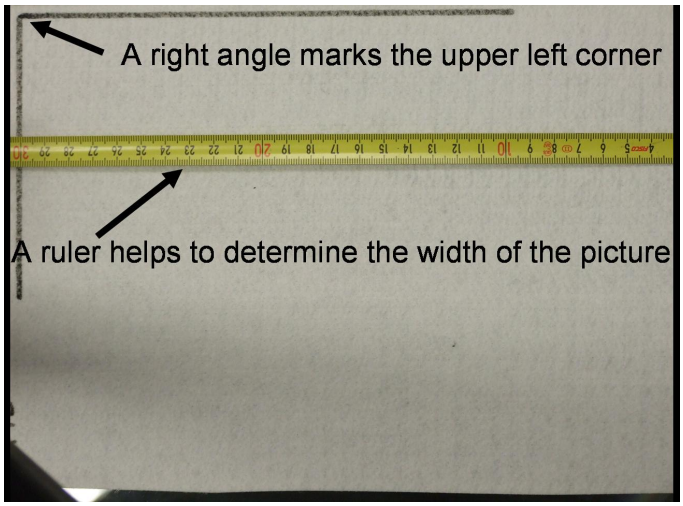

Figure 5.1: Prepared filter sheet with ruler

- The overhead projector is switched on. The user has to wait for 10 minutes to avoid heat up effects.
- The camera menu is switched to *manual M* with the following setting:

  Exposure time: 800

  White balance: Neonlicht 2

  Aperture value: 5.6

  Flash: Stand by

  ISO: 100

  Change the exposure time by using the up and down arrows. Press *menu* and choose *WEISSABGLEICH*. Change the setting to *Neonlicht 2*. Press the *+/-* button on the top of the camera and use the up, and down arrows to change the *aperture value*. Use the right arrow to switch off the *flash*. Press the *F* button and select an *ISO* quality of 100.
- The lights in the room have to be switched off and the curtains drawn. If it is possible the overhead projector should be the only light source in the room.
- The picture can be taken.

5.1.3 Saving and Scaling the Pictures

- To transfer the pictures to the PC, connect the camera with the USB cable to the PC. A program will open automatically and the pictures are saved in a folder.

- Open the picture with the ruler, determine the length of the picture in millimeter and make a note of it.

- The resolution of the pictures is rather high. To decrease the calculation time of the program, the size of the pictures has to be decreased. This is done with *IrfanView*. A description of the program is shown in figure 5.2. Open the pictures of the filter samples with this program. Now select: *File -> BatchConversion/Rename* and a new window will open. The user has to select the pictures which should be decreased on the right side, and click *Add*. On the left side the following settings are recommended:

  Work As: Batch Conversion + Rename

  Batch Conversion Settings: Make a tick at *Use advanced options (for bulk resize…),* and click *advanced*. Select *Set new size as percentage of original* and insert 25%. Click *OK*.

  Determine the output directory and click *Start Batch*. A new window will open with some information. If there are no warnings or errors click *OK*.

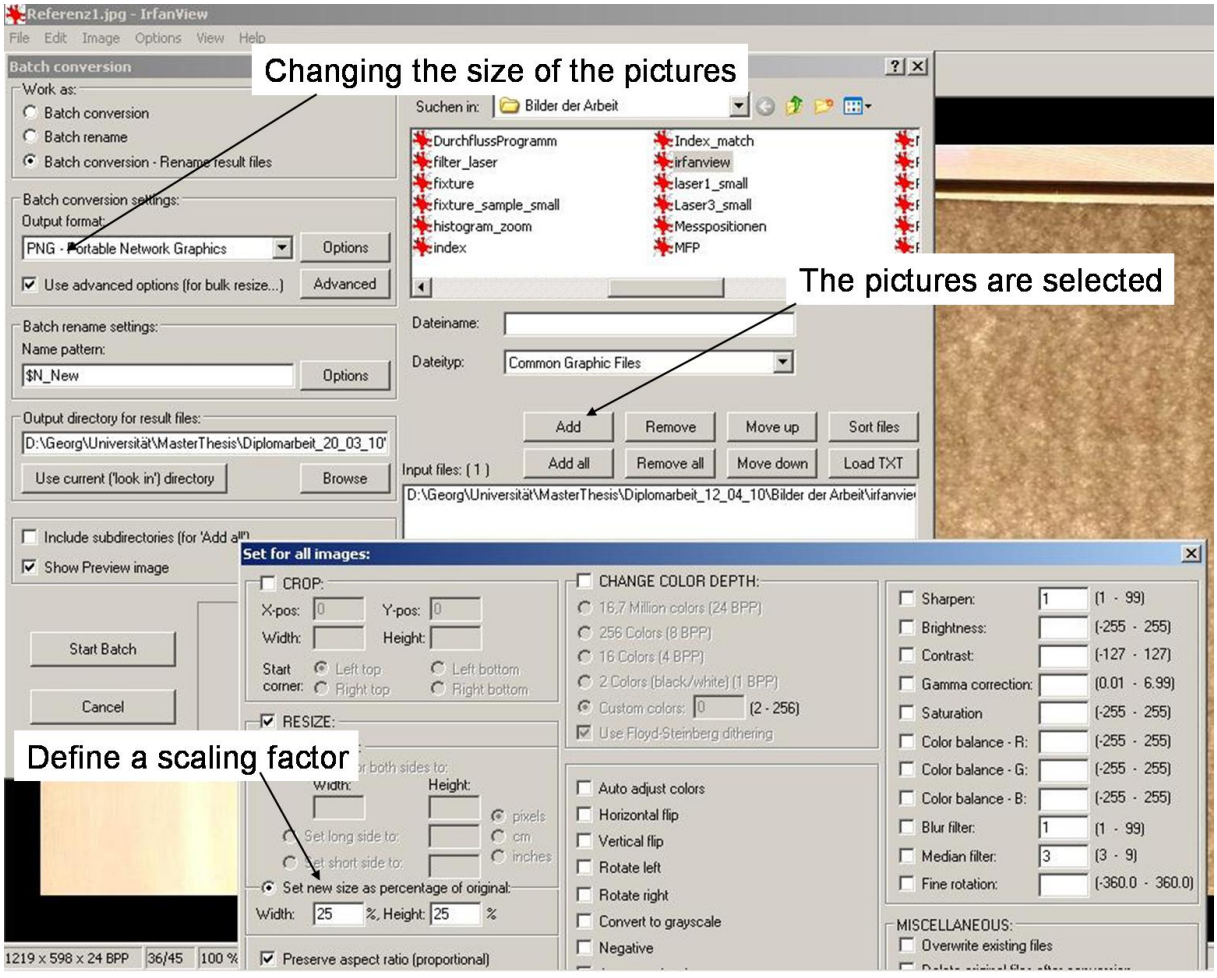

Figure 5.2: Using the program IrfanView

5.1.4 Determination of the Position of Samples

- Start MATLAB and open the program *selectProbeLocation.m.* Run the program. A new dialog box will open where the path can be defined, and the picture of the filter sample selected. Insert the length of the picture in millimeter in the next dialog box, and click *OK*.

- The next step is the light source elimination. The user is asked to define a filter size. In most cases a filter size of 15% is suitable. A new window shows the original picture, the estimated light source and the corrected image as illustrated in figure 3.4. If the estimated light source has a circular shape, click *yes*. If not retry the light source elimination with a higher percentage.

- The user has to choose the area of the picture where the filter sheet is located. Use the scroll bars to change the position of the lines. The lines should be exactly at the edges of the filter sheet. A very important point is the upper left corner of the filter sheet. This is the zero point in the coordinate system for the stencil. If the area is chosen, click *apply*.

- Enter the diameter of the sample in millimeters. The effective size of the fixture for the samples in the filter test circuit is 25 mm. The program calculates the position of the samples. This will take some time.

- The user has to choose an area fraction of the picture which is suitable for the determination of the filter samples. Use the scroll bars to change the position of the lines. The edges of the filter are often not representative as shown in figure 5.3. Therefore, the inner area should be chosen. If the area is chosen, click *apply*.

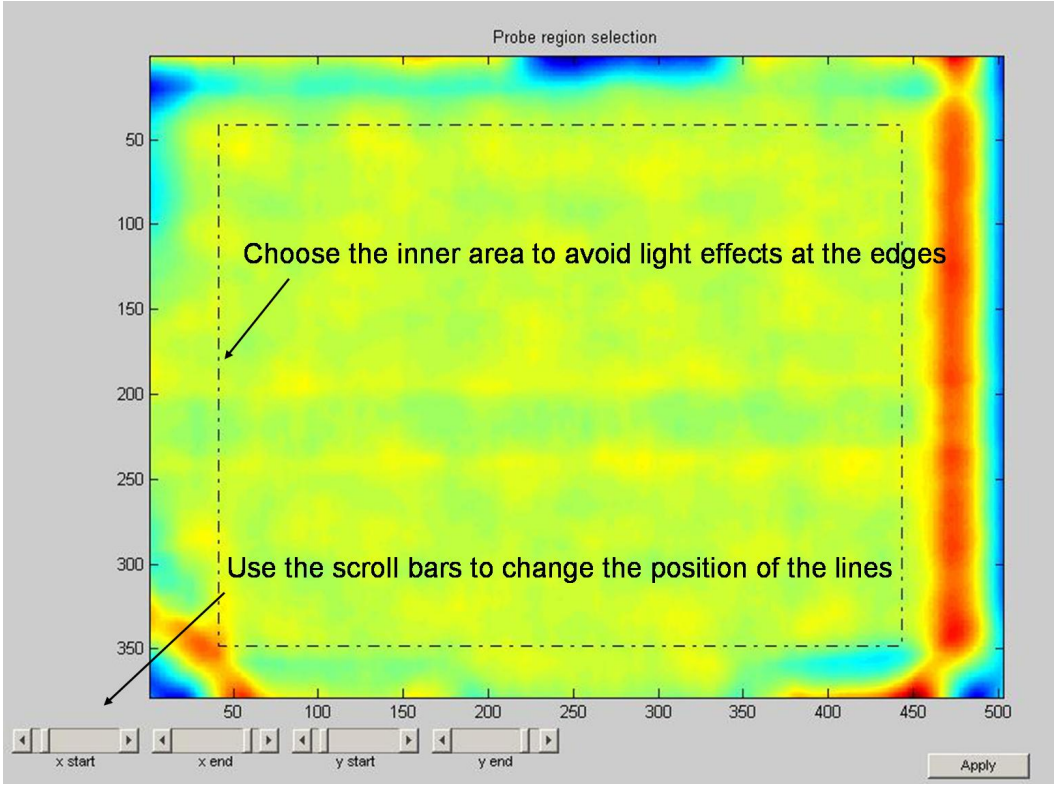

Figure 5.3: Selection of the region of the filter sheet where the samples shall be determined.

- The next dialog box gives the user different opportunities to define the properties of the samples:

  Range paper: The user can define the range (minimum and maximum value) of the grey values.

  Range mean: The user can define the range (minimum and maximum value) of the mean grey value of a filter sample with the diameter which was defined by the user.

  Range standdev: The user can define the range (minimum and maximum value) of the standard deviation of the grey value of a filter sample with the diameter which was defined by the user.

  Number of positions: The user can define on how many different grey values a sample should be taken. If *1* is inserted the program determines the position of the samples at the mean grey value. If *2* is inserted the program determines the position of the samples at the minimum and maximum grey value. If *3* is inserted the program determines the position of the samples at the minimum, the maximum and the mean grey value and so on.

  Number of samples/position: The user can define how many samples at each grey value *position* should be determined.

- The program proposes positions for the different samples as illustrated in figure 5.4. The user has to check whether the position of the samples satisfy the requirements or not. Therefore, it is recommended to check the window with the mean grey values and the window with the standard deviation of the grey values. If the positions of the samples are suitable click *yes*, otherwise click *no* and change the settings.

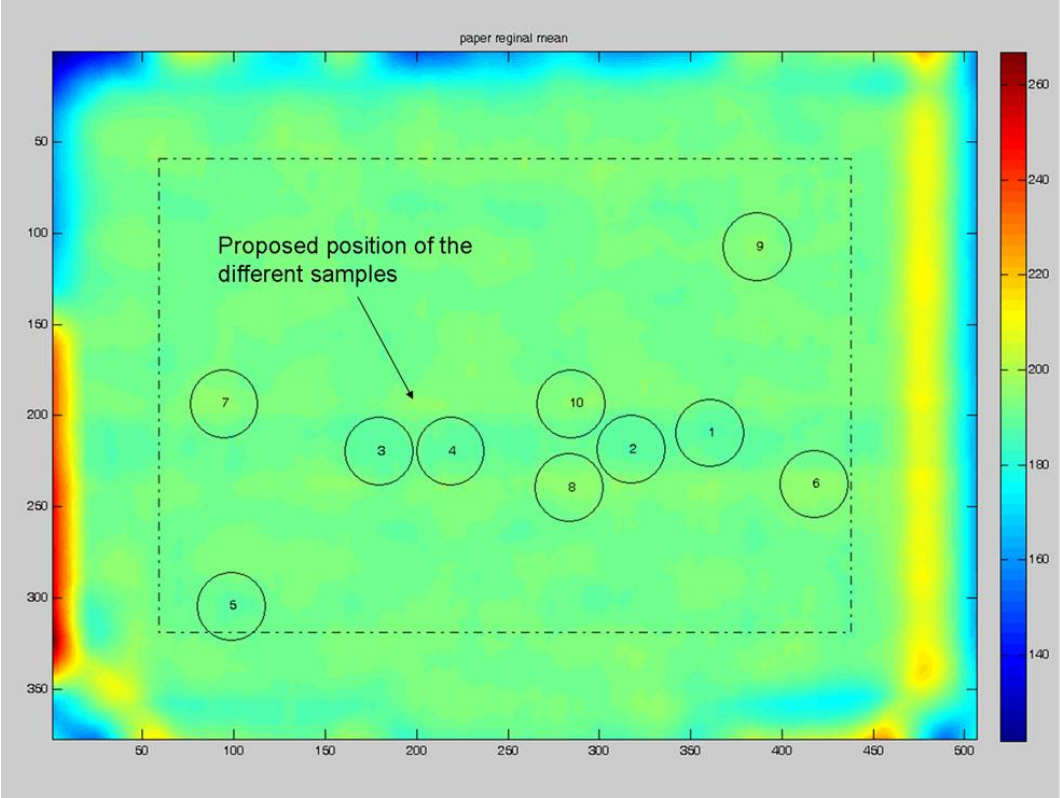

Figure 5.4: Proposed position of the different samples

- It is recommended to save the result, and close all figures. The program creates a new folder in the directory of the current image.

- Open the *statistic.dat* file. In this file the number of each sample and the statistical data is written. Print this file.

- Open the *mask.fig* file. This is a stencil with the positions of the samples for the filter sheet. Print the stencil. Fix the stencil to the filter sheet with some paper clips so that the upper left corner of the stencil is on the upper left corner of the filter sheet.

- The filter samples can be stamped with the help of a punch and a hammer. It is recommended to prepare two cling films. In one of them a paper is placed with the numbers of the different filter samples according to the *statistic.dat* file. The filter samples are laid between the two cling films. Make a point with a permanent marker on the filter to distinguish front and back.

5.2 Working Instruction - Pressure Drop (Without Particles)

Read the following working instruction carefully and thoroughly!

5.2.1 Preparation of the Samples

For the preparation of the samples read the working instruction for the *translucency examination* (see chapter 5.1).

5.2.2 Filter Test Circuit

The arrangement of the filter test circuit is described in chapter 3.2.2.

5.2.3 Sequence of Operations

- Ensure that no pressure is applied on the reservoir [4], and the manual valve (d) is closed. Open the fixture (h) and place the red sealing ring in the right part of the fixture as illustrated in figure 3.7. Insert the grate for the stability of the filter sample. Place the filter sample on the grate. Finally add the blue sealing ring which should avoid leakiness at the edges. The left part of the fixture also contains a grate. Screw the two parts together. Be careful with the pressure gauges [5], and ensure that they are on the same level.

- Turn on the power supply, and make sure that the display of the flow control device [6] is on. Connect the USB – cable of the control box with the computer, and start the *DurchflussregelungMain* program with *LabView8.5*, when the green light on the control box is blinking.

- Fill the reservoir (a) with roughly 6 litre of paraffin oil [14], and close the lid. Switch on the compressor [7], and wait till it reaches the operating pressure. Open the valve which connects the compressor to the reservoir, and adjust the pressure in the reservoir according to the pressure gauge seen in figure 5.5. The pressure is regulated with a valve on the compressor as shown in figure 5.6. It is recommended to use a pressure of 3 to 4 bar for a flow rate of 0.2 to 0.4 litre per minute and a pressure of approximately 6 bar to obtain higher flow rates. The maximum flow rate is 1.0 litre per minute, depending on the pressure drop of the filter medium.

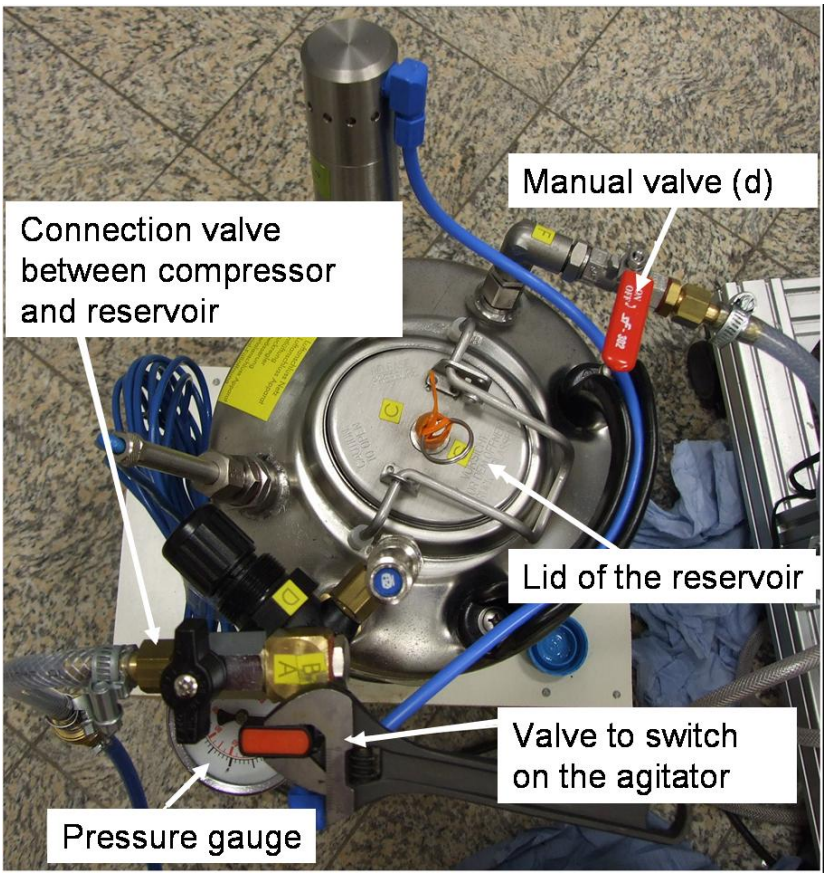

Figure 5.5: Reservoir (a) of the filter test circuit

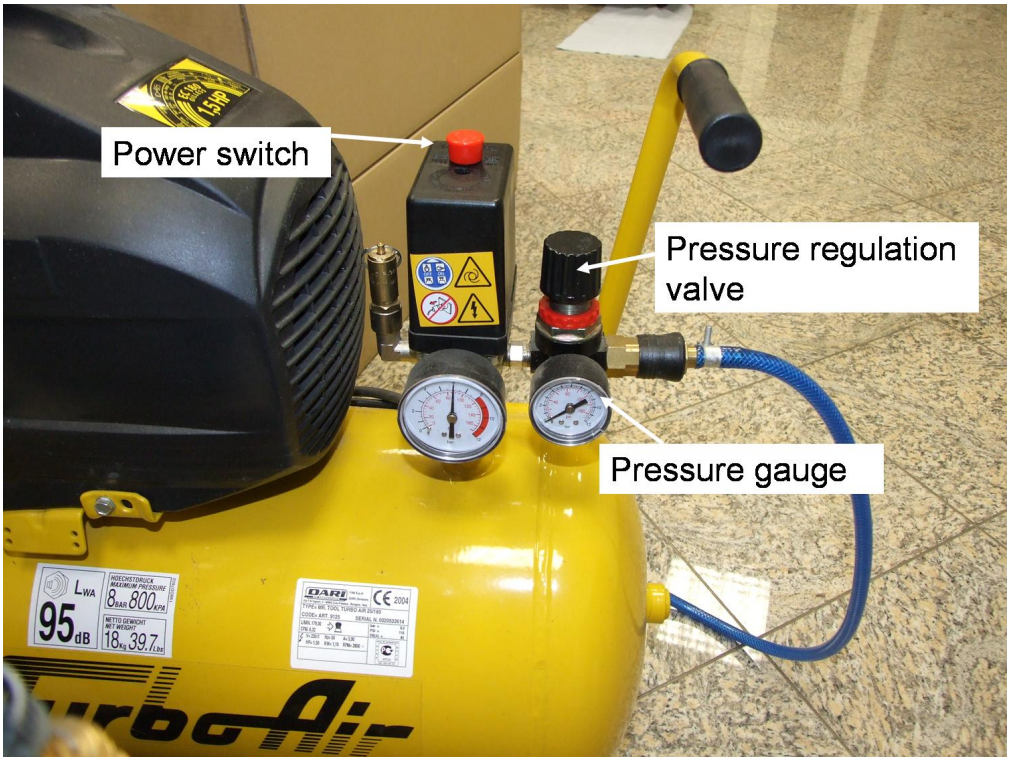

Figure 5.6: Compressor

- Click on the *arrow* in the upper left area of the *DurchflussregelungMain* program, and choose the *Spülen* menu. On the right side are three diagrams as illustrated in figure 5.7. The first diagram shows the pressure against time. The second diagram illustrates the flow rate against time and the third diagram shows the volume against time. Use the right key of the mouse and scale the y – axis of the first diagram. On the left side the user can define the flow rate in litre per minute.

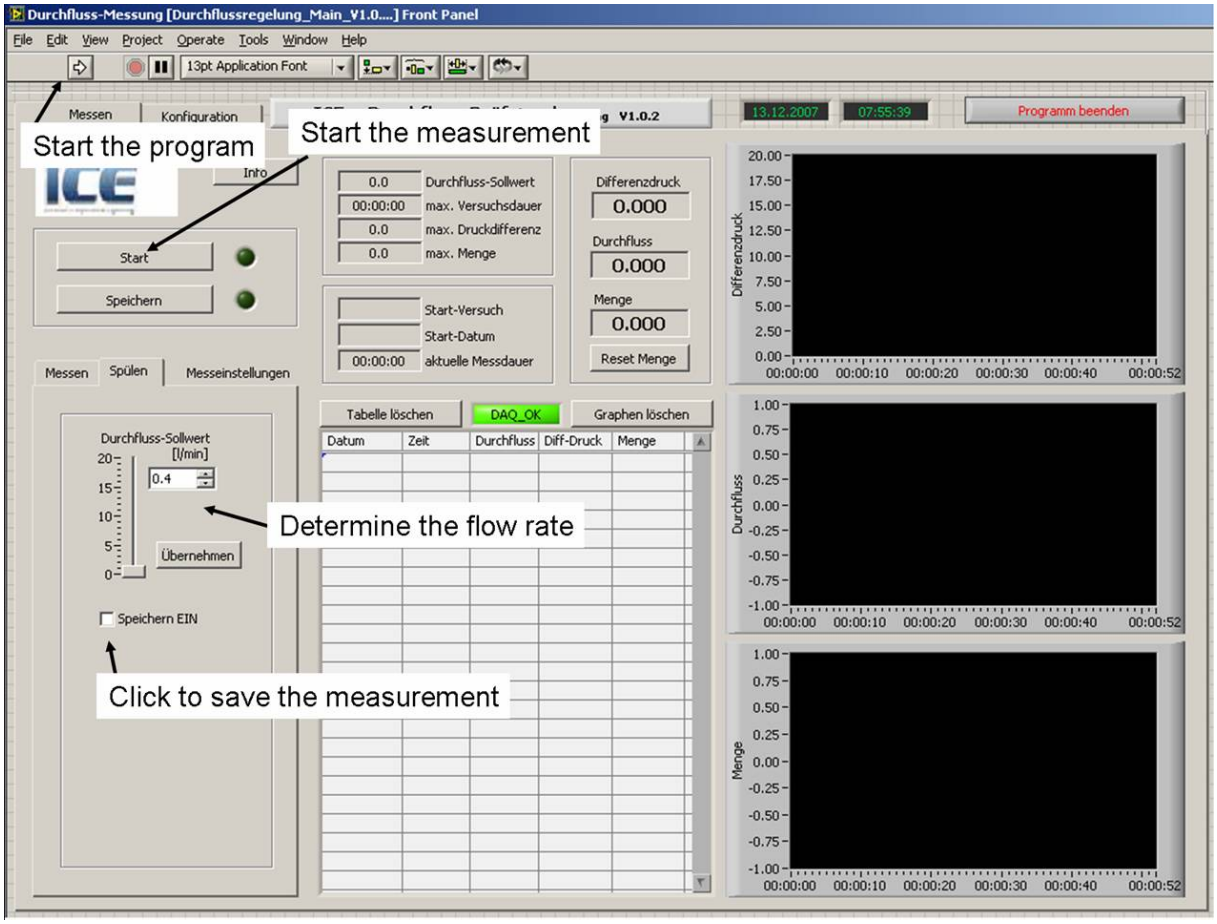

Figure 5.7: Description of the *Durchluss-Messung* program

If it is necessary to save the pressure values, make a tick at *Speichern EIN*. The user has to define the directory where the data is saved. This is done by clicking on *Speichern* and choosing the directory. The program saves a file with the current date. It is important that this file is renamed after the experiment. The file name should contain experiment related information such as: the type of the filter material and the number of the sample.

- If the pressure is applied to the reservoir (a) and the settings in the program are done, ensure that the pipe after the fixture (h) leads into the second reservoir (i). Start the program by clicking on *Starten*. The user is asked to confirm the settings. Insert the path where the file should be saved. If previous measurement data should be

deleted, click *OK*. The two signals next to *Starten* and *Speichern* should be green. Open the manual valve (d) slowly to avoid shock waves because it takes some time till the flow measurement [8] and control devices regulate the flow.

- The program shows the values of the pressure drop of the filter sample. If stationary flow conditions are reached, the user can take a note of the pressure value at the certain flow rate. Then the next flow rate can be adjusted. Usually the pressure drop is evaluated at 0.2, 0.4, 0.6 and 0.8 litre per minute. The applied pressure on the reservoir for 0.2 and 0.4 litre per minute is between 3 and 4 bar and the pressure for 0.6 and 0.8 litre per minute is roughly 6 bar, so the user has to increase the pressure with the pressure regulation valve on the compressor.

- If the experiment is finished, close the manual valve (d) and stop the computer program. Close the valve which connects the compressor to the reservoir, and turn on the agitator. The agitator is operated with pressurized air, so the pressure in the reservoir (a) will decrease till the atmospheric pressure is reached. Then the agitator is turned off, the reservoir is opened and can be refilled with the paraffin oil from the second reservoir (i) by using a funnel. Rename the file with the experimental data.

- The fixture with the filter sample is opened and the filter can be removed.

- The pressure regulation valve on the compressor is opened so that the pressure gauge on the compressor indicates zero.

5.3 Working Instruction - Pressure Drop (With Particles)

Read the following working instruction carefully and thoroughly! Read also the safety data for Rhodamine B particles enclosed to this document and ensure personal protection.

5.3.1 Preparation of the Samples

For the preparation of the samples read the working instructions for *translucency examination* (see chapter 5.1).

5.3.2 Filter Test Circuit

The information of the filter test circuit is shown in chapter 3.2.2.

5.3.3 Sequence of Operations

- Ensure that no pressure is applied on the reservoir [4], and the manual valve (d) is closed. Open the fixture (h) and place the red sealing ring in the right part of the fixture as illustrated in figure 3.7. Insert the grate for the stability of the filter sample. Place the filter sample on the grate. Finally add the blue sealing ring which should avoid leakiness at the edges. The left part of the fixture also contains a grate. Screw the two parts together. Be careful with the pressure gauges [5], and ensure that they are on the same level.

- Turn on the power supply and make sure that the display of the flow control device [6] is on. Connect the USB – cable of the control box with the computer, and start the *DurchflussregelungMain* program with *LabView8.5* when the green light on the control box is blinking.

- Fill the reservoir (a) with roughly 6 litre of paraffin oil [14]. Switch on the scale [9] and tare a clean beaker. Fill it with 3 to 6 mg of Rhodamine B particles [15], depending on the size of the particles. The bigger the particles are, the more is needed in order to compensate for decreasing particle numbers per mg with increasing particle diameter. For personal protection it is recommended to wear gloves, when Rhodamine B particles are used. Put some paraffin oil in the beaker with the help of a syringe, and mix the suspension till larger agglomerates are destroyed. Then the content of the beaker is injected with the syringe in the reservoir and the lid is closed.

  Switch on the compressor [7], and wait till it reaches its operating pressure. During the whole experiment the agitator is switched on, to ensure a constant particle concentration in the suspension. The agitator is operated with pressurized air. In

order to guarantee a constant pressure in the reservoir, the compressor has to work during the whole experiment. The user has to wear ear protection.

Open the valve which connects the compressor to the reservoir, turn on the agitator and adjust the pressure in the reservoir according to the pressure gauge illustrated in figure 5.5. The pressure is regulated with a valve on the compressor as shown in figure 5.6. It is recommended to use a pressure of 3 to 4 bar for a flow rate of 0.2 to 0.4 litre per minute and a pressure of approximately 6 bar at higher flow rates. The maximum flow rate is 1.0 litre per minute, depending on the pressure drop of the filter medium.

Experiment Conditions:

- If the penetration depth is to be evaluated, four samples of the same filter material should be taken. The amount of 6 litre paraffin oil is enough for four filter samples. This procedure ensures that all four filter samples are treated with the same suspension. The user determines one flow rate for all samples e.g. 0.4 litre per minute. A volume of 1.1 litre should flow over each filter.

- Click on the *arrow* in the upper left area of the *DurchflussregelungMain* program, and choose the *Spülen* menu as shown in figure 5.7. On the right side are three diagrams. The first diagram shows the pressure against time. The second diagram illustrates the flow rate against time and the third diagram shows the volume against time. Use the right key of the mouse, and scale the y – axis of the first diagram. On the left side the user can define the flow rate in litre per minute.

  If it is necessary to save the pressure values, make a tick at *Speichern EIN*. The user has to define the directory where the data is saved. This is done by clicking on *Speichern* and choosing the directory. The program saves a file with the current date. It is important that this file is renamed after the experiment at least with the type of the filter material, the number of the sample and the diameter of the particles.

- If the pressure is applied to the reservoir (a) and the settings in the program are done, ensure that the pipe after the fixture (h) leads into the second reservoir (i). The agitator has to run for at least five minutes before the experiment starts, to ensure a constant concentration in the suspension. Start the program by clicking on *Starten*. The user is asked to confirm the settings. Insert the path where the file should be saved. If previous measurement data should be deleted, click *OK*. The two signals next to *Starten* and *Speichern* should be green. Open the manual valve (d) slowly to avoid shock waves because it takes some time till the flow control devices regulates the flow.

- After a volume of 1.1 litre has flown over the filter, close the manual valve (d) and the valve which connects the compressor to the reservoir (a). The agitator is still switched on, and the program is running as well. Wait till the pressure in the reservoir is decreased to atmospheric pressure. Open the fixture for the filter sample (h) and replace the filter with the next sample as described above.

- Open the valve which connects the compressor to the reservoir, and adjust the pressure in the reservoir according to the pressure gauge. The agitator is still switched on. When the desired pressure is reached, open the valve (d) slowly.

- This procedure can be repeated for all four filter samples.

- If the experiment is finished, close the manual valve (d) and stop the computer program. Close the valve which connects the compressor to the reservoir, and wait till the pressure in the reservoir is decreased to atmospheric pressure. Then the agitator is turned off, the reservoir is opened and can be refilled with the paraffin oil from the second reservoir (i) by using a funnel. Rename the file with the experimental data.

- The fixture with the filter sample (h) is opened and the filter can be removed.

- After the experiment is finished, it is important to clean the filter test circuit, especially when particles with other diameters are used. Therefore, insert a new filter sample with a small MFP – value. Screw the fixture and apply a pressure to the reservoir (a). Switch on the agitator. Start the program and open the manual valve (d). All 6 litre have to flow over the clean up filter. When the reservoir (a) is empty release the pressure, open the lid and refill it with the paraffin oil from the second reservoir (i). It is not necessary to change the clean up filter as long as the pressure drop is not too high (< 2 bar). Repeat this cleaning procedure three times. Then the clean up filter has to be changed, and a new filter is used for the fourth time. After the fourth time the clean up filter is checked for pink particles. If the filter is pink or particles can be seen, repeat the cleaning procedure. Otherwise a new experiment can be started.

5.4 Working Instruction - Penetration Depth

Read the following working instruction carefully and thoroughly! Read also the safety data for Rhodamine B particles enclosed to this document, and ensure personal protection. When the laser is activated all persons in the room have to wear proper eye protection.

5.4.1 Determination of the Pressure Drop

For the determination of the pressure drop of the samples read the working instructions for *translucency examination* (chapter 5.1) and pressure drop with particles (chapter 5.3).

5.4.2 Preparation of the Samples and the Devices

The filter samples are loaded with particles [15] of a certain diameter or size distribution. The user has to prepare the filter samples and take 30 to 50 pictures in different distances to the samples.

- Take a fixture and place a sheet of glass in it. Put a black sealing ring on the sheet of glass and fill it with some paraffin oil [14] with the help of a syringe. Lay a filter sample in the sealing ring, ensuring that the filter is parallel to the sheet of glass and the front side is up. Fill some more paraffin oil in the sealing ring taking advantage of the surface tension. Place a second sheet of glass on the sealing ring and fix it with two clamps as illustrated in figure 4.11.

  If the sealing ring is free from larger air bubbles, the connecting piece can be screwed on the fixture. Put the entire fixture in an upright position and wait for at least 30 minutes to make certain that all particles have settled down.

- Switch on the camera [10] and start the *daVis_alt* program. Click *Login*. Open a new session by clicking on *new,* and specify the *project name*. Click on the *camera symbol new*. Select the *Macro* drop-down menu and click on *Execute Function*. A new dialog box will open. Insert the cursor at the *Find String* line, write *DDE* and click on *Refresh*. Choose the *DDE_command*, and click *execute*. Insert the following four parameters in the new dialog box and press enter after each parameter: -1 “” “” “”. Confirm everything with enter. If the whole thing worked the string “result:” should be seen on the left side.

  The camera has to cool down to -11°C. The current temperature is shown on the bottom of the program. During this time the user can enter the *exposure time* by choosing the *PTU controlled recording* menu as shown in figure 5.8. Ensure that a tick is made at *Camera 1*. An *exposure time* of 200.000 µs is recommended. After the working temperature is reached, an *Intensity Correction* has to be carried out. Therefore, click on *Devices,* located in the lower part of the window. Select *Image*

Intense and click on *Intensity Correction*. Delete all ticks and ensure that the lens cap is closed. Click on *Take Dark Image*. If this is done, remove the tick at *Dark image subtraction* and click on *Take Background Image*. Make a tick at *Dark Image* and *Background Image*.

Click on the *Take* button. The camera takes a single picture of the lens cap. A black picture appears on the screen. Click with the right key of the mouse on the picture and select *Buffer Statistics*. All values have to be zero, otherwise repeat the *Intensity Correction*.

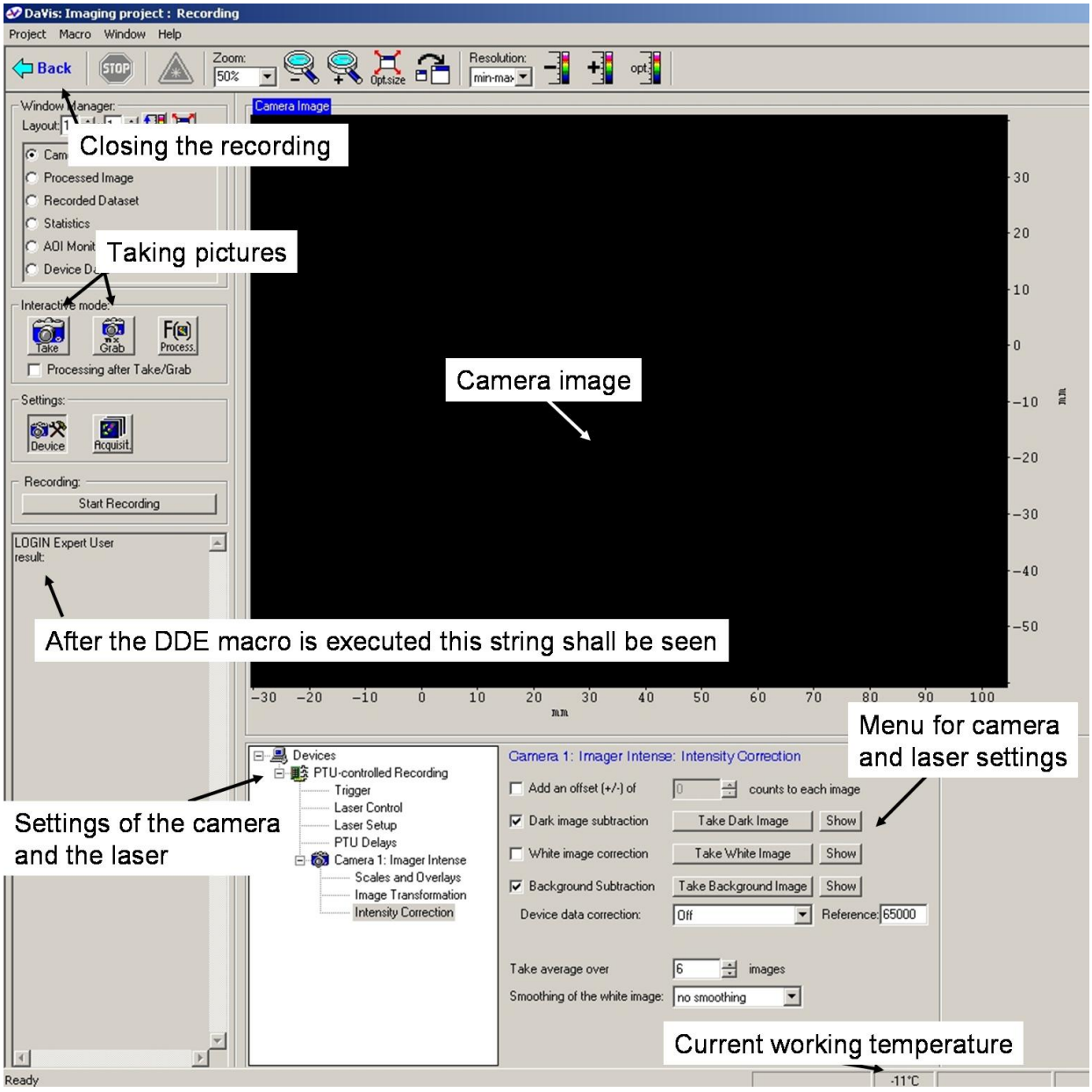

Figure 5.8: Screenshot of the *DaVis* program

- Switch on the power supply for the motion basic system [11], and start the *motion basic* program. Click on the *Erstellen* drop-down menu and select *Kompilieren*. The program checks if everything is correct. Then click again on the *Erstellen* drop-down menu, select *Start Debug -> Go*. The drive set application goes for a trial run. It is very important that the fixture with the sample is not screwed on the suspension, so that the camera cannot crash into it during the trial run.

- Remove the lens cap from the camera and ensure that the filter is fixed to the object lens. Check the setting of the object lens [12]:

  Zoom: 1:1

  Aperture value: 2.8

- Screw the fixture to the fitting and position the camera in front of the fixture as shown in figure 4.8. For that, change to the *motion basic* program and select in the *Extras* drop-down menu *XemoGo*. A new window will open as illustrated in figure 5.9. Choose *Handsteuerung*. Now the user has the possibility to change the coordinates of the camera position. The x-direction is up and down, the y-direction is left and right and the z-direction is the distance between the camera and the fixture with the filter sample.

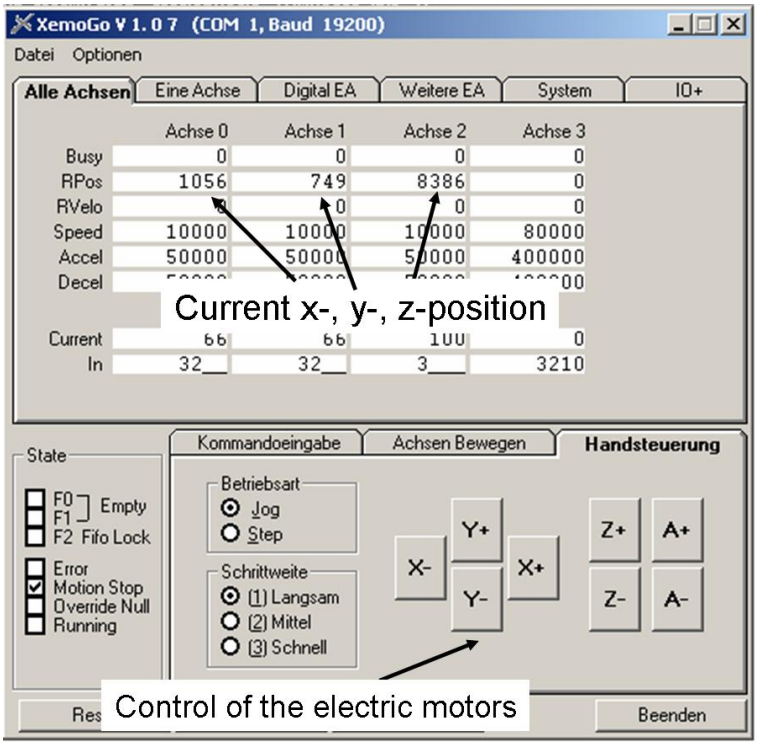

Figure 5.9: Screenshot of the *XemoGo* window

- The user has two possibilities to take a picture. The first one is to click on the *Take* button in the *DaVis* program. A single picture is taken. The other possibility is to click on the *Grab* button. Here the program takes pictures continuously. The exposure time must not be too high because the camera sensor is very sensitive to light.

- Click on the *Grab* button and change the position of the camera with *XemoGo,* so that the filter is in focus. If the pictures are too dark, increase the exposure time, otherwise decrease it. As soon as the filter is focused, try to find the upper and lower end, as well as the right and left edge of the round filter. Make a note of the coordinates, calculate the centre of the circle and position the camera on these coordinates. Stop the grab modus by clicking once more on the *Grab* button. Put a cardboard on the fixture with the sample as shown in figure 4.12.

Close all doors, draw all curtains and switch on the power supply of the laser [13], which is located on the back of the control tower. When the laser is on, every person in the room must wear proper eye protection! Protection glasses, designed to filter 532nm laser light, are found in the laboratory. Turn the key to 1 and press *START* as illustrated in figure 5.10. Wait till the lamp stops to blink and check if the lamp at the *INT* button is on. Then press both *LASER* buttons, so that the laser is activated. A “tick-tick” sound indicates that the laser is working. Remove the safety cap of the laser, fix the diverging lens as shown in figure 4.9 and open the safety lid. Position the laser such that it aims at the filter sample. Press the two *EXT INT* buttons, so that the lamp at the *EXT* is on and press the two *LASER* buttons again. Now the laser can be controlled with the computer program.

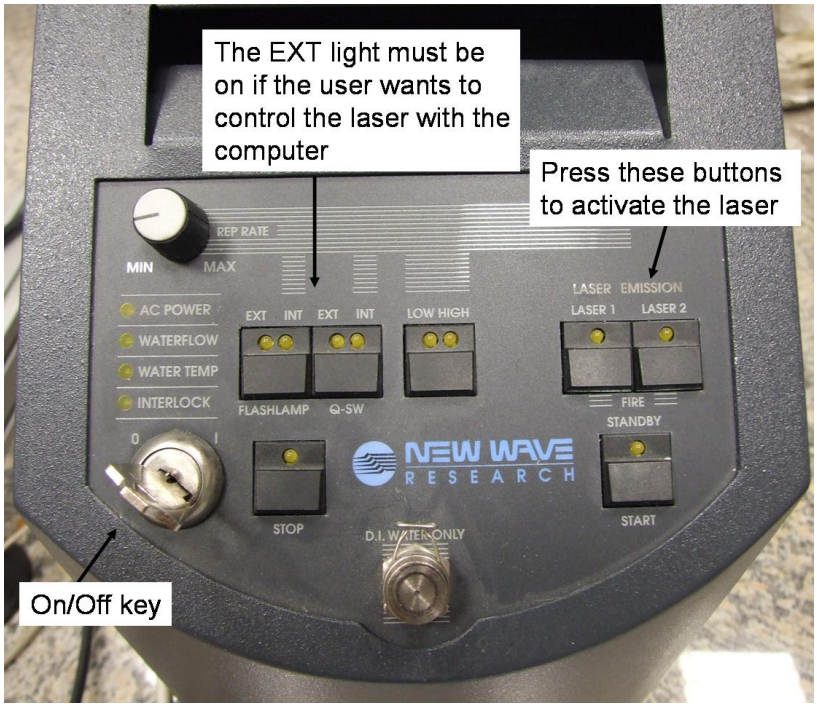

Figure 5.10: Control tower of the laser system.

5.4.3 Taking the Pictures

- Click on the *PTU controlled recording* menu and select *Laser Control -> On*. The default settings are: Ticks at *Laser 1* and *Laser 2 active*; *dt* -> 800µs; *Power* ->100. The laser should be working and a “tick-tick” sound should be heard. Take a photo and check if the exposure time is sufficient. When working with small particle diameters the exposure time may have to be increased. It is important that the pictures are black and only the particles are visible. If the exposure time is too high, light dots may be seen. A possibility to avoid these unwanted light effects is to turn off the lights in the laboratory. Activate the grab modus and find a good position for a picture. Set the z-coordinate to the smallest distance between the camera and the filter sample, where the particles are not in the focus area. Make a note of all three coordinates. Stop the grab modus.

- Close the *XemoGo* window, open the *Cam – Laser* program and fill in the demanded parameters (*Buffernummer* -> 5; *Path* and *Versuchsplan* -> user defined, *Nullpunkt coordinates*) as illustrated in figure 5.11. Insert *2* at the *Relativbew*. *in z-Richtung* field, this means that the camera increases the distance to the sample for 20 µm after every taken picture. Fill in *30* to *50* at the *Anzahl in z-Richtung* field in the z-direction, depending on the amount of pictures, which should be taken, and *1* in the x- and y-direction. Click on the *arrow* button on the upper left side of the window. Two windows will open. Click *Retry* and the camera will make a trial run, position at the determined coordinates, take a picture, change the position, wait a few seconds and make a picture again till it reaches the end point. The user can see the pictures on the screen and has to check whether the quality is sufficient or not. It is recommended that on the fifth picture the first focused particles are seen. If this is not the case the program has to be stopped and the coordinates have to be changed.

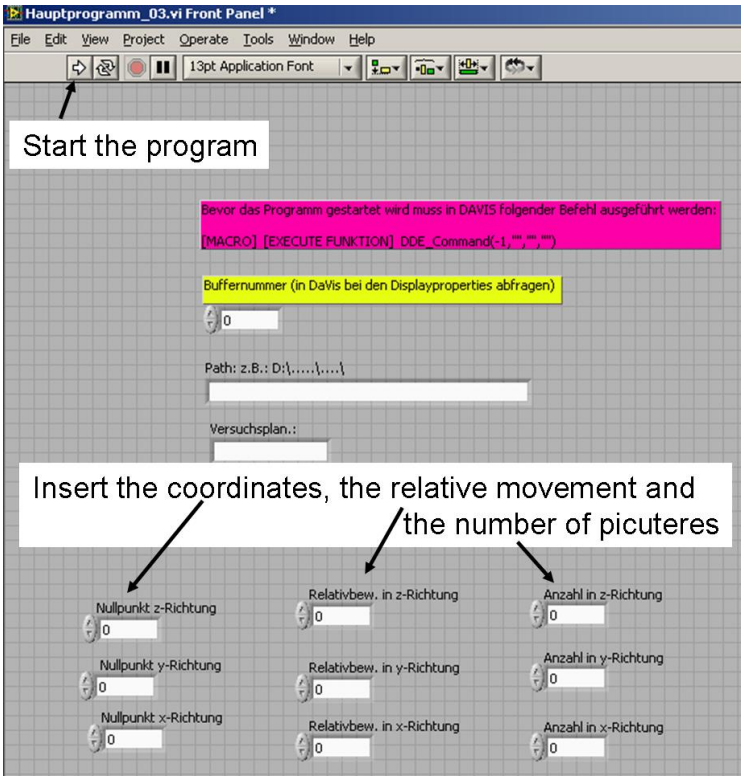

Figure 5.11: Screenshot of the *Cam_Laser* program

- When a set of pictures is finished, click on *Back* in the upper left corner. Click on *Import* and select all pictures; click on *Add to list* and then on *Import Data*. Then click on *Back*, select *Export* and fill in the demanded parameters especially the *Export path* and the *File name,* and click on *Export*. The pictures are saved in the *JPEG* format in a folder. Click on *Back*.

- Click on *New recording* if a new set of pictures should be taken and repeat the above instructions. It is recommended to take at least five different sets of pictures. One in the middle of the filter sample and one set each above, below, left and right from the middle (see figure 5.12). The distance to the middle should be at least 200, which is adequate to 2000µm.

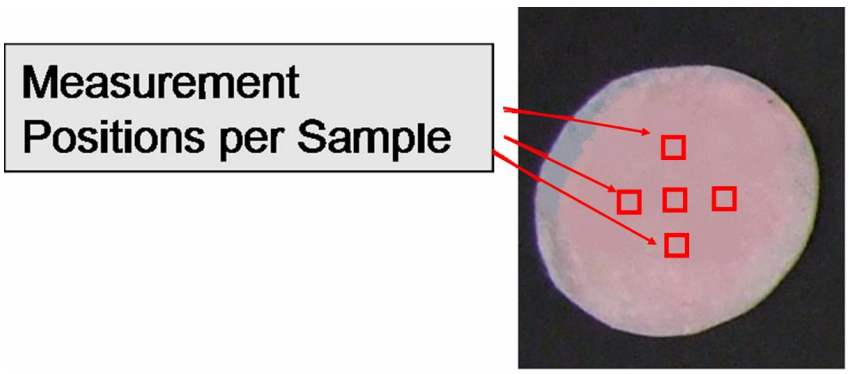

Figure 5.12: Proposed measurement positions per sample

- After the experiment is finished, close all programs and turn of the power supply of the motion basic system, the camera and the laser. If the program asks whether to save changes or not, click on *don't save*. Remove the fixture with the filter sample. Fix the lens cap to the object lens of the camera. Close the lid at the laser, remove the diverging lens and screw the cap.

5.4.4 Evaluating the Pictures

- Open the *processImageStatistics.m* and the *processImage.m* program with *MATLAB*. The *processImageStatistics.m* program is the user interface. The user has to define several parameters:

  noSamples -> How many sets of pictures have been taken?

  noFiles -> How many pictures at each set?

  fileRes -> Compressed resolution of pictures

  spacing -> This equates to the *Relativbew. in z-Richtung* which was defined by the user in the *Cam-Laser* program. The value has to be inserted in millimeter.

  widthFile -> Width of picture at a resolution of *fileRes* in millimeter. This is a determined value for the above mentioned camera settings.

  SaveStats -> The user can define whether the statistic diagrams shall be saved or not, by entering *true* or *false*.

- Run the program. A new window will open where the user can define the path of the set of pictures and choose the first picture. The program will evaluate the set of pictures. When it finishes with the first set, it asks to define the path of the next set and so on. The program saves the results and the statistic evaluation is shown in the *command window*. Copy this information to a word document and save it.

- The *processImage.m* file gives the user the opportunity to change some evaluation parameters:

  Thres -> This is a percentile of the *MaxFocusValue*, which is the maximum focus value in the pictures. If this value is increased, fewer particles are detected. The recommended default value for all particle diameters is *0.05*.

  RadiusExtension -> When particles are very close to each other it can occur that one particle occludes the other. In this case the two particles are seen as one particle. The *RadiusExtension* defines the minimum distance in pixel between two particles, which is required for those two objects to be identified separately. The recommended default value for all particle diameters is *2.*

noOps -> It can occur that undesired light effects cause light spots on the picture. To get rid of these effects the program deletes small light spots. The higher the value of *noOps* is, the bigger are the light spots which are erased. This causes problems when small particles with a diameter less than 40µm are to be evaluated, because then the program also deletes some of these particles. Therefore, it is recommended to use a *noOps* value of *1* for particles smaller than 40µm and a value of *2* for particles bigger than 40µm.

5.5 List of Components and Materials

[1] Tripod: SLIK Professional II

[2] Overhead Projector: 3M 1750

[3] Camera: Fuji Finepix S6500fd

[4] Reservoir: Krautzberger; max. volume 10 litre; max. operating pressure 6 bar

[5] Pressure gauge: JUMO MIDAS; pressure range: 0 – 2.50 bar

[6] Flow control: bürkert; easy FLOW CONTR 8623-2

[7] Compressor: MISTER TOOL; Turbo Air 25/180; max. pressure: 8 bar

[8] Flow measurement: bürkert; 8071 Flow Sensor; flow range: 2 – 100 lph

[9] Scale: KERN; EW 150-3M

[10] Camera: LAVISION; Imager intense

[11] Motion Basic: xemo S360 systec

[12] Object lens: Nikon; AF MICRO NIKKOR 60mm

[13] Laser: New Wave Research; Model: Solo III 15 Hz

[14] Paraffin Oil: Viscosity 160 mPas; Density 0.8676 kg/dm³

[15] Monodisperse fluorescent particles (Rhodamine B PMMA): 19.78 ± 0.18 µm
41.12 ± 0.76 µm
61.35 ± 1.42 µm

6 Application of the Proposed Methods

In this chapter a practical application of the *translucency examination* (see chapter 3) and the evaluation of the particle penetration depth (see chapter 4) is presented. The filter medium *A43 Fulda* was chosen. The characteristics provided by the supplier are listed in table 6.1.

Table 6.1: Characteristics of the filter medium *A43 Fulda* (MAHLE, 2006)

Characteristics	Unit	*A43 Fulda* Required Value	*A43 Fulda* Actual Value
Air permeability	l/m²s	750 ± 140	749
Pore size			
- biggest pore	µm	≤ 115	109
- many pores	µm	83 ± 8	102
- mean flow pore size	µm	32 ± 3	31,9
Thickness			
@ 1bar	mm	1,1 ± 0,1	1,05
@ 0,5 kPa	mm	1,3 ± 0,15	1,41
Weight	g/m²	250 ± 20	232
Burst strength	N/mm²	≥ 0,6	≥ 0,6
Bulge height	mm	-	≥ 6,5

This data can now be extended by information provided by the two novel methods.

6.1 Translucency Examination

With the help of the *translucency examination* five samples with a higher grey value and five samples with a lower grey value were chosen from an *A43 Fulda* filter sheet. The information, obtained by pressure drop measurements, enables the user to determine the maximal and minimal possible pressure drop of this filter sheet.

6.1.1 Experimental Conditions

The pressure drop was assessed in accordance with the working instructions described in chapter 5. Each filter sample was tested at five different flow rates. These flow rates were: 0.2 l/min, 0.4 l/min, 0.6 l/min, 0.8 l/min and 0.9 l/min.

6.1.2 Results

Figure 6.1 and figure 6.2 show the pressure drop of the individual samples of *A43 Fulda* against the flow velocity. The information in the legend refers to the number of the sample (e.g. *P1*) and the current grey value of the sample.

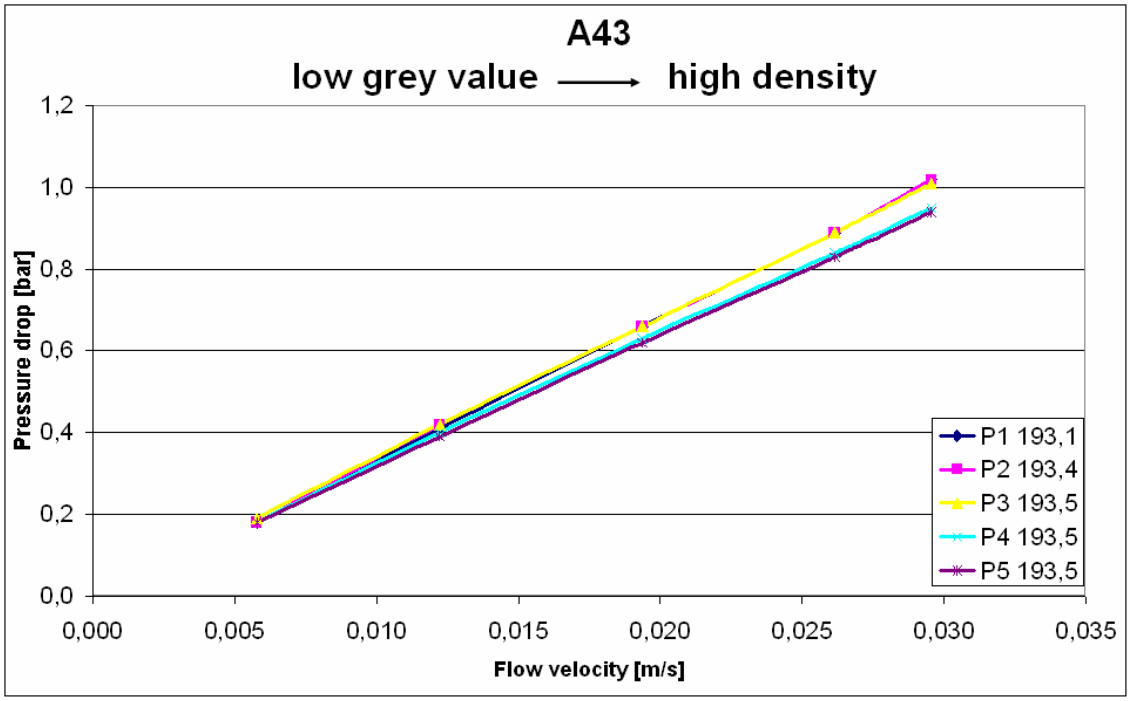

Figure 6.1: Pressure drop of *A43 Fulda* filter samples with low grey values against flow velocity

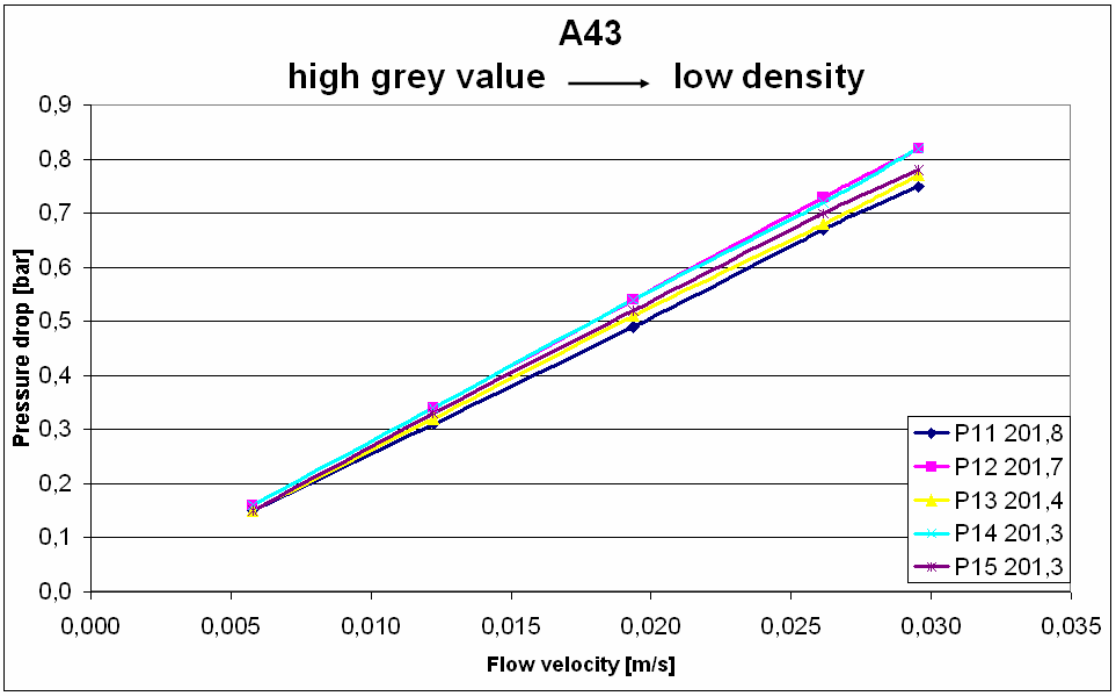

Figure 6.2: Pressure drop of *A43 Fulda* filter samples with high grey values against flow velocity

Figure 6.3 shows a comparison between the mean pressure drop for all flow velocities of *A43 Fulda* filter samples with high and low grey values. The curves in figure 6.3 are simultaneously borderlines for the *A43 Fulda* filter. Every arbitrarily selected sample will feature a local pressure drop which is likely to be within these lines. Therefore, the user has a relatively simple opportunity to determine the highest and the lowest possible pressure drop, and assess the applicability of the filter material for a particular process.

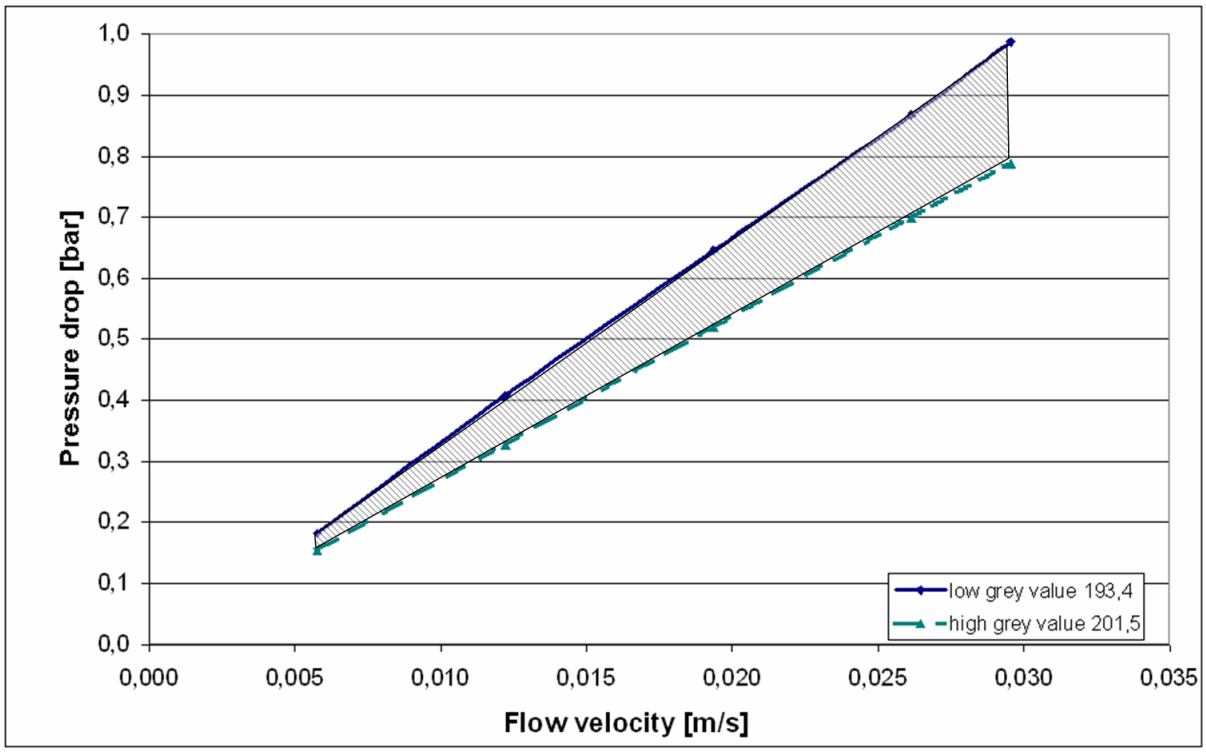

Figure 6.3: Comparison between the mean pressure drop values of an *A43 Fulda* filter against flow velocity

6.2 Particle Penetration Depth

The evaluation of the particle penetration depth offers the opportunity to examine the particle distribution within a filter fibre material. It delivers information on the deposition effects, and can be used to improve the quality of the filter fibre material.

6.2.1 Experimental Conditions

The penetration depth of three different particle sizes was assessed. The diameters of the PMMA Rhodamine B particles were: 19.78 ± 0.18 µm, 41.12 ± 0.76 µm and 61.35 ± 1.42 µm. For each particle size four *A43 Fulda* filters were used. They were selected with the help of the *translucency examination* method in view of an equal grey value, and a low grey value deviation within the sample. The filters were loaded with particles, and five sequences of 40 pictures were taken of each sample. Subsequently, the pictures were evaluated with the

computer algorithm, and the mean depth, as well as the mean deviation were obtained. A detailed working description can be looked up in chapter 5.

6.2.2 Results

The input data for the computer algorithm is a certain amount of pictures. These pictures are evaluated to determine the position of the focused particles. Each particle position is then linked to the number of the corresponding picture. Therefore, the output data does not state the distance of individual particles, but the number of the picture where these particles are located. As the distance in z-direction between two pictures is defined by the steps, which the camera has to make between two photographs, it is reasonable to assume that also particles detected on neighbouring pictures have the same distance in z-direction. As a consequence, the picture number is converted to a distance in micrometer with a scaling factor of 20µm/picture because this is the defined step width of the camera.

In order to assess the property of the filter medium, different statistical values are calculated by the computer algorithm. Firstly, the absolute penetration depth of particles with different diameters is examined (see figure 6.4). The x-axis refers to the numbering of the filter samples and is chosen arbitrarily. For each particle diameter four filters were selected with the help of the *translucency examination*. On every filter sample five measurement positions were examined (see figure 5.12), and the local particle penetration depth was assessed. The mean value of these five measurement positions is printed as an individual data point in figure 6.4.

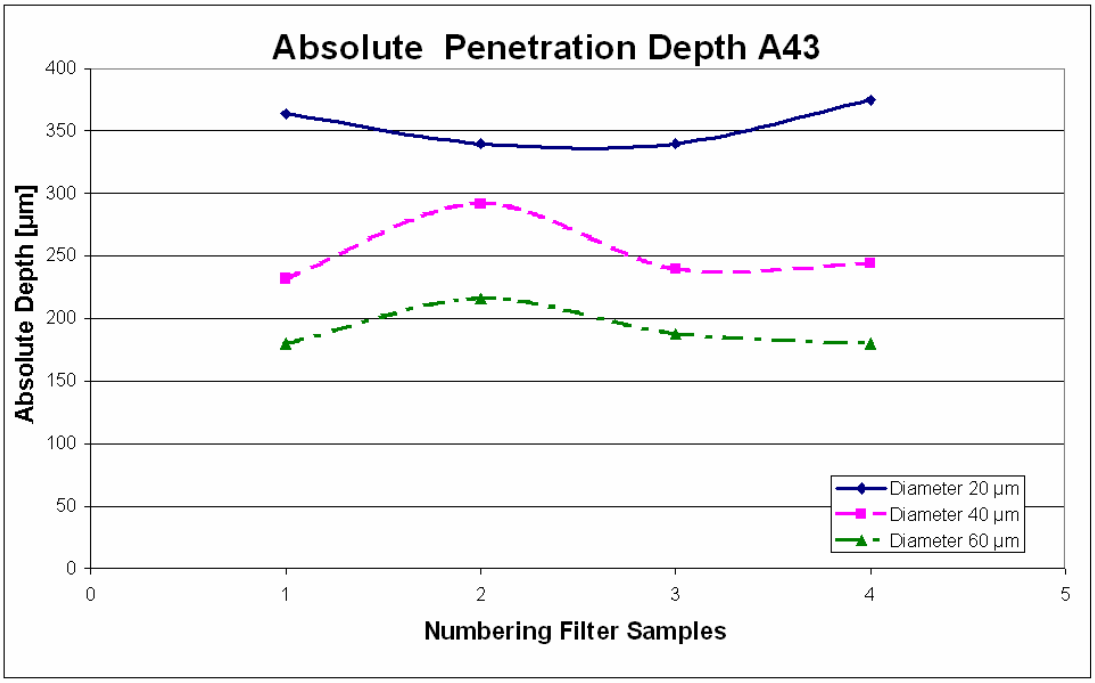

Figure 6.4: Absolute penetration depth of different particle diameters in *A43 Fulda;* data points are averages, calculated from five measurement positions on each filter sample

Due to the fact that it is hardly possible to determine the beginning of the filter, the following definition of the absolute penetration depth is proposed. The distance between the nearest and farthest focused particle is regarded as the absolute penetration depth. When looking at figure 6.4 it is evident that the absolute penetration depth increases with smaller particle diameters. This is an expected result and confirms the applicability of the procedure. The mean absolute penetration depth for particles with a diameter of roughly 60µm is in the region of 200µm, compared to approximately 250µm for particles with a diameter of 40µm. The maximum penetration depth lies almost at 350µm for particles with a diameter of 20µm. One problem is that it is not known if the taken pictures represent the entire thickness of the filter, or if the fibres obstruct the sight trough the filter. This problem can be solved through using special oils which have an optimal match of indices of refraction, as considered in chapter 4.4.3. Another drawback is, that the distance between the nearest and the farthest focused particle is determined, but it is not known whether the nearest particle is deposited close to the outermost fibres of the filter or at some point located more deeply within the filter. Consequently, the next statistical value provides more information on the property of the filter medium.

The mean penetration within the A43 Fulda is the second numerical value which was evaluated with the algorithm (see figure 6.5). Here again the x-axis refers to the numbering of the filter samples, and is chosen arbitrarily. Each of the points is again a mean value of the five different positions of measurement, where the penetration depth was assessed. The mean penetration depth of all particles is calculated, and then related to the position of the nearest focused particle. Once more the increasing mean penetration depth with decreasing particle size can be observed.

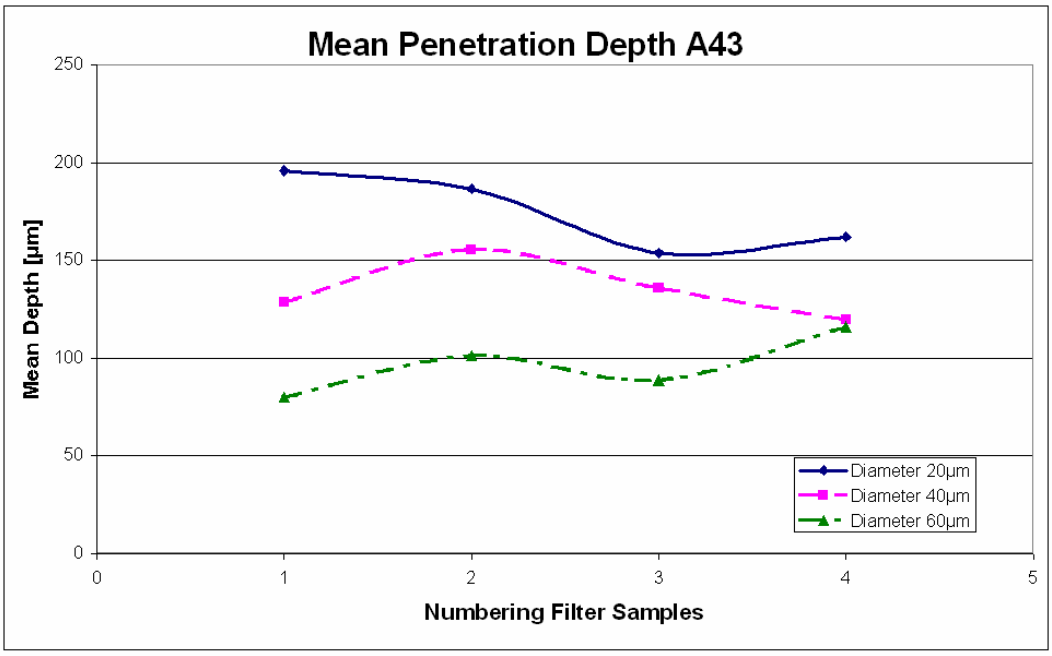

Figure 6.5: Mean penetration depth of different particle diameters in *A43 Fulda;* data points are averages, calculated from five measurement positions on each filter sample

The third evaluated statistical value is the mean *particle spreading* within filter materials. Theoretically the *particle spreading* should increase with decreasing particle diameters because bigger particles will be deposited on the first fibres, while smaller particles spread out more readily within the filter. This assumption is already confirmed by the results shown in figure 6.4 and 6.5. The values of the *particle spreading* are shown in figure 6.6.

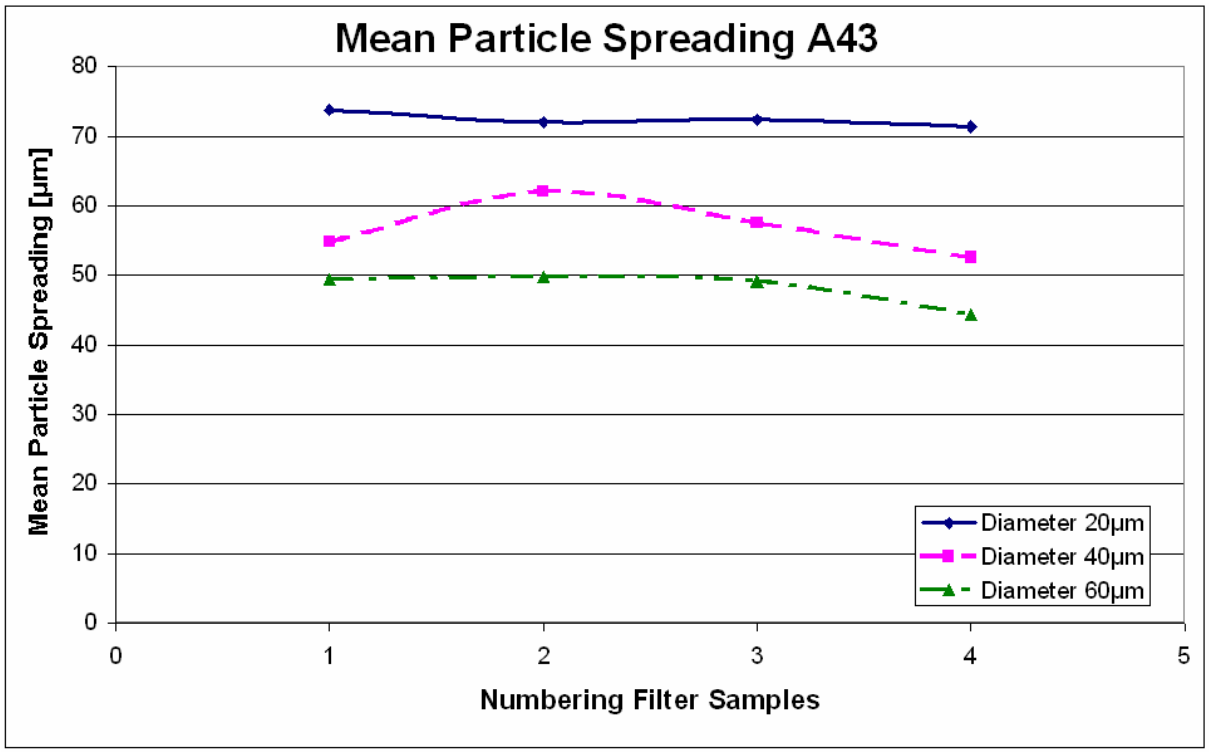

Figure 6.6: Mean *particle spreading* of different particle diameters in *A43 Fulda;* data points are averages, calculated from five measurement positions on each filter sample

Once more the value of each point is the mean value of the five different positions, where the penetration depth was assessed. The theoretical assumption that smaller particles have a higher *particle spreading* is proved to be true. In figure 6.7 a comparison of the 3-D distribution between the penetration depths of particles with different diameters is shown. The side view of the filter is plotted, where the flow direction is from the right hand side to the left. Particles with a diameter of 60µm seem to be stuck nearly in one plane, whereas particles with a diameter of 40µm have a slightly broader distribution in the filter medium. In table 6.1 filter characteristics of the *A43 Fulda* are listed. The mean flow pore size is stated to be 31,9µm. Therefore, it is obvious why the *particle spreading* of particles with a diameter of 20µm is distinctly higher compared to 40µm and 60µm. Particles with a diameter above 30µm are likely to be separated by plugging (sieving effect) because these particles are too big to pass through the pores. Smaller particles, like those with a diameter of 20µm, are deposited on the fibre mainly due to particle inertia and depth filtration effects.

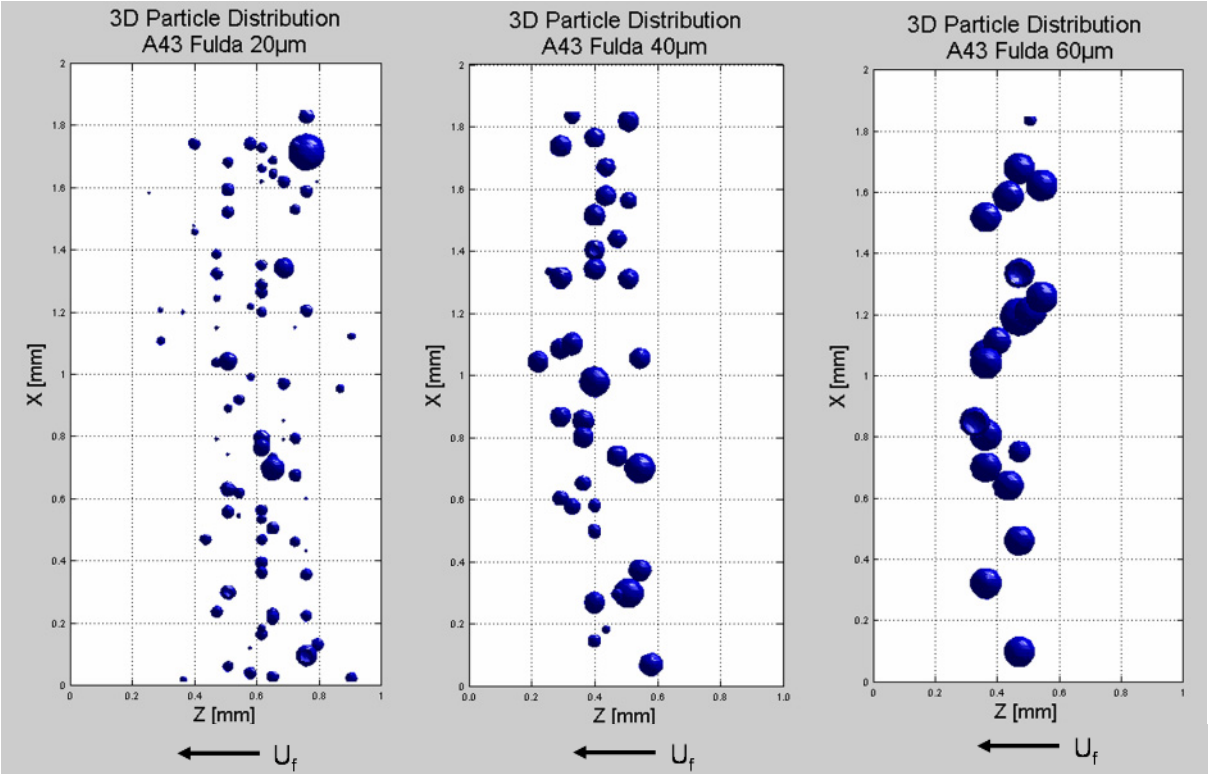

Figure 6.7: Comparison of the penetration depth of different particles sizes in *A43 Fulda*

6.3 Conclusion

The two proposed filter testing methods provide the following additional information for characterizing a filter medium:

- minimal and maximal pressure drop
- data on the particle penetration depth distribution

The minimal and maximal possible pressure drop of the *A43 Fulda* filter is listed in table 6.2.

Table 6.2: Minimal and maximal pressure drop to be expected: *A43 Fulda*

Pressure drop *A43 Fulda*		
Grey value	193,4	201,5
Flow velocity	Δ p	Δ p
m/s	bar	bar
0,17	0,18	0,15
0,36	0,41	0,33
0,57	0,65	0,52
0,76	0,87	0,70
0,86	0,99	0,79

The pressure drop of each arbitrarily chosen sample should range between the threshold values listed in table 6.2. With the improvements, suggested in chapter 3.6, it should be possible to assess other filter sheets of the type *A43 Fulda* only by means of their grey values. This means that if the grey value of the sample is within 193,4 and 201,5 also the pressure drop should lie between the minimum and the maximum pressure value, listed in table 6.2.

The evaluation of the particle penetration depth provides the following information:

Firstly, that particles with diameters distinctly higher than the MFP-value are deposited in the filter *A43 Fulda* nearly in one plane. They are too big to penetrate the filter.

Secondly, that the distribution of particles within the filter fibres augments with decreasing particle diameters.

7 Conclusion

This master thesis started with a description of the state of the art in filter testing, and ended with the presentation and application of two novel and innovative filter testing methods. The brief overview at the beginning gave an idea about the quantity of different procedures to assess filter materials. Nevertheless, it was possible to develop and verify two new filter testing methods.

The assumption that grey values of a picture of a filter sample and the local pressure drop correlate is proven. With the help of the *translucency examination* the dependence can be confirmed. Furthermore, it is shown that the application of the novel *translucency examination* method leads to a noticeable decrease of the measurement error of selected samples compared to arbitrarily chosen ones. Another surprising finding, observed during the development process, is that the permeability of filter materials is not constant for relevant flow velocities. The deformation of the filter materials causes a change of the MFP-value. Especially glass fibre filters tend to have a non-linear behaviour which results in the fact that the measured pressure drop is higher compared to the pressure drop to be expected based on the assumption of non-deformability.

The second method provides the opportunity to look into a filter material. With the interplay of a laser, fluorescence particles, a drive set and a high resolution camera it is possible to obtain a 3-D reconstruction of the distribution of particles within filter fibre geometry. It is confirmed that particles with a smaller diameter have a deeper penetration depth into the filter than particles with a bigger diameter. Furthermore, the distribution within the filter medium is broader for smaller particles.

The core of this master thesis is a thorough description of the proposed filter testing methods, which can be used as an instruction manual for every filter testing laboratory. One goal of the detailed description of these working instructions is, to enable the usage of the procedures without any deeper background knowledge.

Subsequent to the theoretical and practical development process the application of the proposed methods was described. One filter material was chosen and assessed with the help of the *translucency examination*. Furthermore, the determination of the particle penetration depth was carried out. These additional pieces of information, retrievable by the novel testing methods, extend the state of the art knowledge of the filter material.

To sum up, this master thesis contains the know-how of two novel and innovative filter testing methods. The *translucency examination* meets the guideline that the procedure should be affordable for every laboratory. It is an user-friendly process which does not require long settling-in periods. The results, obtained by the *translucency examination*, can be used by filter fibre producers, as well as other companies that use filters in their processes, and need a fast and simple evaluation method for the quality of these filters. The

determination of the particle penetration depth offers new opportunities especially for filter fibre producers. The knowledge and verification of separation processes in real fibre geometry can help to improve the production and the quality of filter fibres. An application of the two methods in other fields, such as the paper industry is conceivable as well.

8 Appendix A

8.1 Safety data Rhodamine B

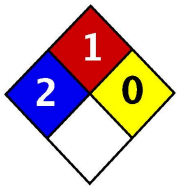

Material Safety Data Sheet
Rhodamine B, O MSDS

Section 1: Chemical Product and Company Identification

Product Name: Rhodamine B, O

Catalog Codes: SLR1465

CAS#: 81-88-9

RTECS: Not available.

TSCA: TSCA 8(b) inventory: Rhodamine B, O

CI#: 45170

Synonym: Rhodamine 123 Basic Violet 10; (9-(o-carboxyphenyl)-6-(diethylamino)-3H-xanthen-3-ylidene)diethylammonium chloride

Chemical Name: Not available.

Chemical Formula: C28H31ClN2O3

Contact Information:

Sciencelab.com, Inc.
14025 Smith Rd.
Houston, Texas 77396

US Sales: **1-800-901-7247**
International Sales: **1-281-441-4400**

Order Online: ScienceLab.com

CHEMTREC (24HR Emergency Telephone), call: 1-800-424-9300

International CHEMTREC, call: 1-703-527-3887

For non-emergency assistance, call: 1-281-441-4400

Section 2: Composition and Information on Ingredients

Composition:

Name	CAS #	% by Weight
Rhodamine B, O	81-88-9	100

Toxicological Data on Ingredients: Rhodamine B, O: ORAL (LD50): Acute: 887 mg/kg [Mouse].

Section 3: Hazards Identification

Potential Acute Health Effects: Hazardous in case of skin contact (irritant), of eye contact (irritant), of ingestion, of inhalation.

Potential Chronic Health Effects:
Hazardous in case of skin contact (irritant), of eye contact (irritant), of ingestion, of inhalation.
CARCINOGENIC EFFECTS: Not available.
MUTAGENIC EFFECTS: Not available.
TERATOGENIC EFFECTS: Not available.
DEVELOPMENTAL TOXICITY: Not available.

Section 4: First Aid Measures

Eye Contact:

p. 1

Check for and remove any contact lenses. Immediately flush eyes with running water for at least 15 minutes, keeping eyelids open. Cold water may be used. Do not use an eye ointment. Seek medical attention.

Skin Contact:
After contact with skin, wash immediately with plenty of water. Gently and thoroughly wash the contaminated skin with running water and non-abrasive soap. Be particularly careful to clean folds, crevices, creases and groin. Cold water may be used. Cover the irritated skin with an emollient. If irritation persists, seek medical attention. Wash contaminated clothing before reusing.

Serious Skin Contact:
Wash with a disinfectant soap and cover the contaminated skin with an anti-bacterial cream. Seek immediate medical attention.

Inhalation: Allow the victim to rest in a well ventilated area. Seek immediate medical attention.

Serious Inhalation: Not available.

Ingestion:
Do not induce vomiting. Examine the lips and mouth to ascertain whether the tissues are damaged, a possible indication that the toxic material was ingested; the absence of such signs, however, is not conclusive. Loosen tight clothing such as a collar, tie, belt or waistband. If the victim is not breathing, perform mouth-to-mouth resuscitation. Seek immediate medical attention.

Serious Ingestion: Not available.

Section 5: Fire and Explosion Data

Flammability of the Product: May be combustible at high temperature.

Auto-Ignition Temperature: Not available.

Flash Points: Not available.

Flammable Limits: Not available.

Products of Combustion: These products are carbon oxides (CO, CO2), nitrogen oxides (NO, NO2...), halogenated compounds.

Fire Hazards in Presence of Various Substances: Not available.

Explosion Hazards in Presence of Various Substances:
Risks of explosion of the product in presence of mechanical impact: Not available.
Risks of explosion of the product in presence of static discharge: Not available.

Fire Fighting Media and Instructions:
SMALL FIRE: Use DRY chemical powder.
LARGE FIRE: Use water spray, fog or foam. Do not use water jet.

Special Remarks on Fire Hazards: Not available.

Special Remarks on Explosion Hazards: Not available.

Section 6: Accidental Release Measures

Small Spill:
Use appropriate tools to put the spilled solid in a convenient waste disposal container. Finish cleaning by spreading water on the contaminated surface and dispose of according to local and regional authority requirements.

Large Spill:

Use a shovel to put the material into a convenient waste disposal container. Finish cleaning by spreading water on the contaminated surface and allow to evacuate through the sanitary system.

Section 7: Handling and Storage

Precautions:
Keep away from heat. Keep away from sources of ignition. Empty containers pose a fire risk, evaporate the residue under a fume hood. Ground all equipment containing material. Do not ingest. Do not breathe dust. Wear suitable protective clothing In case of insufficient ventilation, wear suitable respiratory equipment If ingested, seek medical advice immediately and show the container or the label. Avoid contact with skin and eyes

Storage:
Keep container dry. Keep in a cool place. Ground all equipment containing material. Keep container tightly closed. Keep in a cool, well-ventilated place. Combustible materials should be stored away from extreme heat and away from strong oxidizing agents.

Section 8: Exposure Controls/Personal Protection

Engineering Controls:
Use process enclosures, local exhaust ventilation, or other engineering controls to keep airborne levels below recommended exposure limits. If user operations generate dust, fume or mist, use ventilation to keep exposure to airborne contaminants below the exposure limit.

Personal Protection:
Splash goggles. Lab coat. Dust respirator. Be sure to use an approved/certified respirator or equivalent. Gloves.

Personal Protection in Case of a Large Spill:
Splash goggles. Full suit. Dust respirator. Boots. Gloves. A self contained breathing apparatus should be used to avoid inhalation of the product. Suggested protective clothing might not be sufficient; consult a specialist BEFORE handling this product.

Exposure Limits: Not available.

Section 9: Physical and Chemical Properties

Physical state and appearance: Solid.

Odor: Not available.

Taste: Not available.

Molecular Weight: 479.02 g/mole

Color: Not available.

pH (1% soln/water): Not available.

Boiling Point: Decomposes.

Melting Point: 165°C (329°F)

Critical Temperature: Not available.

Specific Gravity: Not available.

Vapor Pressure: Not applicable.

Vapor Density: Not available.

Volatility: Not available.

Odor Threshold: Not available.

Water/Oil Dist. Coeff.: Not available.

Ionicity (in Water): Not available.

Dispersion Properties: See solubility in water.

Solubility: Partially soluble in cold water.

Section 10: Stability and Reactivity Data

Stability: The product is stable.

Instability Temperature: Not available.

Conditions of Instability: Not available.

Incompatibility with various substances: Not available.

Corrosivity: Non-corrosive in presence of glass.

Special Remarks on Reactivity: Not available.

Special Remarks on Corrosivity: Not available.

Polymerization: No.

Section 11: Toxicological Information

Routes of Entry: Eye contact. Inhalation. Ingestion.

Toxicity to Animals: Acute oral toxicity (LD50): 887 mg/kg [Mouse].

Chronic Effects on Humans: Not available.

Other Toxic Effects on Humans: Hazardous in case of skin contact (irritant), of ingestion, of inhalation.

Special Remarks on Toxicity to Animals: Not available.

Special Remarks on Chronic Effects on Humans: Not available.

Special Remarks on other Toxic Effects on Humans: Not available.

Section 12: Ecological Information

Ecotoxicity: Not available.

BOD5 and COD: Not available.

Products of Biodegradation:
Possibly hazardous short term degradation products are not likely. However, long term degradation products may arise.

Toxicity of the Products of Biodegradation: The products of degradation are more toxic.

Special Remarks on the Products of Biodegradation: Not available.

Section 13: Disposal Considerations

Waste Disposal:

Section 14: Transport Information

DOT Classification: Not a DOT controlled material (United States).

Identification: Not applicable.

Special Provisions for Transport: Not applicable.

Section 15: Other Regulatory Information

Federal and State Regulations:
Pennsylvania RTK: Rhodamine B, O
Massachusetts RTK: Rhodamine B, O
TSCA 8(b) inventory: Rhodamine B, O
SARA 313 toxic chemical notification and release reporting: Rhodamine B, O

Other Regulations: Not available..

Other Classifications:

WHMIS (Canada): CLASS D-2B: Material causing other toxic effects (TOXIC).

DSCL (EEC): R36/38- Irritating to eyes and skin.

HMIS (U.S.A.):

Health Hazard: 2

Fire Hazard: 1

Reactivity: 0

Personal Protection: E

National Fire Protection Association (U.S.A.):

Health: 2

Flammability: 1

Reactivity: 0

Specific hazard:

Protective Equipment:
Gloves.
Lab coat.
Dust respirator. Be sure to use an approved/certified respirator or equivalent. Wear appropriate respirator when ventilation is inadequate.
Splash goggles.

Section 16: Other Information
References: Not available. **Other Special Considerations:** Not available. **Created:** 10/09/2005 06:21 PM **Last Updated:** 11/06/2008 12:00 PM *The information above is believed to be accurate and represents the best information currently available to us. However, we make no warranty of merchantability or any other warranty, express or implied, with respect to such information, and we assume no liability resulting from its use. Users should make their own investigations to determine the suitability of the information for their particular purposes. In no event shall ScienceLab.com be liable for any claims, losses, or damages of any third party or for lost profits or any special, indirect, incidental, consequential or exemplary damages, howsoever arising, even if ScienceLab.com has been advised of the possibility of such damages.*

9 Appendix B

9.1 References

Akshaya, Jena; Krishna, Gupta (2009): Characterization of the pore structure of complete filter cartridges using high flow porometry. Porous Materials Inc., USA. Retrieved July 30, 2009: http://porousmaterialsinc.com/publications/docs/AFS_Topical_Conf_paper.pdf

Boiger, Gernot (2009): Development and Verification of a Novel Lagrangian, (Non-)Spherical Dirt Particle and Deposition Model to Simulate Fluid Filtration Processes using OpenFOAM®. PhD thesis. Montanuniversität Leoben, ICE Strömungsforschung GmbH. Austria.

Box, George E. P.; Hunter, William G.; Hunter J. Stuart (1978): Statistics for experimenters: An Introduction to Design, Data Analysis, and Model Building. New York: Wiley.

Conrad, Jeff (2006): Depth of Field in Depth. Large Format Page. Retrieved October 15, 2009: http://www.largeformatphotography.info/articles/DoFinDepth.pdf

Eltoukhy, Helmy A.; Kavusi, Sam (2003): A Computationally Efficient Algorithm for Multi-Focus Image Reconstruction. Proc. of SPIE Electronic Imaging. Pages: 332-341.

EN 779 (1994): Partikel-Luftfilter für die allgemeine Raumlufttechnik. Berlin: Beuth.

Huang, Wei; Jing, Zhongliang (2007): Evaluation of focus measures in multi-focus image fusion. Pattern Recognition Letters. Vol. 28. No. 4. Pages: 493-500.

ISO 4548-12 (2000): Methods of test for full-flow lubricating oil filters for internal combustion engines. Part 12: Filtration efficiency using particle counting, and contaminant retention capacity. Geneva: ISO.

Klauth, Peter; Bauer, Reimar; Ralfs, Carla; Ustohal, Petr; Vanderborght, Jan; Vereecken, Harry; Klumpp, Erwin (2007): Fluorescence macrophotography as a tool to visualise and quantify spatial distribution of deposited colloid tracers in porous media. Colloids and Surfaces A: Physicochem. Eng. Aspects. Vol. 306. Pages: 118–125.

LaVision (2002): DaVis Flow Master Hardware Manual for DaVis 6.2. Göttingen: Produced by LaVision GmbH.

MAHLE (2006): Laborbericht. MAHLE Filtersysteme GmbH, Stuttgart. Fulda Filtervlies A43.

Maruthi, R.; Sankarasubramanian, K.(2007): Multi Focus Image Fusion based on the Information Level in the Regions of the Images. Journal of Theoretical and Applied Information Technology. Vol. 3. No. 4. Pages: 80-85.

Mataln, M.; Boiger, G.; Brandstätter, W.; Gschaider, B. (2007): Simulation of Particle Filtration Processes in Deformable Media. Part 1: Fluid-Structure Interaction. ICE Stroemungsforschungs GmbH. Montanuniversitaet Leoben.

Schnitzer, Ch.; Ripperger S. (2007): Die Barrierewirkung von Geweben. Teil 4: Modellierung der Durchströmung von Multifilamentgeweben. In: F&S Filtrieren und Separieren. Vol. 21. Pages: 226-231.

TOPAS (2008): Pore Size Meter for Filter Papers, Woven Materials, Non-Wovens and other Porous Materials PSM 165. Topas GmbH, Dresden. Retrieved August 20, 2009: http://www.topas-gmbh.de/dateien/prospekt/100/165/165prspe.pdf

VDI 3677 (1997): Filternde Abscheider. Oberflächenfilter. Filtering separators. Surface filters. Düsseldorf: Verein Deutscher Ingenieure.

VDI 3926 (1994): Prüfung von Filtermedien für Abreinigungsfilter. Testing of Filter Media for Cleanable Filters. Düsseldorf: Verein Deutscher Ingenieure.

Wang, Chiu-Sen (2001): Electrostatic forces in fibrous filters – a review. Powder Technology. Vol.118. Pages: 166-170.

9.2 List of Abbreviations

Latin Symbols

A_F	Filter area (in m²)
a_x	standard thickness (in mm)
D	aperture diameter (in mm)
d	particle diameter (in µm)
D_F	fibre diameter (in m)
DoF	Depth of field (in m)
D_p	pore diameter (in m)
f	focal length (in m)
F_d	flow rate through the dry filter material (in l/min)
F_w	flow rate through the wet filter material (in l/min)
k	number of different grey values
K_D	permeability (in m²)
K_D'	thickness-related permeability (in m)
ΔL	thickness of the fibre layer (in m)
l_a	starting length (in mm)
l_s	shrinkage length (in mm)
m	magnification
m_A	weight per unit area (in g/cm²)
Mgroup	mean pressure drop of a group
Mgv	mean pressure drop of a certain grey value at all flow velocities
Mov	mean pressure drop of all individual pressure values
Mv	mean pressure drop at a certain flow velocity of all grey values
N	f-number of camera
n	number of different flow velocities
p	pressure (in Pa)

Δp	pressure drop of the fibre layer (in Pa)
R	radius blur circle (in mm)
r	number of replications
Res	resolution (in pixel/µm)
r_r	relative particle radius (pixel)
S	distance of sensor plane to the lens (in mm)
s	thickness of the filter (in m)
S_e	sum of squares error
S_{FV}	sum of squares flow velocity
S_{GV}	sum of squares grey value
S_I	sum of squares interaction
SoS	sum of squares total
S_V	specific surface area (in m^{-1})
U	object distance between object and lens (in m)
U_{far}	farthest object plane with a blur circle less than or equal R
U_{near}	nearest object plane with a blur circle less than or equal R
V	image distance between depicted object and lens (in m)
$\dot{V}$	flow rate (in m³/h)
v_F	specific area load (in m³/(m²·h))
V_{px}	pore portion (in %)
$\bar{\bar{y}}$	grand average
$\bar{y}_i$	block average
$\bar{y}_t$	treatment average

Greek Symbols

γ	surface tension (in N/m)
ε	layer porosity (in %)
η_f	dynamic viscosity (in Pas)
θ	contact angle of the wetting liquid with the sample
μ	correction factor
ρ_{RX}	gross density of filter medium (in g/cm³)
ρ_N	density of fibre material (in g/cm³)

9.3 List of Tables

9.4 List of Figures

Figure 4.26: Set-up of a simple scene to verify the functionality of the 3-D particle reconstruction method. Boiger, Gernot (2009): Development and Verification of a Novel Lagrangian, (Non-)Spherical Dirt Particle and Deposition Model to Simulate Fluid Filtration Processes using OpenFOAM®. PhD thesis. Montanuniversität Leoben, ICE Strömungsforschung GmbH. Austria. p. 226

Figure 4.27: Comparison between a real picture of a sphere distribution and the 3-D result of the computer algorithm. Boiger, Gernot (2009): Development and Verification of a Novel Lagrangian, (Non-)Spherical Dirt Particle and Deposition Model to Simulate Fluid Filtration Processes using OpenFOAM®. PhD thesis. Montanuniversität Leoben, ICE Strömungsforschung GmbH. Austria. p. 227

Figure 4.28: Comparison of the resolution in pixel per µm between different optical bellows settings and different object lenses.

Figure 4.29: Photographed filter sample area (Resolution: 460 x 337) with different optical bellows settings.

Figure 4.30: Comparison of the index match between filter samples and different oils

Figure 5.1: Prepared filter sheet with ruler

Figure 5.2: Using the program IrfanView

Figure 5.3: Selection of the region of the filter sheet where the samples shall be determined.

Figure 5.4: Proposed position of the different samples

Figure 5.5: Reservoir (a) of the filter test circuit

Figure 5.6: Compressor

Figure 5.7: Description of the *Durchluss-Messung* program

Figure 5.8: Screenshot of the *DaVis* program

Figure 5.9: Screenshot of the *XemoGo* window

Figure 5.10: Control tower of the laser system.

Figure 5.11: Screenshot of the *Cam_Laser* program

Figure 5.12: Proposed measurement positions per sample

Figure 6.1: Pressure drop of *A43 Fulda* filter samples with low grey values against flow velocity